X-RAY AND OPTICAL OBSERVATIONS OF HIGH MASS X-RAY BINARIES

A THESIS SUBMITTED TO
THE GRADUATE SCHOOL OF NATURAL AND APPLIED SCIENCES
OF
MIDDLE EAST TECHNICAL UNIVERSITY

BY

ELİF BEKLEN

IN PARTIAL FULFILLMENT OF THE REQUIREMENTS
FOR
THE DEGREE OF DOCTOR OF PHILOSOPHY
IN
PHYSICS

SEPTEMBER 2010

Approval of the thesis:

X-RAY AND OPTICAL OBSERVATIONS OF HIGH MASS X-RAY BINARIES

submitted by **ELİF BEKLEN** in partial fulfillment of the requirements for the degree of **Doctor of Philosophy in Physics Department, Middle East Technical University** by,

Prof. Dr. Canan Özgen
Dean, Graduate School of **Natural and Applied Sciences** _____

Prof. Dr. Sinan Bilikmen
Head of Department, **Physics** _____

Prof. Dr. Altan Baykal
Supervisor, **Physics, METU** _____

Assis. Prof. Dr. S. Çağdaş İnam
Co-supervisor, **E.E. Dept., Başkent Univ.** _____

Examining Committee Members:

Prof. Dr. Berahitdin Albayrak
Astronomy and Space Sciences, Ankara University _____

Prof. Dr. Altan Baykal
Physics Department, METU _____

Prof. Dr. Ümit Kızıloğlu
Physics Department, METU _____

Prof. Dr. Nilgün Kızıloğlu
Physics Department, METU _____

Assis. Prof. Dr. Sinan Kaan Yerli
Physics Department, METU _____

Date: _____

I hereby declare that all information in this document has been obtained and presented in accordance with academic rules and ethical conduct. I also declare that, as required by these rules and conduct, I have fully cited and referenced all material and results that are not original to this work.

Name, Last Name: ELİF BEKLEN

Signature :

ABSTRACT

X-RAY AND OPTICAL OBSERVATIONS OF HIGH MASS X-RAY BINARIES

Beklen, Elif
Ph.D, Department of Physics
Supervisor : Prof. Dr. Altan Baykal
Co-Supervisor : Assis. Prof. Dr. S. Çağdaş İnam

September 2010, 87 pages

In this thesis, X-ray and optical observations of accretion powered pulsars are presented. By using archival RXTE observations we work on the X-ray spectral and pulse timing analysis of 4U 1538-52, 4U 1907+09, SMC X-1 to have more detailed information about their orbital and spin parameters. For 4U 1538-52 and SMC X-1, we determined new orbital epochs. By using long term pulse history of 4U 1907+09, we were able to work spin-down trend of the system and also calculate the change in the spin-down rate. Using Fermi/GBM observations we can monitor bright accreting pulsar systems. We are producing long term histories of pulse frequency and flux of 20 continuosly monitoring systems. Adding Swift/BAT observations to GBM observations, for 4U 1626-67, we did reveal the characteristics belong to spin-down trend before and spin-up behaviour after torque reversal seen in 2008 February. Two newly discovered IGRJ06074+2205 and IGRJ01583+6713 sources are identified as X-ray binary systems and we found parameters of them like distance, magnitudes, by using both optical photometric and spectroscopic observations.

Keywords: Accreting powered pulsars, Pulse Timing, Spin down, Spin up, X-ray binaries

ÖZ

YÜKSEK KÜTLELİ X-IŞINI ÇİFTLİ SİSTMELERİN X-IŞINI VE OPTİK ARALIKTAKİ GÖZLEMLERİ

Beklen, Elif

Doktora, Fizik Bölümü

Tez Yöneticisi : Prof. Dr. Altan Baykal

Ortak Tez Yöneticisi : Y. Doç. Dr. S. Çagdaş İnam

Eylül 2010, 87 sayfa

Bu tezde, aktarım güçlü atarcaların gözlemleri sunulmaktadır. RXTE arşiv gözlemleri kullanılarak 4U 1538-52, 4U 1907+09, SMC X-1'in X-ışını tayfsal ve atarca zamanlama analizleri çalışılıp yörüngesel ve atma parametreleri hakkında detaylı bilgi edinilmiştir. 4U 1538-52 and SMC X-1 için yeni yörüngesel dönem değerleri bulunmuştur. 4U 1907+09 için uzun zamanlı atma hareketi izlenerek kaynağın yavaşlaması ve yavaşlama oranı çalışılmıştır. Fermi/GBM uydusunun gözlemleri kullanılarak parlak aktarım atarcaları da gözlenilmektedir. Şu ana kadar sürekli gözlenen 20 kaynağın uzun zamanlı atma frekansı ve akı hareketi gözlen mektedir. GBM gözlemlerine Swift/BAT gözlemleri de eklenerek, 4U 1626-67 için, Şubat 2008 de görülen dönme momentinin dönüşümünün öncesinde görülen yavaşlama ve sonrasında görülen hızlanma davranıslarina dair özellikler belirlenmiştir. Yeni keşfedilen iki kaynağın, IGRJ 06074+2205 ve IGRJ 01583+6713 X-ışını çiftli sistemler olduğu ve uzaklık, parlaklık değerleri gibi parametreler optik fotometri ve tayfsal gözlemlerle tespit edilmiştir.

Anahtar Kelimeler: Aktarım güçlü atarcalar,Zamanlama,Yavaslama,Hızlanma,X-ışını çiftleri

To my lovely family

ACKNOWLEDGMENTS

I would like to express my deep and sincere gratitude to my supervisor, Prof. Dr. Altan Baykal. His wide knowledge and his logical way of thinking have been of great value for me. His understanding, encouraging and personal guidance have provided a good basis for the present thesis.

I wish to express my warm and sincere thanks to Dear Assis.Dr. S.Çagdaş İnam. He was always be a good co-supervisor but futhermore he became, and I am sure will continue to be, very good friend for me.

I express my most sincere gratitude to Prof.Dr. Ümit Kızıloğlu and Prof.Dr. Nilgun Kızıloğlu, firstly, for their kindly and warm behaviours. Nextly, for their discussion and suggestion for my every question.

I am grateful to Assoc. Dr.Şölen Balman for her discussions on any kind of my question and to Assis. Dr. Sinan Kaan Yerli for his very helpful answers especially to my latex and any kind of problems that I encounter in my computer.

I feel so happy and lucky to be able to study and collaborate with Prof.Dr. Mark H. Finger, Prof.Dr.Colleen A.Wilson-Hodge, Dr.Valerie Connaughton, Dr.Ascension Camero and all GBM pulsar and occultation team members for sharing, firstly, their knowledge. During my stay in Huntsville, (AL) they were always helpful to me for everything.

My another thanks are due to Dr. Pablo Reig for his knowledge and sincere behaviours during my studies at University of Crete, Heraklion. I did learn many things belongs to optical studies. Also to all University of Crete Physics Department and Skinakas Observatories Technical Staff.

I would like to thank TÜBİTAK projects TBAG-106T040 and TBAG-109T748 for financial supports during the last years. They were really important support during my research. During my reasearch in University of Crete was totally supported by the European Union funded ”Transfer of Knowledge” program entitled ASTRONS (Astrophysics of Neutron Star)

project MKTD-CT-2006-042722, this financial support of course was decided to given me by Astrophysics Team Member of Sabancı University, it was honor for me to know Prof. Dr. Ali Alpar, Assoc. Dr. Ersin Göğüş, Assoc. Dr. Ünal Ertan, Assoc. Dr. Emrah Kalemci. Also another thank goes to METU for partial support through the project METU-BAP-08-11DPT2002120510, a part of program (ÖYP) of collaboration between Süleyman Demirel University and METU.

My dear family; my mother, my father, my sister and lovely nephew Umut (lucky to be your aunt). Without their encouragement and understanding it would have been impossible for me to finish this work. They did not only support they did also share my ideal,feel my desire as me. Thanks for everything you did for me. My husband M.Ali Barto for development talks, thoughts since I meet you, make me improve so much.

I would like to thanks to my all dear friends, I feel their encouragement every time. Also, to our Department administrative workers, Zeynep Eke, Gülşen Özdemir, Sevim Aygar thank you for support and any help during my stay in METU.

TABLE OF CONTENTS

ABSTRACT iv

ÖZ v

ACKNOWLEDGMENTS vii

TABLE OF CONTENTS ix

LIST OF TABLES xi

LIST OF FIGURES xii

CHAPTERS

1 INTRODUCTION 1

1.1 History of Neutron Star and Accretion Powered Pulsars 1

1.1.1 Torque Reversal in Accreting Powered Pulsars 4

1.1.2 Quasi Periodic Oscillation (QPO) 5

1.2 Thesis Contents 6

2 SMC X-1 9

2.1 Introduction 9

2.2 Observations and Analysis 10

2.2.1 Pulse Timing Analysis and Timing Solution 12

2.2.2 Pulse Period History and Change of Rate 13

2.2.3 Power Spectra and QPO Features 20

2.3 Spectral Analysis 20

2.4 Discussion 23

3 4U 1907+09 26

3.1 Introduction 26

3.2 Observations and Analysis 27

3.2.1 Timing Analysis 27

3.2.2 Energy Spectrum Analysis . . . 30
3.3 Discussion . . . 33
4 4U 1538-52 . . . 36
4.1 Introduction . . . 36
4.2 Observations and Timing Analysis . . . 37
4.3 Discussion . . . 40
5 OBSERVATIONS OF ACCRETION-POWERED PULSARS WITH FERMI/GBM . . . 43
5.1 Pulsar Monitoring and Data Analysis Process . . . 44
5.2 Pulse Searches . . . 45
5.3 Detected Sources . . . 46
5.4 4U 1626-67 . . . 52
5.5 Observations and Timing Analysis . . . 53
5.6 Swift/BAT observation and Timing Analysis . . . 54
5.7 RXTE Observation and Analyse . . . 56
5.7.1 Hardness Ratio . . . 56
5.7.2 Spectral analysis . . . 58
5.8 Discussion . . . 58
6 SPECTROSCOPIC AND PHOTOMETRIC OBSERVATIONS OF IGRJ 06074+2205 AND IGRJ 01583+6713 . . . 65
6.1 Introduction . . . 65
6.2 Observations . . . 67
6.3 Results . . . 68
6.3.1 Photometric Results . . . 68
6.3.2 Spectral Classification . . . 69
6.3.3 Reddening and Distance Measurements . . . 70
6.4 Discussion . . . 72
7 CONCLUSION . . . 74
REFERENCES . . . 78
CURRICULUM VITAE . . . 86

LIST OF TABLES

TABLES

Table 1.1 List of QPOs 6

Table 2.1 RXTE observations of non-pulsating data of SMC X-1 11

Table 2.2 Orbital Epoch Measurements of SMC X-1 14

Table 2.3 Timing Solution of SMC X-1 15

Table 2.4 Pulse Period History with several and RXTE observations of SMC X-1 . . . 16

Table 2.4 continued 17

Table 2.4 continued 18

Table 2.4 continued 19

Table 2.5 Spectra parameters from Two Different Region 22

Table 3.1 Observation list for 4U 1907+09 27

Table 3.2 Timing solution of 4U 1907+09 29

Table 3.3 RXTE pulse period measurements of 4U 1907+09 31

Table 3.4 Sample Spectral Parameters of Individual PCA Observations of 4U 1907+09 32

Table 4.1 Orbital Parameters of 4U 1538-52 38

Table 4.2 Orbital epochs by pulse timing analysis 41

Table 5.1 Detected accreting pulsars with Fermi/GBM 47

Table 5.2 Detected accreting pulsars with Fermi/GBM 50

Table 5.3 RXTE/PCA and HEXTE continuum spectral fits 59

Table 6.1 Results of photometric measurements of the counterparts 68

Table 6.2 Equivalent widths of the Hα lines 70

LIST OF FIGURES

FIGURES

Figure 2.1 RXTE-PCA Observation Dates shown on RXTE-ASM Lightcurves 10

Figure 2.2 Arrival times (pulsation cycles) (top panel), and residuals after fitting arrival times to a circular (middle panel) and elliptical orbital model (lower panel) . 14

Figure 2.3 Orbital Epoch Arrival Times SMC X-1 15

Figure 2.4 Top panel and middle panel. Pulse frequency history and residuals of SMC X-1 after a linear fit obtained from 5 different intervals listed in Table 2.4. bottom panel. Frequency derivative history. Dashed lines in top and middle panels and horizontal error bars in the bottom panel indicate time intervals in which linear fits were performed. The last (rightmost) interval almost consists of pulse frequency values obtained from our analysis. 21

Figure 2.5 High energy cut-off and folding energy trend of SMC X-1 between MJD 50093 and 53000 22

Figure 2.6 Photon index and nH trend of SMC X-1 between MJD 50093 and 53000 . 23

Figure 2.7 Photon index and nH trend of SMC X-1 24

Figure 3.1 Pulse phase and its residuals fitted to the orbital model presented in (Table 3.2) 28

Figure 3.2 Plot of pulse period history. Solid line and the residuals correspond to the previous spin-down rate found by Baykal et al. 2001([10]). 30

Figure 3.3 Evolution of 3-25 keV unabsorbed flux, Hydrogen column density, power law index, cut-off energy, e-folding energy, and reduced χ^2 in orbital phase. 33

Figure 4.1 2-30 keV RXTE-PCA light curve of 4U 1538-52 between July 31 and August 7, 2003. Two 26s binned $\sim$ 3ksec samples of this light curve corresponding to single RXTE orbits are presented on the upper left and the upper right. 38

Figure 4.2 Top panel. Pulse arrival time delays and best-fit elliptical orbital model given in Table 4.1. (Note that pulse profiles are obtained with respect to the reference time 52855.0585 MJD). Residuals after removing best orbital model. 39

Figure 4.3 Pulse frequency history of 4U 1538-52. The rightmost point corresponds to most recent RXTE observation of ID 80016. 40

Figure 4.4 The phase residuals of orbital epoch for 4U 1538-52. The orbital phases are estimated relative the constant orbital period ($T_{\pi/2} - n < P_{orbit} > - < T_{\pi/2} - n < P_{orbit} >>$), where n is the orbital cycle number. The rightmost point corresponds to the most recent RXTE observation of ID 80016. 41

Figure 5.1 The LAT (silver box at the top) was integrated on the spacecraft at General Dynamics Advanced Information Systems in December 2006. 44

Figure 5.2 A fit of the background rates belongs to the data 2009 Oct 1 in the 12-25 keV band. The upper panel shows the rates and the fit, the bottom panel shows the residuals. 45

Figure 5.3 The Corbet Diagram showing distribution of accreting pulsars as in spin period versus orbital period configuration, with GBM detected sources 48

Figure 5.4 Frequency and the pulsed flux history between 12-25 keV for A 0535+26 . 49

Figure 5.5 Frequency and the pulsed flux history between 12-25 keV for EXO 2030+375 50

Figure 5.6 Frequency and the pulsed flux history between 12-25 keV for Cen X-3 . . 51

Figure 5.7 Frequency and the pulsed flux history between 12-25 keV for Vela X-1 . . 52

Figure 5.8 Frequency and the pulsed flux history between 12-25 keV for Her X-1 . . . 52

Figure 5.9 Pulse frequency history of 4U 1626−67, showing all available historical data from 1997 to 2003. The 1990 June (~MJD 48000) torque reversal is clearly seen. 53

Figure 5.10 Fermi/GBM pulse frequency measurements of 4U 1626-67 since 2008 August. A change in the sign of the torque was found after 18 years of the source spinning down. 54

Figure 5.11 Swift-BAT pulse frequency history covering this second reversal torque (from 2004 Oct to the present time). Error bars are smaller than the plotted symbols. 55

Figure 5.12 Top panel. Swift-BAT spin-up rate history of 4U 1626-67. Middle panel. Average 15-50 keV BAT count rate vs. time. Error bars are smaller than the plotted symbols. Bottom panel. BAT count rate vs. spin-up rate for all the period (circles). A correlation pattern is observed specially during the torque reversal (only square symbols). 56

Figure 5.13 Top panel. Long term hardness ratio analysis of 4U 1626-67. Swift-BAT count rates (15-50 keV) were selected as the hard band and RXTE/ASM count rate (1.5-12 keV) as the soft band. Bottom panel. Hardness-intensity diagram. During the reversal a transition from hard to soft is seen. 57

Figure 5.14 Times of transient outburst observed with GBM 60

Figure 5.15 Pulse frequency history of 4U 1626-67 from 1997 up to 2009. The 1990 June and the 2008 Feb reversals are clearly seen. 61

Figure 5.16 The X-ray flux history of 4U 1626-67 relative to the flux measured by HEAO 1, in the same energy band, from previous works ([28]) circles; ([143]) triangle; ([99]) stars) and two recent RXTE/PCA observations (unfilled squares) in the 2-20 keV band. The cross point is inferred from PCA flux and the fractional change in the Swift-BAT rate, since no spectral changes during the transition have been observed in this work. 63

Figure 6.1 The blue band spectrum (3800-4800 (Å)) of IGRJ 06072+2205 taken on 26 December 2007 68

Figure 6.2 Hα emission line in the red spectrum of IGRJ 06074+2205 taken on 07 November 2007 73

CHAPTER 1

INTRODUCTION

1.1 History of Neutron Star and Accretion Powered Pulsars

After the discovery of the neutron by Chadwick 1932([27]), Baade & Zwicky 1934([8]) proposed the existence of the neutron stars. This idea was realized from their investigation of the explosive endpoint of massive stars, Supernovae. The supernovae represented the transitions from normal stars into neutron stars, which would be at an ultra high density and with a small radius [8]. This is the rst precise prediction that neutron stars can be formed in core-collapsed supernova explosion.

Since the gravity of a neutron star is extremely strong, general relativistic effects have to be taken into account in calculating the stellar structure. The rst relativistic calculations of neutron star models, had shown the existence of stable equilibrium stars which are much more dense than white dwarfs [142]. There were pre- dictions that neutron stars can be rapidly rotating compact objects with strong magnetic field [77]. In 1962, the most powerful persistent extra-solar X-ray source, Scorpius X-1, had been discovered with the X-ray detector on an Aerobee rocket [62]. This discovery made people to speculate that neutron stars could be observable in X-rays. (Zel′dovich & Guseynov 1965) and (Hayakawa & Matsouka 1964) ([198],[72]) had independently predicted that binary systems which comprise a compact object, either a neutron star or a white dwarf and a massive normal stars could generate X-ray emission. When a compact star is accreting matter from its main sequence companion star, thermal X-rays would be generated.

Todays, we exactly know that Accretion-Powered Binary X-ray Pulsars are rotating, highly magnetized $B \gtrsim 10^{12}G$ neutron stars which are capturing matter from a stellar companion

([152], [43], [104]). The dipole axis of the magnetosphere is thought to be tilted with respect to the spin axis of the netron star. The accreting matter is channeled by the magnetosphere onto the magnetic poles and is gravitationally accelerated (to a velocity of ~0.1c) and in a time it reaches the surface of the neutron star. Later, at the polar surface this matter gets slower and it releases its gravitational energy as X-ray and gamma-ray radiation. If the magnetic rotation axes are misaligned and if the beamed emission from the magnetic poles rotates through the line of sight, the pulsations can be observed ([128]). Also we know that if the magnetic field is not so high $B \leq 10^{11}G$, then the accretion disk may touch or come close to the neutron star surface, so the pulsation can not be observed. The pulse profiles of the X-ray pulsars tend to be (mostly) broad and sinusoidal, particularly 10 keV. The pulse shapes can be described as either single-peaked or double-peaked (some of them especially at low energies have complex structures). This shape make us to identify whether the emission comes from one or both magnetic poles.

The pulse emission powered by the release of gravitational energy described as

$$L_x = (GM_x\dot{M}/R_x) = 10^{37} ergs^{-1}(M_x/(1.4)M_{sun})(\dot{M}/10^{-10}M_{sun}yr^{-1})((R_x/10km)^{-1}) \quad (1.1)$$

where L_x is the bolometric X-ray luminosity, M_x and R_x are the mass and radius of the neutron star and $\dot{M}$ is the mass accretion rate.

Accreting X-ray binaries can be divided into a number of different categories based on their observational (such as X-ray, optical) and physical characteristics. But mainly the classification is made based on the mass of the companion star ([38],[137]) in the system, which $M_{comp} \lesssim M_{sun}$ named as low mass X-ray binaries (LMXBs), $1 \gtrsim (M_{comp}) \gtrsim 10(M_{sun})$ classified as intermediate mass X-ray binaries (IMXB), and if $M_{comp} \geq 10(M_{sun})$ then classified as high mass X-ray binaries (HMXBs).

LMXBs are the systems with late type or degenerate dwarf companions (Her X-1, 4U 1626-67, GX 1+4, etc). These systems are steady, low-luminosity X-ray sources. HMXBs are the systems with a massive early type supergiant or a O,B main sequence star (BeX systems). Early type supergiant systems also divide into two groups. First, systems with short pulse periods and high X-ray luminosities (SMC X-1, Cen X-3), in which mass accretion occurs via Roche-lobe overflow mediated by an accretion disk. Secondly, systems with long pulse periods and moderate X-ray luminosities (Vela X-1), in which the mass accretion is supported by accretion of the supergiant's stellar wind. These systems are steady X-ray sources and tend

to be very luminous ($\geq 10^{37} ergs^{-1}$). Nearly 300 X-ray binary systems have ben detected in the Galaxy, with pulse periods ranging from 0.069 to 23.5 min. More than half of these binaries belongs to LMXBs. Around 115 of them belong to HMXBs, and $\approx$ %70([113],[114]) is comprised from Be X-ray binaries. They comprise a neutron star in a wide eccentric orbit around main sequence Be companion (A 0535+62, EXO 2030+375). In these systems, X-ray outbursts typically occur during periastron passage of the neutron star close to the circumstellar disc of the Be star ([141]).

Most Be/Xray binaries are transient systems. Persistent BeX display much less X-ray variability and lower flux ($L_x \leq 10^{35} ergs^{-1}$) and contain slowly rotating neutron stars ($P_{spin} \geqslant$100 s). The variability time scales in Be/Xray binaries range from seconds to years. Pulse periods cover the range 3.61412 s. On longer time scales (months to years), the variability is also apparent in the optical and IR bands and it is attributed to structural changes of the circumstellar disk. Sometimes, the Be star loses its disk. When this occurs the Hα line shows an absorption profile and the X-ray activity ceases.

X-ray bursts have been observed to occur in three different shapes; i) Type I (or normal) outbursts. Those are regular outbursts and peaks of these bursts occur at or very close to periastron passage. They have a short life time and almost cover small fraction of the orbital period. They are generally repeated in each orbital period cycle. They are characterized by lower X-ray luminosities ($L_X \lesssim 10^{37}$ erg s^{-1}).

ii) Type II (or giant) outbursts. They arise from a dramatic expansion of the circumstellar disk and are characterized by high X-ray luminosities ($L_X \sim 10^{38}$ erg s^{-1}), show increases of the X-ray flux. They reach the Eddington luminosity for a neutron star so they become very bright sources. Eddington luminosity is a limit which is set on steady accretion by the radiation pressure on the infalling matter. It is set by equating radiation pressure with gravity.

$$L_{Edd} = 4(\pi)cGM_x(m_p)/(\sigma)_T = 1.8 \times (10_{38}) ergs^{-1}(M_x/(1.4)M_{sun}) \tag{1.2}$$

where m_p is the proton mass and $(\sigma)_T$ is the Thomson scattering cross-section.

The accretion disk may occur during Type II outbursts. Those outbursts don't have a strick phase dependence and typically much longer than Type I outbursts, with outburst time measured generally in months.

iii) Type "outburst free" (quiescence), where the accretion is partially or completely halted

([170], [134], [22]).

1.1.1 Torque Reversal in Accreting Powered Pulsars

The spin periods of most pulsars change with time. This change is related to the torque exerted on the star. For accreting powered pulsars the torque is the accretion of matter with a specific angular momentum ([152], [104]).

$$N_o = \dot{M} l_{in} \tag{1.3}$$

where $l_{in} = (GMr_{in})^{1/2}$ is the specific angular momentum of the matter at the inner edge of the disk. Addition to this torque, there are also internal torques due to coupling of the superfluid interior and the outer crust of the neutron star. As a result, the net torque is produced by filtering of external torque fluctuations in the vicinity of the coupling between the crust and superfluid interior ([105],[106]).

Torque reversals which have been observed in the accreting pulsars, can be detected in Her X-1, Cen X-3, GX 1+4, OAO 1657-415, Vela X-1 ([22]) and 4U 1907+09 ([83]). Her X-1 and 4U 1626-67 has a Roche-lobe filling low mass companion, where matter from the companion flows from the L1 point into an accretion disk ([155]). Studies of accretion torque in Her X-1 are made difficult by the obstruction caused by the warped accretion disk which is viewed from near edge-on, resulting in attenuation or complete eclipsing of the pulsar ([147]), make flux measurements unreliable probes of the mass accretion rate. For 4U 1626-67, see discussion in Chapter 5. Cen X-3 has a high mass companion which almost overflows its Roche-lobe with a focused wind from companion flowing into the accretion disk ([45]). In Cen X-3 the dense wind results in a large column density, with source occasionally being completely obscured. In GX 1+4 ([76]), OAO 1657-415 ([30]), 4U 1907+09 ([59]) and Vela X-1 ([50]) the optical companion underfills its Roche lobe and accretion is done from a wind, with perhaps the transient formation of an accretion disk if the accreting angular momentum is large enough. Vela X-1 is the prototype for a supergiant wind fed system, where accretion is done by direct capture from the wind. In this case the transfer of angular momentum is very inefficient. Detailed timing analysis show that the frequency history of Vela X-1 is consistent with a random walk, or equivalently the power spectrum of the torque is white noise ([48]). However, rare short high flux states have been observed where transient disk accretion may occur ([100]). It is likely transient accretion disks occur in GX 1+4, OAO 1657-415, 4U

1907+09 and play an essential part in there frequency histories.

1.1.2 Quasi Periodic Oscillation (QPO)

QPOs, in X-ray binaries, were first identified in white dwarf systems and then in neutron star systems ([180], and [129]). Generally it is thought to be related to the rotation of the inner accretion disk ([145]). The general description can be done as, any inhomogeneous matter distribution or blobs of matter in the inner disc may result in QPO in the power spectrum. In power spectrum,we search narrow peaks corresponding to the pulse frequency of the pulsar and also its harmonics, QPOs can be distinguish as the appearance of aperiodic variabilities like broad bumps. For accretion powered X-ray pulsars, these features are important in giving information about the interaction between the accretion disc and the neutron star magnetosphere. In accretion powered systems, detecting of these features can be between the range of 10-400 mHz and we may generalize it as, low magnetic field netron stars and black hole binaries show in a wide range of frequency from a few Hz to a few hundred Hz, whereas low frequency QPOs, between 10m Hz to 1 Hz, can be detected from high magnetic field neutron stars. QPOs have been detected in 16 high magnetic accretion-powered pulsars. Few of these belongs to LMXB class and many of them are classified as HMXBs. In Table 1.1, we can see QPO features of both transient and persistent pulsars. In this thesis, we also detect QPOs for 4U 1907+09 (see Chapter 3) and SMC X-1 (see Chapter 2). The QPOs are transient events for all types of pulsars, except 4U 1626-67 (for discussion see[94] and [89]). Persistent pulsars do not show persistent features. For transient pulsars, appearing of QPOs are differ in some situations. For the transient pulsars that show QPOs, if the feature is not detected in some part of the outburst, then it is not detected in all the outbursts. Whereas, if the feature is detected during an outburst, then it is usually present in whole outbursts ([51], [135]). There models for explaining Hz QPOs for HMXBs, the most populars are the *Magnetosphere Beat Frequency Model (MBMF;* [1]) and the *Keplerian Frequency Model (KFM*;[180]). In the MBFM, QPO frequency is calculated as the difference between the spin frequency and the Keplerian frequency of the inner edge of the accretion disc $\nu_{QPO} = \nu_k - \nu_s$ ([166]). In the other model, KFM, QPO features are generated from the modulation of the X-rays by inhomogeneities in the accretion disc, at the Keplerian frequency. We kmow that Keplerian frequency can not be smaller than the spin frequency of the neutron star, otherwise the mass accretion flow to the neutron star from companion star is expected to be stopped at the magnetospheric boundary

by central inhibition of accretion ([170]). In detecting QPOs we use the correlation between the X-ray intensity and the QPO centroid frequency ([52]). When the mass accretion rate becomes bigger, the accretion disk come closer to the neutron star. For both model, such a linear correlation is expected but for some sources although the X-ray luminosity vary, the QPO frequency is founded as almost constant.

1.2 Thesis Contents

In Chapter 2, we present timing and spectral analysis by using RXTE observations of **SMC X-1** accreting powered system between January 1996 and December 2003. The pulse period history and timing solution of the source shows that the source is still in spinning up since its discovered. The long term spin-up rate is $2.65343816(7) \times 10^{-11}$ Hz s^{-1}. We obtain new orbital epoch and using this epoch and previous results we calculate the orbital decay as $\dot{P_{orbit}}/P_{orbit}$ of $-3.402(7)\times10^{-6}$ yr^{-1}. We found that all spectral parameters except Hydrogen

Table 1.1: List of QPOs

Source	Type	ν_s (mHz)	ν_{QPO} (mHz)	ν_{QPO}/ν_s (mHz)	Reference
Transient pulsars					
KS 1947+300	HMXB	53	20	0.38	1
SAX J2103.5+4545	HMXB	2.79	44	15.77	2
A0535+26	HMXB	9.7	50	5.15	3
V0332+53	HMXB	229	51	0.223	4
4U 0115+63	HMXB	277	62	0.224	5
XTE J1858+034	HMXB	4.53	110	24.3	6
EXO 2030+375	HMXB	24	200	8.33	7
XTE J0111.2-7317	HMXB	32	1270	39.68	8
GRO J1744-28	LMXB	2100	20000	9.52	9
Persistent pulsars					
SMC X-1	HMXB	1410	10	0.0071	10
Her X-1	LMXB	806	13	0.016	11
LMC X-4	HMXB	74	0.65-20	0.0087-0.27	12
Cen X-3	HMXB	207	35	0.17	13
4U 1626-67	LMXB	130	48	0.37	14
X Per	HMXB	1.2	54	45	15
4U 1907+09	HMXB	2.27	69	30.4	16

(1)[90], (2)[79], (3)[51], (4)[172], (5)[168], (6)[145], (7)[2], (8)[92], (9)[199], (10)[3], (11)[132], (12)[131], (13)[171], (14)[165], (15)[173], (16)[85]

column density did not show variation from previous studies. And hydrogen column density increases the X-ray flux gets lower.

In Chapter 3, we present the results of timing and spectral studies of archival RXTE-PCA observations of 4U 1907+09, and report a change in the spin down rate of this system. From previous studies it is known that this source showed two flares, namely a primary and a secondary occurring near periastron and apastron and our RXTE observations also included flaring activities of the source. The source showed continues spin down at a rate of $\dot{\nu} = (-3.54 \pm 0.02) \times 10^{-14} Hzs^{-1}$ for more than 15 years. The spin down rate is found as $\dot{\nu} = (-1.887 \pm 0.042) \times 10^{-14}$ Hz s^{-1}.

By using timing analysis of RXTE and IXAE observations give information about transient oscillations with periods of about 18.2s and 14.4s respectively. It was suggested that those transient oscillations can be responsible for the slowing-down of the pulsar due to the presence of a transient retrograde accretion disc.

In Chapter 4, we will discuss the timing studies on accreting powered system HMXB **4U 1538−52** in between July 31 and August 7, 2003 by RXTE-PCA data. We determine new orbital epochs for both circular and elliptical orbital models. Both model results are in agreement with each other. The orbital period derivatives that we found ($\dot{P}/P = (0.4 \pm 1.8) \times 10^{-6}$ yr^{-1}) is also in agreement with previous measurement
($\dot{P}/P = (2.9 \pm 2.1) \times 10^{-6}$ yr^{-1}). The spin-up rate of the neutron star between observation times is found as 2.76×10^{-14} Hz sec^{-1}.

Using the Gamma Ray Burst Monitor (GBM) on board Fermi, we can monitor accreting pulsar systems. In chapter 5 we will work on Fermi-GBM results. We present the results of long term histories of each individual sources from the beginning of the GBM's mission and up to now 20 sources, 8 of them are persistent and 12 of them are transients, are monitored. Basicly, we use the rates from GBM's 12 NaI detectors in the 8-55 keV range to detect and monitor pulsations with periods between 0.5 and 1000 seconds. Two different pulse searches, daily blind and source individual search, are the main components of this study. **4U 1626+67** is one the monitored source by GBM and we will discuss the new torque reversal observed after about 18 years of steadily spinning-down trend. In this work, all available GBM data since its launch in 2008 June 11 and hard X-ray Swift/BAT data starting from 2004 October to the end of 2007 are used. Between 2004 October and end of 2007 the spin-down rate is

averaged at a mean rate of $\sim \dot{\nu} = -4.8 \times 10^{-13}$ Hz s^{-1} until the torque reversal reported here. This second detected torque reversal was centered near MJD 54500 (2008 Feb 4) and it lasted approximately 150 days. During the reversal the source also underwent an increase in flux by a fraction of ∼2.5 and the steady spin-up rate is averaged at a mean rate of $\sim \dot{\nu} = 4.0 \times 10^{-13}$ Hz, s^{-1}. Also there is detailed long-term timing analysis of this source and a long term spectral hardness ratio study in order to see whether there are spectral changes around this new observed torque reversal.

In Chapter 6, we work on two Be type binary systems, **IGRJ06074+2205** and **IGRJ01583+6713**, discovered by INTEGRAL instruments in 2003 and 2005. We present optical band studies of them, photometric and spectroscopic measurements taken from different optical observatories. The spectral type of the companion of IGRJ06074+2205 is defined by using blue spectrum of itself and standard star. The equivalent width of the Hα line gives us information on the disc around Be star, from the lines we define the lines as emission lines. Also it is possible to have idea about interstellar reddening between the star and the observer, by using both photometric and spectroscopic results. Lastly, we could be able to make prediction about the distance of IGRJ06074+2205, which is consistent with other studies about it.

Finally in the last chapter, there is conclusion on our results.

CHAPTER 2

SMC X-1

2.1 Introduction

A high mass X-ray binary system SMCX−1 consists of a neutron star with a low mass M_x= $1.06^{+0.11}_{-0.10} M_\odot$ ([127]). X-ray pulsations were detected every 0.71 s ([115]). The system accretes from young B0 super giant companion star Sk 160 ([185],[112]) with a mass of M_{opt}= 15.6±1.5 ([127]). The source is observed with several satellites since it was discovered during a rocket flight ([150]). It is the most X-ray luminous known HMXB therefore it is a good example of wind disruption by X-ray ionization. It is the first detected HMXB in SMC galaxy. The system show X-ray eclipses occurring once in every orbital period of 3.8992 ([163]).

SMC X-1 has a super orbital flux variations ∼ 55 days. These super-orbital flux variations are different according to 35 day cycle of Her X-1, since the length of successive cycles are highly variable ([195], [176]). The long term superorbital period was firstly reported by Gruber& Rothschild 1984([69]) and then continued to be studied by Levine et al. 1993([110]) with RXTE observations and Wojdowski et al. 1998([195]) with several observations. This superorbital is thought to be due to precession of a warped accretion disk.

Using pulse timing analysis, the spin and orbital parameters of the source was examined. From the rates of change in the orbital period were found in the studies by Levine et al. 1993([110]) and Wojdowski et al. 1998([195]) ($P_{orb}/\dot{P}_{orb}$ of $\sim 3.4 \times 10^{-6}\mathrm{yr}^{-1}$), the results were almost same and the values represent that there is an significant orbital decay in the system. Mostly, the change in pulse spin rate of the source was studied in detail, with the pulse spin values obtained by several observations. The source is spinning up since it was discovered, with a change in spin-up rate.

2.2 Observations and Analysis

The RXTE-PCA (Proportional Counter Array)([87]) consists of an array of 5 Proportional Counters (PCU) operating in the 2-60 keV energy range, with a total effective area of approximately 7000 cm^2 and a field of view of $\sim 1^\circ$ FWHM. Besides PCA data, we also used RXTE-ASM data (All Sky Monitor) to get ASM lighcurve which is generated using all three Scanning Shadow Cameras, and are quoted as nominal 2-10 keV rates in ASM counts per second. In this work we used "one-day average" data belongs to the source. Each "one-day average" data point represents the one-day average of the fitted source fluxes from a number (typically 5-10) of individual ASM dwells.

We analyzed all archival RXTE-PCA observations of SMC X-1 between 1995 January and 2004 January and approximately 139 pointed observations with a total exposure of around 250 ks were used. During the observations between 1998 October 16 and 1998 November 24, nearly $\sim$ 23 ks, the source was observed during the outburst of the nearby transient X-ray pulsar XTEJ0111.2-7317 ([29]) which is located at 30' from SMC X-1. Due to contamination

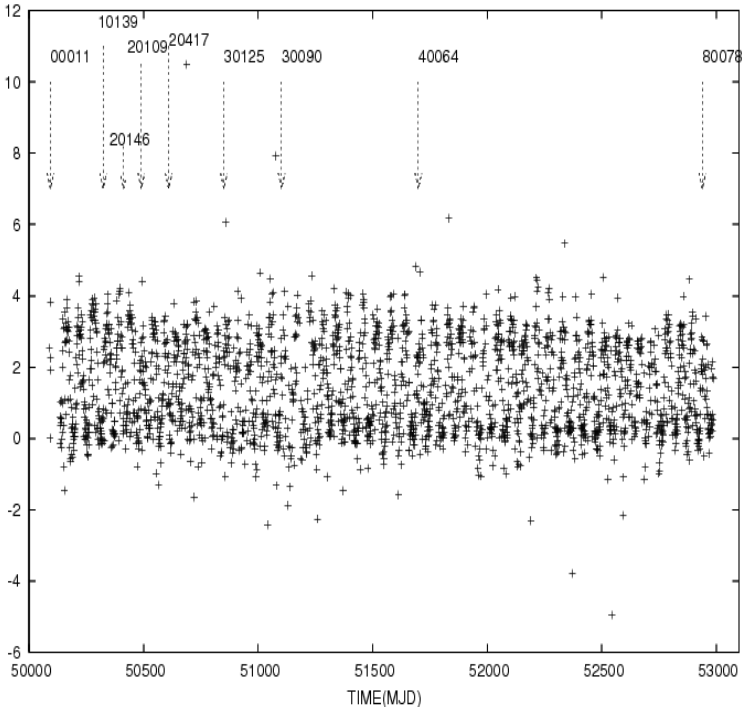

Figure 2.1: RXTE-PCA Observation Dates shown on RXTE-ASM Lightcurves

all pulse timing and X-ray spectral studies we excluded them. Some data belong to exclipsing duration of this source. They were also examined and ignored during all analyses due to be low count statistics. In Table 2.1 data are listed in which SMC X-1 no pulsation observed.

We used all of the five PCUs during whole analysis. Top xenon layers for all Proportional Counter Units were selected for the better statistics. For the observations before May 2000, analysis are made by using all PCU top xenon layers. For the observations after May 2000, for which the propane layer for PCU 0 was lost, only the top xenon layers of other four PCU units were used for spectral analysis.

All PCA bservation dates are indicated on RXTE/ASM lightcurves between MJD 50088 and 54572, in (Figure 2.1) it's labeled according to proposal ID. During the observations between 1998 October 16 and 1998 November 24, nearly ~ 23 ks, the source is observed during the outburst of the nearby transient X-ray pulsar XTEJ0111.2-7317 ([29]). All pulse timing and X-ray spectral studies are done also for these data. The 31s transient source located at 30' from SMC X-1 was easily detected from the power spectra of the data, so to prevent the

Table 2.1: RXTE observations of non-pulsating data of SMC X-1

Obs. ID	Obs. Date	exposure time
20109-02-01-00	1997-01-25	3829
20146-06-03-00	1997-01-25	1015
20109-02-04-00	1997-03-13	2847
30125-05-01-00	1998-01-13	1456
30125-05-02-00	1998-02-06	3756
30125-05-03-01	1998-03-11	2234
30125-05-03-02	1998-03-11	1436
30125-05-08-00	1998-08-10	2979
30125-05-08-01	1998-08-11	2311
30125-05-10-00	1998-10-02	3043
30125-05-10-01	1998-10-03	2853
80078-01-01-07	2003-10-27	10523
80078-01-01-08	2003-10-27	4823
80078-01-03-00	2004-01-27	21028
80078-01-03-01	2004-01-27	49238
80078-01-03-02	2004-01-28	4160
80078-01-03-04	2004-01-28	27725
80078-01-03-03	2004-01-29	31779
80078-01-05-05	2004-01-30	7411
80078-01-05-00	2004-01-30	16173

contamination due that source, we entirely ignored those data.

2.2.1 Pulse Timing Analysis and Timing Solution

During whole analysis the standard PCA analysis tools 'FTOOLS' version 6.3 software commands were used. For timing analysis, all lightcurves (3-20 keV with 0.035s) were generated with the photon arrival times from Good Xenon data and for the background lightcurves the background estimator models from the RXTE team were used, which is based on the rate of very large events (VLE), detector activation, and cosmic X−ray background. Finally, the background lightcurves were subtracted from the source light curve obtained from the event data 'lcmath'. Then background subtracted lightcurves were corrected to the barycenter of the solar system.

From the long archival data, pulse periods were found by folding the time series on trial periods ([109]). Master pulses were generated from these long observations by folding the data on the period which had the greatest power in the periodogram. Pulse arrival times were found by cross-correlating the pulse profiles obtained from $\sim$ 200s long segments with constructed master pulses. Both the master and independent sample pulse profiles consisted of 20 phase bins. Cross-correlation was performed by using the Fourier harmonic representation of pulses ([47]). If master pulse and sample pulse are shown with g(ϕ) and f(ϕ), we can define the Fourier series as;

$$g(\phi) = (G_o) + \sum_{k=1}^{m} (G_k cosk(\phi - \phi_k)) \tag{2.1}$$

$$f(\phi) = (F_o) + \sum_{k=1}^{m} (F_k cosk(\phi - \phi_k + \Delta\phi_k)) \tag{2.2}$$

with harmonic number m. Between the sample and master pulse, the pulse phase offset is shown as $\delta\phi$ and it is used during the estimation of pulse frequency derivatives.

As a timing solution of SMC X-1, initially we found pulse arrival times obtained from a series of observations with a time span of $\sim$ 6 days around MJD 50324.7. These pulse arrival times can be fitted to an expression to obtain timing solution ([46]).

$$\nu = (\nu_o) + \dot{\nu}(t - t_0) + \frac{1}{2}\ddot{\nu}(t - (t_0))^2 + \frac{2\pi(\nu_0)}{P_{orbit}} x(cos(l) + ecos(w)cos(2l) + esin(w)sin(2l)) \tag{2.3}$$

where e is the eccentricity, w is the longitude of periastron, t_0 is the mid-time of the observation, (ν_0)is the pulse frequency at (t_0), $\ddot{\nu}$ and $\ddot{\nu}$ are the first and second time derivative of

the pulse frequency, $l = 2\pi(t - T_{\pi/2})/P_{orbit} + \pi/2$ is the mean orbital longitude at t; $T_{\pi/2}$ is the epoch when the mean orbital longitude is equal to 90 °; P_{orbit} is the orbital period of the system, $x = a/csin(i)$ is the light traveltime for the projected semimajor axis (where i is the inclination angle between the line of sight and the orbital angular momentum vector), and P_{orbit} is the orbital period.

We firstly assumed a circular orbit (e=0) and therefore this expression became,

$$\delta t = \frac{\delta P}{P}(t - t_0) + \frac{1}{2}\frac{\dot{P}}{P}(t - t_0)^2 + xcos(l). \tag{2.4}$$

Also in order to improve the fit, we used the whole expression since it contains terms corresponding to an eccentric orbit

The periodic trend of the pulse arrival times yields an eccentric orbit (e=0.00089(6)) with an orbital period of 3.89220909(4) days (numbers in parenthesis denote 1σ uncertainties in the least significant figures hereafter).

Table 2.3 presents the timing solution of SMC X-1. Figure 2.2 presents the pulse arrival times from the observations with a time span of about 6 days around 30 August 1996 after the removal of the quadratic trend (or intrinsic -$\dot{P}$) together with the residuals of circular (e=0) and eccentric orbit models respectively.

In Table 2.2, we present the orbital epoch ($T_{\pi/2}$) measurements from different observatories and orbital cycle number (N). In Figure 2.3, we present observed minus calculated values of orbital epochs ($T_{\pi/2} - n < P_{orbit} > - < T_{\pi/2} - n < P_{orbit} >>$) relative to the constant orbital period ($< P_{orbit} >$= 3.892188 days). It should be noted that the last point indicated as ”RXTE Point” is our result and other points were already published before (see Figure 7 in [195]). A quadratic fit to the epochs from all experiments yielded an estimate of the rate of period change $\dot{P}_{orb}/P_{orb} = -3.402(7) \times 10^{-6}$ yr^{-1}.

2.2.2 Pulse Period History and Change of Rate

Beginning from the first detection of the pulse, all pulse history of the source is listed in Table 2.4.

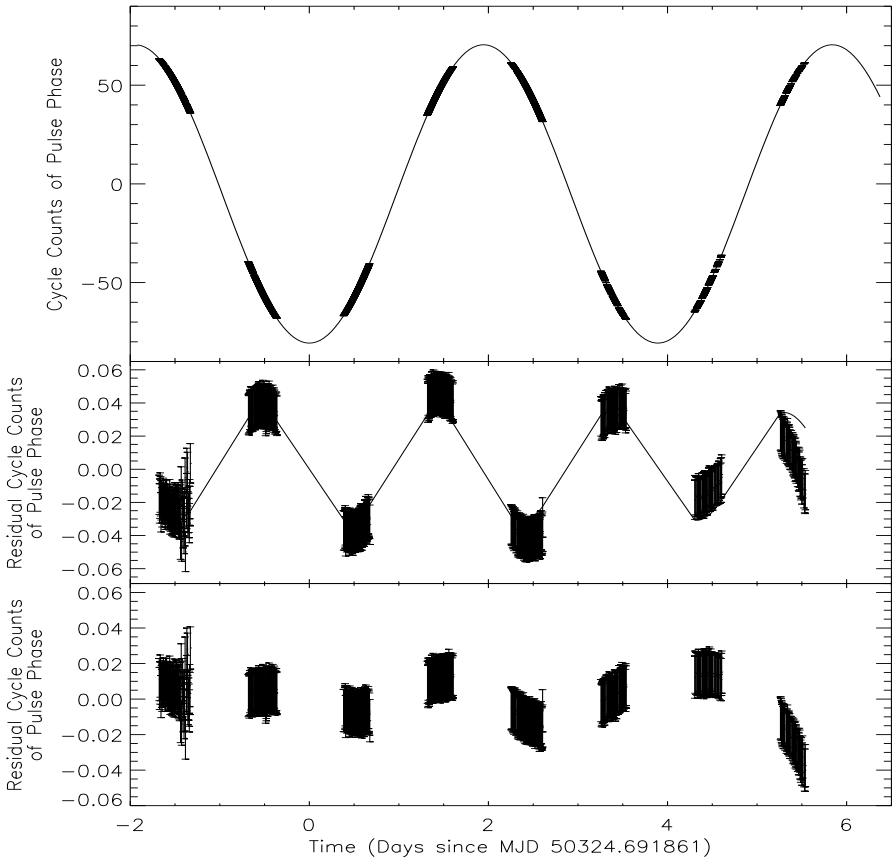

Figure 2.2: Arrival times (pulsation cycles) (top panel), and residuals after fitting arrival times to a circular (middle panel) and elliptical orbital model (lower panel)

Table 2.2: Orbital Epoch Measurements of SMC X-1

$T_{\pi/2}$ (MJD)	N	Observatory	Reference
40963.99(2)	-481	Uhuru	[195],[163]
42275.65(4)	-144	Copernicus	[195],[177]
42836.1828(2)	0	SAS 3	[195],[151]
42999.6567(16)	42	Ariel V	[195],[44]
43116.4448(22)	72	Cos B	[195],[24]
46942.47237(15)	1055	Ginga	[195],[110]
47401.744476(7)	1173	Ginga	[195],[110]
47740.35906(3)	1260	Ginga	[195],[110]
48534.34786(35)	1464	ROSAT	[195]
49102.59109(82)	1610	ASCA	[195]
49137.61911(50)	1619	ROSAT	[195]
50091.170(63)	1864	RXTE	[195]
50324.691861(8)	1924	RXTE	[82]

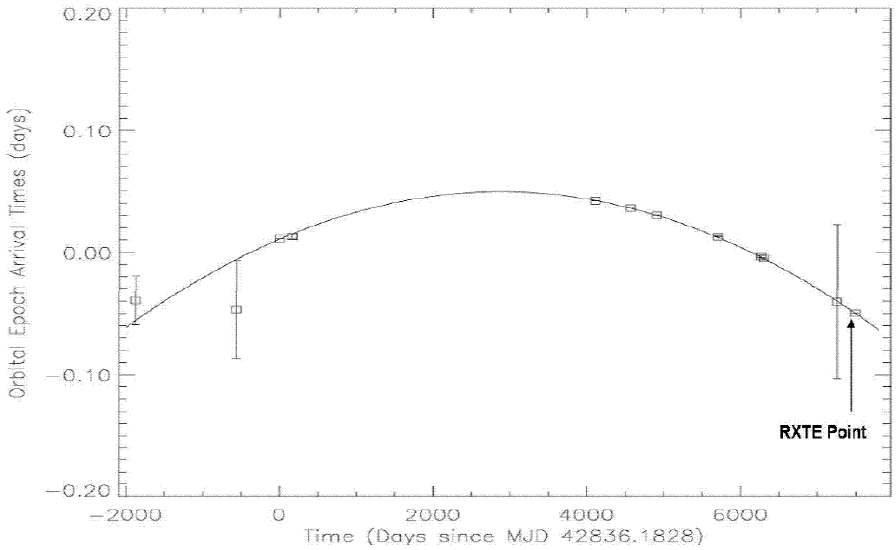

Figure 2.3: Orbital Epoch Arrival Times SMC X-1

Table 2.3: Timing Solution of SMC X-1

Parameters	Model (This Work)
Timing Epoch (MJD)	50326.62356961(9)
ν (Hz)	1.413630801(4)
$\dot{\nu}$ (10^{-11} Hz.s^{-}1)	3.279(5)
Orbital Period (days)	3.89220909(4)
a/c sin I (lt-s)	53.4876(9)
Orbital Epoch	MJD 50324.691861(8)
$\dot{P_{orbit}}/P_{orbit}$ (10^{-6} yr^{-1})	-3.402(7)
Eccentricity	0.00089(6)
w (longitude of periastron)	166(12)

Table 2.4: Pulse Period History with several and RXTE observations of SMC X-1

Proposal ID or Observatory	MJD (days)	Pulse Period[1]	References
Uhuru	41114.200	0.71748(26)	[73]
Aerobee	41999.600	0.7164(2)	[196]
Apollo-Soyuz	42613.799	0.7152(4)	[73]
SAS 3	42836.183	0.71488585(4)	[195]
Ariel V	42999.6567	0.7147337(12)	[195]
Einstein	43985.907	0.713684(32)	[195]
EXOSAT	45998.500	0.7116079958(4)	[103]
Ginga	46942.4724	0.710592116(36)	[110]
HEXE	47399.500	0.7101362(15)	[103]
Ginga	47401.744	0.710140670(15)	[110]
HEXE	47451.500	0.7100978(15)	[103]
HEXE	47591.000	0.7099636(15)	[103]
Ginga	47740.3591	0.709809901(32)	[110]
ROSAT 1	48534.3479	0.70911393(34)	[195]
ROSAT 2	48892.4191	0.7088166(6)	[195]
ASCA	49102.5911	0.7086390(9)	[195]
ROSAT 3	49137.6191	0.7085992(5)	[195]
ROSAT	50054.000	0.70769(6)	[91]
RXTE	50091.170	0.70767330(8)	[195]
00011	50093.048	0.70767394(66)	This work
00011	50093.115	0.70767392(196)	This work
00011	50093.181	0.70767470(68)	This work
10139	50323.016	0.707405055(75)	This work
10139	50323.349	0.70740810(262)	This work
10139	50324.010	0.7074006241(380)	This work
10139	50325.069	0.70739917(17)	This work
10139	50326.009	0.707400173(32)	This work
10139	50327.268	0.7073979(9)	This work
10139	50327.941	0.707395126(32)	This work
10139	50328.993	0.707393636(32)	This work
10139	50329.940	0.707395151(32)	This work
20146-20109-20417	50411.87	0.7073020(85)	This work
20146-20109-20417	50442.90	0.7072548(78)	This work
BeppoSAX-1	50460.900	0.7072282(81)	[139]

[1] errors indicated in the parenthesis gives the value for each pulse period in 1σ

Table 2.4: continued

Proposal ID or Observatory	MJD (days)	Pulse Period[1]	References
20146-20109-20417	50489.366	0.7072005(7)	This work
20146-20109-20417	50504.524	0.7071852(78)	This work
20146-20109-20417	50505.169	0.7071842(9)	This work
BeppoSAX-2	50507.600	0.7071801(44)	[139]
20146-20109-20417	50531.806	0.7071487(48)	This work
20146-20109-20417	50535.679	0.7071436(7)	This work
20146-20109-20417	50551.398	0.7071241(5)	This work
20146-20109-20417	50556.346	0.7071237(75)	This work
BeppoSAX-3	50562.100	0.7071144(71)	[139]
20146-20109-20417	50566.861	0.7070982(45)	This work
20146-20109-20417	50579.511	0.7070880(81)	This work
20146-20109-20417	50583.009	0.70708425(26)	This work
20146-20109-20417	50583.030	0.7070837(7)	This work
ROSAT	50593.799	0.707065(10)	[91]
20146-20109-20417	50597.960	0.70706039(104)	This work
20146-20109-20417	50598.980	0.7070606(7)	This work
20146-20109-20417	50609.319	0.70704348(251)	This work
20146-20109-20417	50617.757	0.7070436(48)	This work
20146-20109-20417	50617.898	0.7070466(260)	This work
20146-20109-20417	50646.787	0.7070038(36)	This work
20146-20109-20417	50675.866	0.7069694(64)	This work
20146-20109-20417	50711.833	0.706929(10)	This work
20146-20109-20417	50738.053	0.7068983(51)	This work
20146-20109-20417	50767.442	0.7068606(52)	This work
20146-20109-20417	50795.116	0.706829(36)	This work
30125	50850.541	0.70676817(232)	This work
30125	50883.272	0.70672955(1109)	This work
ROSAT	50898.200	0.706707(10)	[91]
30125	50910.965	0.70669418(10937)	This work
30125	50949.407	0.70665576(277)	This work
30125	50949.751	0.70665243(2774)	This work
30125	50950.048	0.70664981(547)	This work
30125	51007.374	0.70659188(3077)	This work
30125	51007.975	0.70659264(349)	This work
30125	51060.725	0.70652581(2701)	This work
30125	51060.791	0.70652477(2014)	This work
30125	51061.265	0.70652606(906)	This work

[1] errors indicated in the parenthesis gives the value for each pulse period in 1σ

Table 2.4: continued

Proposal ID or Observatory	MJD (days)	Pulse Period[1]	References
30090-30125	51102.221	0.70647607(4241)	This work
30090-30125	51106.083	0.70647259(1141)	This work
30090-30125	51108.060	0.70649826(889)	This work
30090-30125	51109.781	0.70650057(1347)	This work
30090-30125	51111.866	0.70649266(1107)	This work
30090-30125	51113.711	0.70649280(203)	This work
30090-30125	51115.709	0.70649099(284)	This work
30090-30125	51117.607	0.70648863(994)	This work
30090-30125	51119.586	0.70648654(184)	This work
30090-30125	51121.160	0.70645975(119)	This work
30090-30125	51121.515	0.70645783(67)	This work
30090-30125	51121.637	0.70645430(5328)	This work
30090-30125	51121.724	0.70645748(1928)	This work
30090-30125	51125.443	0.70645499(3264)	This work
30090-30125	51127.234	0.70645028(823)	This work
30090-30125	51129.376	0.70644772(4891)	This work
30090-30125	51131.300	0.70644694(2665)	This work
30090-30125	51133.301	0.70644117(2888)	This work
30090-30125	51151.014	0.70641806(1399)	This work
30090-30125	51151.416	0.70642326(1310)	This work
40064	51699.405	0.70580792(436)	This work
40064	51699.666	0.70580405(462)	This work
40064	51699.736	0.70580918(1612)	This work
40064	51699.876	0.70580980(776)	This work
40064	51700.172	0.70581109(2972)	This work
40064	51700.233	0.70581164(100)	This work
40064	51700.383	0.70581162(999)	This work
40064	51700.593	0.70581175(473)	This work
40064	51700.663	0.70581144(235)	This work
40064	51700.803	0.70581082(689)	This work
40064	51700.896	0.70581221(2831)	This work
40064	51701.152	0.70580888(2225)	This work
40064	51701.315	0.70580732(169)	This work
40064	51701.590	0.70580527(6630)	This work
40064	51701.660	0.70580609(2154)	This work
40064	51701.869	0.70580514(1653)	This work
40064	51701.957	0.70580507(13)	This work

[1] errors indicated in the parenthesis gives the value for each pulse period in 1σ

Table 2.4: continued

Proposal ID or Observatory	MJD (days)	Pulse Period[1]	References
Chandra	51833.808	0.7057147(3)	[183]
INTEGRAL	52843	0.704596(8)	[123]
80078	52939.611	0.70448827(245)	This work
80078	52939.680	0.70448753(281)	This work
80078	52939.749	0.70448789(94)	This work
80078	52940.527	0.70448689(249)	This work
80078	52940.596	0.70448703(1693)	This work
80078	52940.665	0.70448733(1584)	This work
80078	52940.734	0.70448721(76)	This work
80078	52940.805	0.70448768(150)	This work
80078	52940.958	0.70448832(660)	This work
80078	52941.304	0.70448935(2475)	This work
80078	52941.373	0.70449072(1878)	This work
80078	52941.442	0.70449134(1798)	This work
80078	52941.511	0.70449152(550)	This work
80078	52941.813	0.70449323(196)	This work
80078	52942.289	0.70449226(116)	This work
80078	52942.565	0.70449009(166)	This work
80078	52942.652	0.70448883(377)	This work
80078	52942.825	0.70448836(13891)	This work
80078	52942.891	0.70448819(17390)	This work
80078	52943.688	0.70448299(288)	This work
80078	52981.226	0.70444990(19572)	This work
80078	52981.527	0.70444757(6242)	This work
80078	52982.064	0.70443464(505)	This work
80078	52983.496	0.70443455(1715)	This work
80078	52984.033	0.70443753(289)	This work
80078	52984.360	0.70443871(2235)	This work
80078	52984.480	0.70444011(1763)	This work
80078	52984.687	0.70444081(604)	This work
80078	52984.890	0.70444066(780)	This work
80078	52985.326	0.70443804(370)	This work
80078	52986.311	0.70443088(1216)	This work
80078	52987.433	0.70443021(1912)	This work
80078	52987.640	0.70443111(2148)	This work

[1] errors indicated in the parenthesis gives the value for each pulse period in 1σ

We investigated the spin-up variability between MJD 40000 and 53000. We see that the source continues to showing spin-up behaviour as defined previously. But,the source does not show a constant spin-up rate. Between MJD 40000 and 43500, the source is in spin-up with a rate of $(0.93237\pm0.00030)\times 10^{-6}$ s.s^{-1} during this duration. Between 43500 and 47400, the spin-up

rate becomes (1.076157±0.000007)×10^{-6} s.s^{-1}, raising in the spinning up. But later again a decreasing in spinning up with rate value of (0.95531845±0.00000154)× 10^{-6} s.s^{-1} between 47400 and 49200 has been seen.

During the spin period history, we investigate the 'RXTE Observations' zone (between MJD 50093.048 and 52987.640, each having $\sim$ 1 – 2ksec exposure). we roughly obtained pulse periods using the periodogram and then refined these periods by the use of a linear fit to the arrival times. Errors were estimated using the scattering of arrival time values (i.e. errors were related to the errors of the linear coefficient of the fit). These periods were corrected for the binary motion of the pulsar using the orbital parameters listed in Table 2.3. The spin period variation does not have any relation according to the flux variation. Spin rate is (1.1450525±0.0000475)× 10^{-6} s.s^{-1} between MJD 50000 and 53000, we see an increasing in again spining-up of the source. Figure 2.4 shows also the whole pulse period history of the source, and it is evident that the source spins up continuosly between MJD $\sim$ 40000 and MJD $\sim$ 53000 with a varying spin-up rate.

2.2.3 Power Spectra and QPO Features

Power spectra are obtained in two energy ranges. We searched the powerlaw indexes of these spectra seperately at both low and high frequencies in 3.2-21.0 keV, whereas only one power-law index in between 2.0-3.2 keV is derived. The general trend for powerlaw index is constant even though flux varitation, which means that power spectra are stable. Significantly, accretion geometry is almost same. Also some features has been apeared in those power spectra. During analysis, features were seen considerably in some cases as a bump and sometimes as an insignificant peak at $\sim$ 0.05, 0.06 Hz. These features have appeared at any energy range discussed above.

2.3 Spectral Analysis

We used the same data set that we used for timing study. The process was also same for X-ray spectral analysis. For spectral analysis the Standard 2 data were used. Spectrum, background and response matrix files were created using again ftools analysis software. We used background subtracted spectra in our analysis. The background files were created by

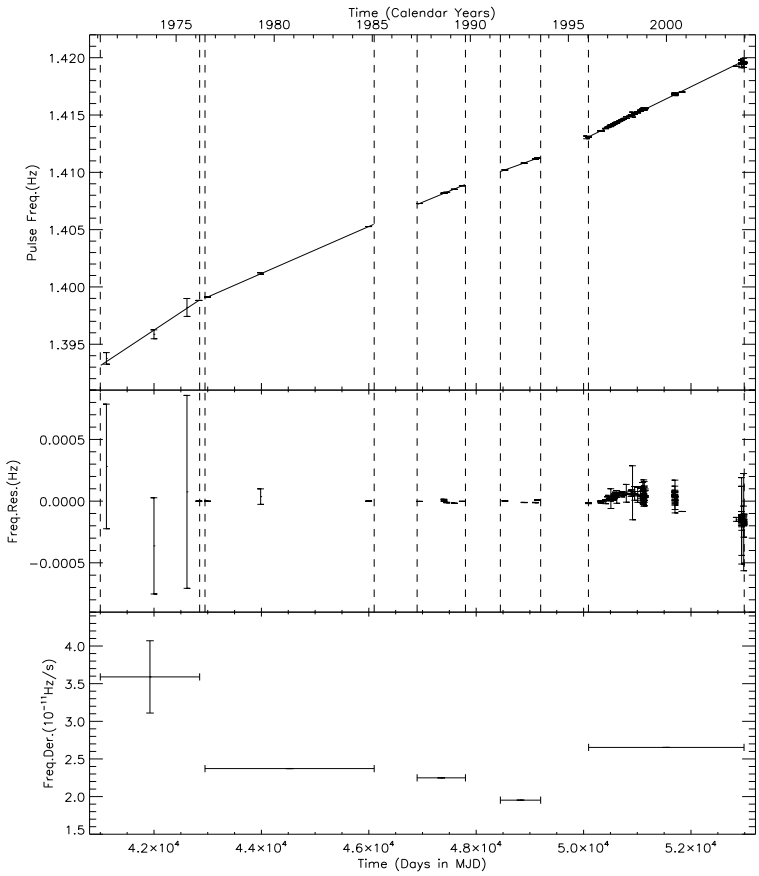

Figure 2.4: Top panel and middle panel. Pulse frequency history and residuals of SMC X-1 after a linear fit obtained from 5 different intervals listed in Table 2.4. bottom panel. Frequency derivative history. Dashed lines in top and middle panels and horizontal error bars in the bottom panel indicate time intervals in which linear fits were performed. The last (rightmost) interval almost consists of pulse frequency values obtained from our analysis.

'pcabackest'. Energy channels corresponding to the 3-25 keV energy range were used to fit the spectra. We ignored photon energies lower than 3 keV and higher than 20 keV and 1% systematic error was added to the errors.

We fitted X-ray spectra with two models by using XSPEC11 spectral package. We used a power law model with a high energy cutoff and a gaussian component is fixed again to 6.7 keV([3]). Also we tried a model by adding a partial covering absorption factor as done in XMM data of this source by Neilsen et al. 2004([140]), but the model did not improve the fit.

For best fit parameters of the spectral model for two different regions corresponding to differ-

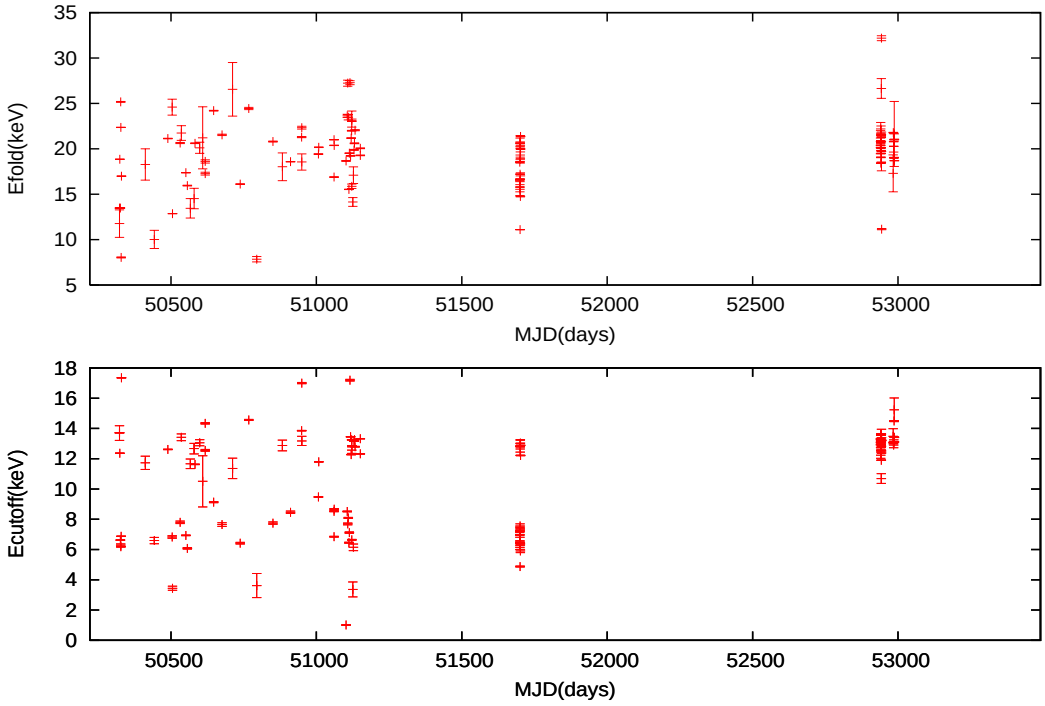

Figure 2.5: High energy cut-off and folding energy trend of SMC X-1 between MJD 50093 and 53000

ent flux values of the system during pulsating can be identified in Table 2.5.

In general, we found that power law index, high energy cut-off and e-fold energy values were almost constant, the ranges between respectively ~ 0.831±0.107 and 1.670±0.110, 5.90 and 14.56, lastly 7.84 and 32.19 For high energy cutt-off and folding energy ranges see Figure 2.5.

Table 2.5: Spectra parameters from Two Different Region

Obs ID	10139-01-01-00	20146-06-02-00
MJD	50323.349	50442.905
nH($10^{22} cm^{-2}$)	12.039±0.748	2.214±0.290
Powerlaw Index	1.184±0.043	1.176±0.074
E_{cutoff}(keV)	13.697±3.424	6.595±1.649
E_{fold} (keV)	11.765±4.118	10.020±3.507
(χ^2_ν) (degrees of freedom)	0.868(47)	1.055(47)
Obserbed flux (10^{-10} ergs cm^{-2} s^{-1})(3-25 keV)	$2.3866^{+0.0282}_{-0.102}$	$20.673^{+0.043}_{-0.157}$
Unabsorbed flux (10^{-10} ergs cm^{-2} s^{-1})(3-25 keV)	$2.8281^{+0.002}_{-0.012}$	$21.553^{+0.039}_{-0.078}$

The hydrogen column density shows decrease in low fluxes between the energy range of 3.0 and 25.0 keV, the range is between 2.005± 0.087 and 21.11±1.86. Nearly after flux of 5 × 10^{-10} ergs cm^{-2} s^{-1} also nH value goes constantly. In (Figure 2.6), we showed the photon index and hydrogen column density behaviours according to time. Then we showed in Figure 2.7 that photon index and hydrogen column density variations make sense for us according to flux (3-25 keV) variations. However, we did not see such variation in cut-off and folding energies in accordance to flux.

2.4 Discussion

By analysing of the all RXTE observations archive data, the trend of spin period show that the neutron star spins up for 30 years, with different spin-up rates. According to RXTE observations duration, source's spin-up rate shows increasing within %20 according to previous spin-up behavior. For RXTE observations duration $\dot{P}_{pulse}/P_{pulse}$=(1.61805096±0.00006863)×10^{-6} s^{-1}.

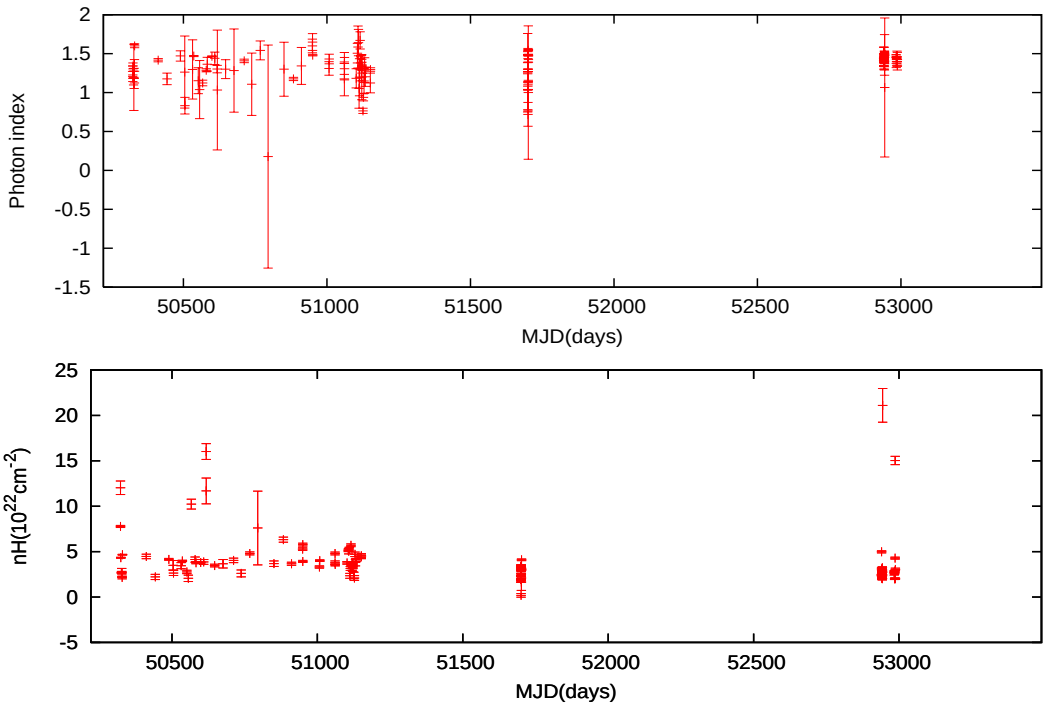

Figure 2.6: Photon index and nH trend of SMC X-1 between MJD 50093 and 53000

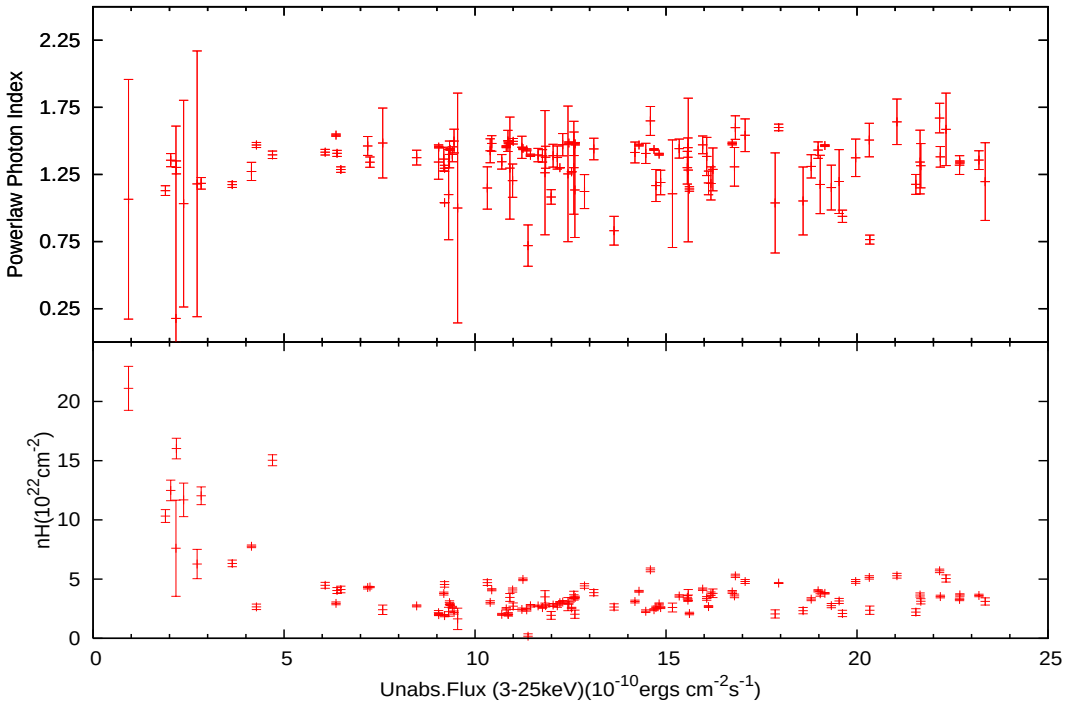

Figure 2.7: Photon index and nH trend of SMC X-1

We can express the spin-up rate of a source with a persistent accretion as

$$\dot{\nu} \simeq 2.2 \times 10^{-12} \mu_{30}^{2/7} m_x^{-3/7} R_6^{6/7} I_{45}^{-1} L_{37}^{6/7} \mathrm{Hz\,s^{-1}}, \tag{2.5}$$

where $\dot{\nu}$ is first time derivative of the spin frequency, μ_{30} is the magnetic moment of the neutron star in units of 10^{30} Gauss cm^3, m_x is the mass of the neutron star in units of solar mass, R_6 is the radius of the neutron star in units of cm, I_{45} is the moment of inertia of the neutron star in terms of 10^{45} g cm^2, and L_{37} is the luminosity of the neutron star in units of 10^{37} erg s^{-1} ([67]). Using a distance value of 61 kpc ([95]) and a flux of 1.2×10^{-9} ergs cm^{-2} s^{-1}, luminosity of SMC X-1 is $\sim 5.5 \times 10^{38}$ erg s^{-1}. Assuming magnetic moment of 10^{30} Gauss cm^3, mass of $1.4 M_\odot$, radius of 10^6 cm, moment of inertia of 10^{45} g cm^2, we find $\dot{\nu}$ to be $\sim 5.9 \times 10^{-11}$ Hz s^{-1}. This value is compatible within the order of the observed spin-up rate value of the source.

Figure 2.3 explicitly shows that the eccentric orbit model is a better fit compared to the circular orbital model. From the timing solution of the source the binary orbit has an eccentricity

of 0.00089(6). Previous studies gave a circular orbit solution ([195]) and an upper limit of 0.00004([110]) for eccentricity for this source. Our present value is more than 20 times greater than the upper limit found by Levine et al. 1993([110]). We believe that our value will be important for future studies.

From timing analysis, we obtained a new orbital epoch of SMC X-1 from RXTE observations. Using this new epoch and previous results ([195]), we found that there is an orbital decay with $P_{orbit}^{\cdot}/P_{orbit}$ of $-3.402(7)\times10^{-6}$ yr^{-1} which is similar to the values founded by previous studies ([195]),[110]). Levine et al. 1993([110]) proposed that the major cause of change in the orbital period is tidal interactions as for the case in Cen X-3 ([96]), and LMC X-4 ([111]). SMC X-1 is unlike Her X-1 for which the mass accretion were thought to be primarily related to the orbital period decay ([49]).

From the spectral analysis, we found that all of the spectral parameters except Hydrogen column density did not vary significantly. Hydrogen column density was found to be higher as X-ray flux gets lower. The same correlation of hydrogen column density and X-ray flux is also observed in Her X-1 ([81]). It may be due the fact that soft absorption becomes stronger whenever there is a partial obscuration of the neutron star due to the X-ray eclipses and warping of the accretion disk. The increase in Hydrogen column density may also be related to the simple absorbed power law model. SMC X-1 has soft excess especially for energies $\lesssim$ 3 keV ([146]). Although we used photon energies greater than 3 keV in our analysis, tail of a soft spectral component may affect low energies in our analysis and as a result we might have interesting changes in energy spectrum as variations in Hydrogen column density parameter.

Hydrogen column density changes just during the low flux values, the hydrogen column density is very high when the flux is low as expected but after some flux value the column density although the flux increases, the density goes constant. The increased soft X-ray pulsation is absorbed due to hydrogen column. Whereas, the other parameters belongs to model do not show any changes according to flux.

CHAPTER 3

4U 1907+09

3.1 Introduction

4U 1907+09 is an accretion powered X-ray pulsar accreting plasma from a blue supergiant companion star. It was discovered as an X-ray source during the Uhuru survey ([63]), it has been observed by using various X-ray observatories as Ariel V ([120]), Tenma ([116]), EXOSAT ([37]), Ginga ([119],[130]), BeppoSAX ([42]), XMPC ([32]), ASCA ([158]), IXAE ([136]) and RXTE ([85],[84],[86],[158],[10],[6]), INTEGRAL ([59]).

Marshall & Ricketts ([120]) determined the binary orbital period to be 8.38d using Ariel V observations. They reported that they found two flares, a primary and a secondary which is respectively occurring near periastron and apastron. Later EXOSAT and RXTE observations ([84],[86]) did clearly show that these flares are locked to orbital phases separated by ~ 0.45 orbital period. The pulsar was founded in an eccentricity of ~0.2 around its companion ([116],[37])

As a discussion the possibility of that the two flares can be caused by an equatorial disc-like envelope (circumstellar disc) around its companion star ([116], [37]). When the neutron star crosses the disc, the mass accretion rate onto the neutron star increases temporarily. We expect to see two peaks while the neutron star passes twice through the circumstellar disc of the companion star in every cycle. We also expect a transient accretion disc formation around the neutron star while the neutron star passes through this circumstellar disc. For the formation of the circumstellar disc around the companion star, the companion must most likely be a Be type star.

The first identification on companion star was done as highly reddened star ([167]). But it

was also discussed as an O or B type supergiant due to the presence of strong and broad Hα emission. The optical companion of 4U 1907+09 is determined as an O8/O9 supergiant with a dense stellar wind with the recent optical studies ([41]) also the discussion on these two flares by using equatorial disc-like envelope idea make the result as Be type companion star. Using Tenma observations, Makishima et al. 1984([116]) also found the pulse period of the source to be 437.5 sec.

The timing measurements and studies from EXOSAT ([37]) and RXTE observations ([84],[86], [10]) showed continuous spin-down trend of the neutron star. The spinning down rate almost founded as $\dot{\nu} = (-3.54 \pm 0.02) \times 10^{-14} Hzs^{-1}$ for more than 15 years ([10]).

3.2 Observations and Analysis

The Proportional Counter Array (PCA)([87]) on board the RXTE consists of five identical proportional counter units (PCUs) coaligned to the same point in the sky, with a total effective area of approximately 6250 cm^2, and a field of view of $\sim 1^0$ FWHM, operating in the 2-60 keV energy range. The number of active PCUs is varied between one and five during the observations. Observations after 2000 May 13 the background level for one of the PCUs (PCU0) increased so for these observations in the analysis PCU0 were ignored.

3.2.1 Timing Analysis

This study includes the results of timing and spectral studies of this pulsar by using archival RXTE-PCA observations which is listed as (Table 3.1). In order to obtain background sub-

Table 3.1: Observation list for 4U 1907+09

Time of Observation start end dd mm yyyy dd mm yyyy	XTE Prop. ID	Number of Observations
17 02 1996-23 02 1996	10155	8
25 11 1996-14 12 1997	10154-20146	24
26 07 1998-01 10 1998	30093	14
10 03 2001-06 03 2002	60061	38

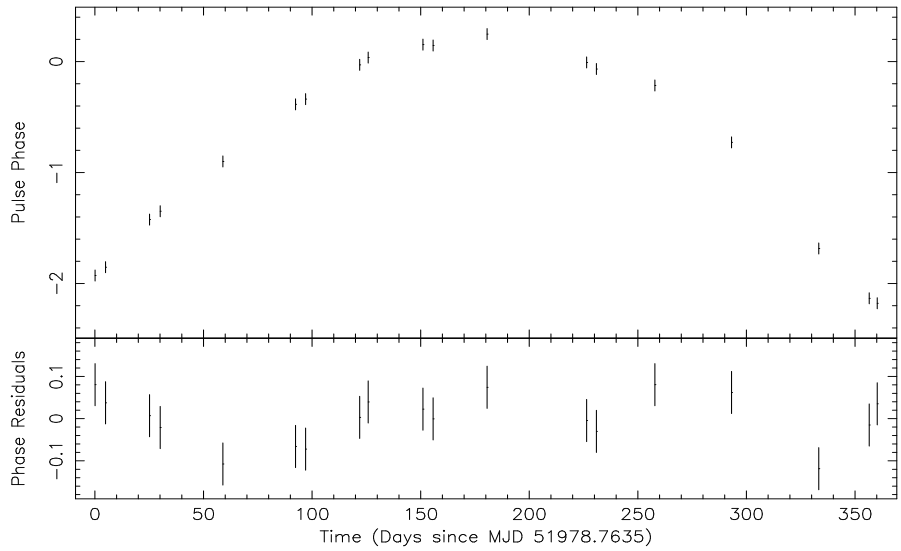

Figure 3.1: Pulse phase and its residuals fitted to the orbital model presented in (Table 3.2)

tracted light curves, we generated the background using the background estimator models based on the rate of very large solar events, spacecraft activation and cosmic X-ray emission with the standard PCA analysis tools. Then we subtracted background light curves from the source light curves obtained from the event data. The background subtracted light curves were also corrected to the barycenter of the solar system and to the binary orbital motion of 4U 1907+09 around its companion. For the correction of binary orbital motion, we used the orbital parameters deduced by In 't Zand, Baykal & Strohmayer et al. 1998([85]).

For timing analysis we fold the light curve outside the intensity dips from long data string around 7-10 ksec on statistically independent trial periods ([109]). As described in previous chapter, we get pulse phases obtained from cross correlation analysis and are presented Figure 3.1.

To estimate pulse frequency derivatives, again the pulse phases calculated from the cross-correlation analysis are fitted to the quadratic polynomial

$$\delta\phi = \phi_o + \delta\nu(t - t_o) + \frac{1}{2}\dot{\nu}(t - t_o)^2 \tag{3.1}$$

which is called second-order Taylor expansion. where $\delta\phi$ is the pulse phase offset deduced from the pulse timing analysis, t_o is the mid-time of the observation, ϕ_o is the phase offset at t_o, $\delta\nu$ is the deviation from the mean pulse frequency (or additive correction to the pulse

frequency), and $\dot{\nu}$ is the pulse frequency derivative of the source.

The pulse frequency derivative from the sequence of 19 pulse phases spread over 360 days was measured as $\dot{\nu} = (-1.887 \pm 0.042) \times 10^{-14}$ Hz s^{-1}. This value approximately ~ 0.60 times lower then previous measurements of pulse frequency derivatives which was measured over 383 days times span ([10]). In this and the previous observations ([10]) time span of the observations are similar ($\sim$ over year) and both observations have low timing noise. However the spin-down rate is lowered by a factor of 0.6 times in latter observations.

In order to see the spin-down trends clearly we estimate the pulse frequency histories by taking the derivatives of each pairs of pulse phases from the pulse phases of this work and previous work([10]) and presented in Table 3.3 and Figure 3.2 along with previous frequency measurements.

From timing analysis This source shows transient oscillations as a result of timing analysis of RXTE ([85]) and IXAE ([136]) observations with periods of about 18.2s and 14.4s. These transient oscillations during flaring activities shows the formation of a transient accretion disk. Due to spin-down trend, it may be suggested to be related to the presence of a transient retrograde accretion disc.

In this work, the whole dataset of 4U 1907+09 was also analyzed for possible detection of

Table 3.2: Timing solution of 4U 1907+09

$T_{\pi/2}$ (Orbital Epoch) (MJD)	50134.76 ∓ 0.06 [b]
$P_{orb}(d)$	8.3753 ∓ 0.0001 [b]
$a_x$sin i (lt s)	83 ∓ 2 [b]
e	0.28 ∓ 0.04 [b]
w	330 ∓ 7 [b]
t_0 (MJD) [c]	52154.6183 ∓ 0.0005
Pulse Period (s)	441.0932 ∓ 0.0003
Pulse Period derivative (s $s^{-}1$)	$(3.653 \mp 0.081) \times 10^{-9}$
Pulse freq. derivative (Hz $s^{-}1$)	$(-1.887 \mp 0.042) \times 10^{-14}$

[a] Confidence intervals are quoted at 1σ level.
[b] Orbital parameters are taken from [85]. P_{orb}=orbital period, $a_x$sin i=projected semimajor axis, e=eccentricity, w=longitude of periastron.
[c] Mid-time of the observation used in pulse timing.

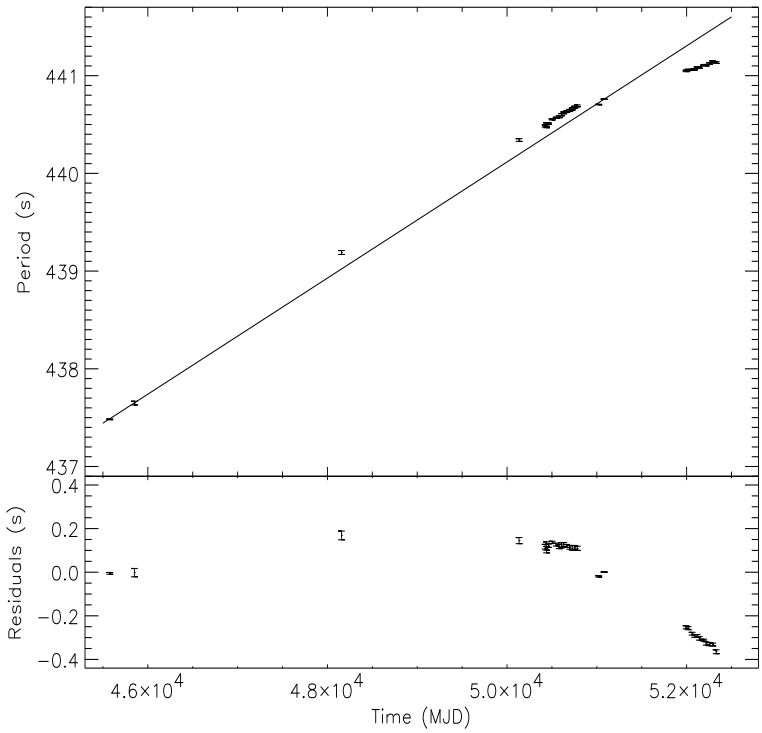

Figure 3.2: Plot of pulse period history. Solid line and the residuals correspond to the previous spin-down rate found by Baykal et al. 2001([10]).

any transient oscillations around $\sim 14 - 18$s, similar to those reported from previous RXTE ([85]) and IXAE ([136]) observations. "In the power spectra of 3-25 keV RXTE-PCA light curve, we searched for transient oscillations around ~ 0.06 Hz in the 0.50s binned ~ 170 light curve segments of length of 512s. In order to test the significance of these oscillations, we used the approach of [181]. As the result of this search, we found only 3 512s segments in the whole dataset with the transient oscillations of significance exceeding 5σ at MJD $\sim$ 50136, $\sim$ 51079 and $\sim$ 51087. Our results about transient oscillations are marginal, and therefore inconclusive. Future observations may be useful to observe and analyze possible transient oscillations of the source."

3.2.2 Energy Spectrum Analysis

"The complete dataset of 4U 1907+09 were also analyzed to investigate whether there is any significant spectral evolution accompanied with the change in the spin down rate of the pulsar or not. Spectra, background and response matrix files were created using FTOOLS 6.0

data analysis software. Background spectra were generated using the background estimator models based on the rate of very large events, spacecraft activation and cosmic X-ray emission." Spectral analysis and error estimation of the spectral parameters were performed using XSPEC version 11.3.2. We extracted individual 3-25 keV PCA spectra each corresponding to a single pulse period. For these spectra, energies lower than 3 keV were ignored due to uncertainties in background modeling while energies higher than 25 keV were ignored as a result of poor counting statistics. In order to take into account the X-ray background from the

Table 3.3: RXTE pulse period measurements of 4U 1907+09

Epoch (MJD)	Pulse Period (s)	Reference
45576	437.483±0.004	[116]
45850	437.649±0.019	[37]
48156.6	439.19±0.02	[130]
50134	440.341±0.014	[85]
50424.3	440.4854±0.0109	This work
50440.4	440.4877±0.0085	[10]
50460.9	440.5116±0.0075	This work
50502.1	440.5518±0.0053	This work
50547.1	440.5681±0.0064	This work
50581.1	440.5794±0.0097	This work
50606.0	440.6003±0.0115	This work
50631.9	440.6189±0.0089	This work
50665.5	440.6323±0.0069	This work
50699.4	440.6460±0.0087	This work
50726.8	440.6595±0.0105	This work
50754.1	440.6785±0.0088	This work
50782.5	440.6910±0.0097	This work
51021.9	440.7045±0.0032	[10]
51080.9	440.7598±0.0010	[10]
51993.8	441.0484±0.0072	This work
52016.8	441.0583±0.0071	This work
52061.5	441.0595±0.0063	This work
52088.0	441.0650±0.0063	This work
52117.4	441.0821±0.0062	This work
52141.2	441.0853±0.0082	This work
52191.4	441.1067±0.0046	This work
52217.2	441.1072±0.0077	This work
52254.3	441.1259±0.0074	This work
52292.0	441.1468±0.0065	This work
52328.8	441.1353±0.0090	This work

Galactic ridge and the nearby supernova remnant W49B, we followed the approach used by [158] as we extracted overall "dip" state spectra of the source for each of the proposal IDs listed in Table 3.1 and the corresponding background spectra. We found that the count rate and the spectral shape of the dip state spectra were consistent with the models of the diffuse emission from the Galactic ridge ([179]). So, these dip state observations were used as additional background spectra in spectral fits of the source spectrum. These additional background spectra were created by subtracting the corresponding dip state model background spectrum from the dip state source spectrum using "mathpha" FTOOL. A power-law model with low-energy absorption ([133]), multiplied by an exponential high energy cut-off function ([188]) was used to model 3-25 keV spectra of the source. We found no evidence of a statistically significant iron line emission at $\sim$ 6.4 keV which is consistent with the previous RXTE spectral fits ([158]). An additional cyclotron resonance absorption line ([118]) component at $\sim$ 19 keV was required to fit the spectra. The parameters of cyclotron absorption line was found to be consistent with the fundamental cyclotron line parameters found from BeppoSAX observations of the source ([42]). Obtaining the spectral fits, we fixed the cyclotron absorption line energy at 19 keV. The result of the spectral fits as a function of orbital phase were presented in Figure 3.3. In the fig, vertical dashed lines indicate the orbital phase corresponding to periastron passages. Points marked with triangles indicate observations between March 2001 and March 2002 (proposal ID 60061) for which spin-down rate of the source was lower. The dotted lines indicate $\pm\sigma$ from the periastron. Sample model parameters were listed in Table 3.4.

Table 3.4: Sample Spectral Parameters of Individual PCA Observations of 4U 1907+09

Parameter	MJD 50547	MJD 52061
Hydrogen Column Density (10^{22}cm^{-2})	5.51 ∓ 0.50	9.13 ∓ 0.23
Power Law Photon Index	1.20 ∓ 0.04	1.21 ∓ 0.03
Power Law Norm. (10^{-2}.cts.cm^{-2}.s^{-1})	4.04 ∓ 0.09	2.83 ∓ 0.15
Cut-off Energy (keV)	12.9 ∓ 0.2	13.7 ∓ 0.3
E-folding Energy (keV)	7.0 ∓ 0.5	9.6 ∓ 0.5
Cyclotron Depth	0.14 ∓ 0.05	0.20 ∓ 0.02
Cyclotron Energy (keV)	19.0 (fixed)	19.0 (fixed)
Cyclotron Width (keV)	1.12 ∓ 0.10	1.71 ∓ 0.34
3-25 keV Unabsorbed X-ray Flux (10^{-10}ergs.cm^{-2}.s^{-1})	6.36 ∓ 0.14	4.69 ∓ 0.25
Reduced χ^2 (43 d.o.f.)	0.74	0.98

3.3 Discussion

The spin-down rate of 4U 1907+09 obtained in between March 2001 and March 2002 was found to be ~ 0.60 times lower than both the previous RXTE measurements of spin-down rate between November 1996 - December 1997 by ([10]) and the long term spin-down trend of the

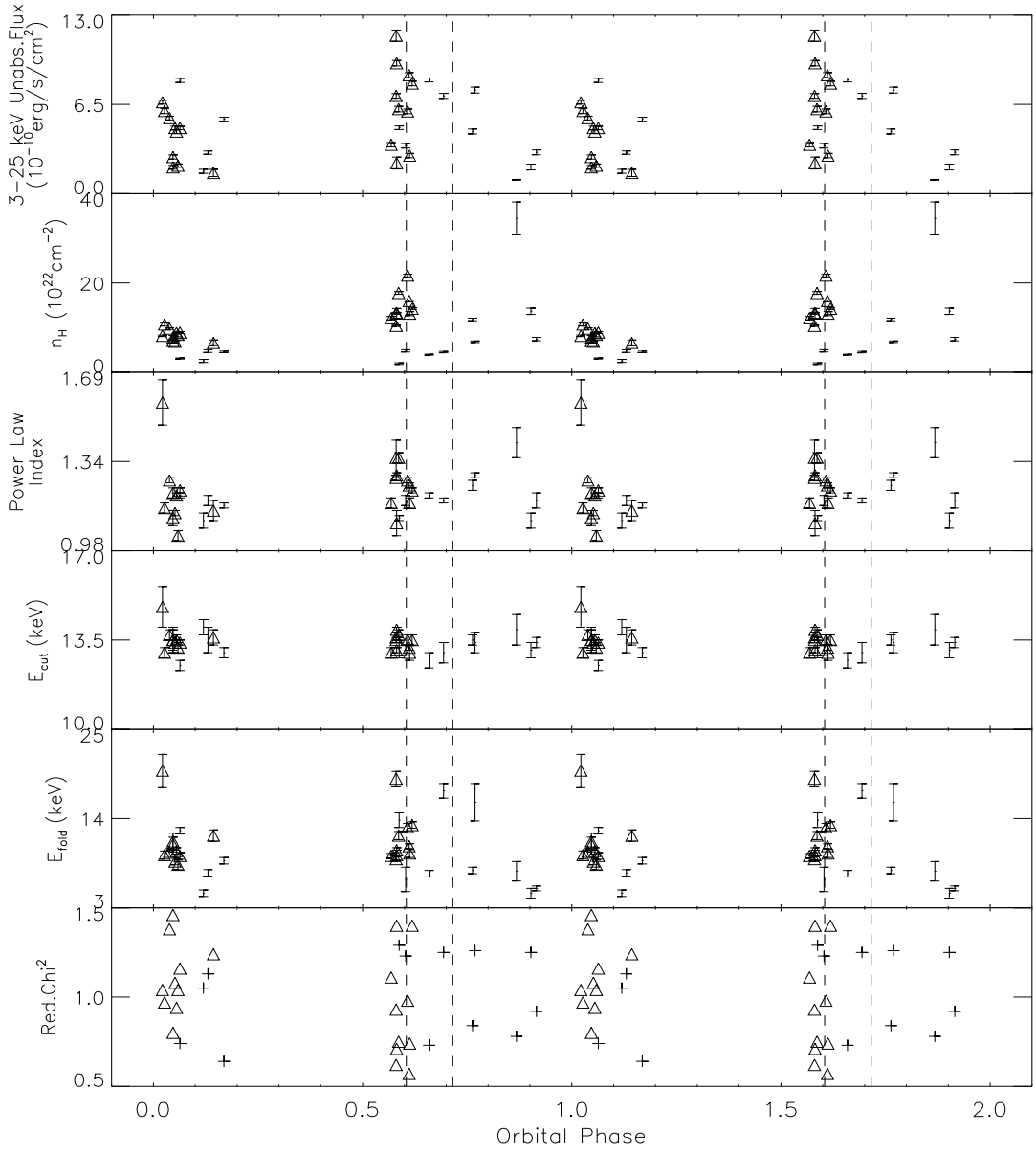

Figure 3.3: Evolution of 3-25 keV unabsorbed flux, Hydrogen column density, power law index, cut-off energy, e-folding energy, and reduced χ^2 in orbital phase.

source in between 1983 and 1997 (See Figure 1 in [10]). In the recent studies and the previous RXTE observations show that time span of the observations were similar ($\sim$ over year) and in both observations posses low timing noise. However, spin down rate is lowered by a factor of 0.6 in the last RXTE observations. It is also interesting to observe that the spin-down rate is consistent with zero around MJD 51000 before this significant change in spin-down rate. Since the discovery of the source, our pulse frequency measurements are significant due to including the first time resolved spin-down rate variations. The steady spin-down rate ([10]) and the presence of transient oscillations ([85],[136]) in 4U 1907+09 support the idea that the source accretes from retrograde transient accretion disc. The possibility of a prograde disc for which the magnetospheric radius should be close to the corotation radius so that the magnetic torque overcomes material torque is not likely to be the case for this system ([85]). If the disc is retrograde and the material torque is dominant, using ([67]) accretion disc model, a decrease in spin-down rate of the neutron star should be a sign of a decrease in the mass accretion rate coming from the accretion disc. If the disc accretion is the only accretion mechanism, this decrease in mass accretion rate should also lead to a decrease in X-ray flux of the system.

From the X-ray spectral analysis of the source, we found no clear evidence of a correlation between 3-25 keV flux and the change in spin-down rate. The flux levels were about the same for latter observations with low spin-down rate compared to the rest of the observations. This was not our expectation if we only consider disc accretion and may be because of the fact that the total mass accretion rate is not only due to only disc accretion, but also accretion from stellar wind may contribute to the total mass accretion rate (see also [158]). In case of accretion from both transient disc and wind, the change in mass accretion rate from the accretion disc might not cause a substantial change in X-ray flux. However, it is important to note that the orbital coverage of the latter (proposal ID 60061) observations is poor and limited to the phase locked flares in orbital phases $\sim$ 0.05 and $\sim$ 0.6. Future observations of the source may be helpful to have a better understanding of a possible relation between spin-down rate and X-ray flux.

Examining spectral parameters plotted in Figure 3.4 especially for flare parts, we also found an evidence of an increase in Hydrogen column density (n_H) for the latter observation with lower spin-down rate. On the other hand, there is no clear evidence of a variation of the other spectral parameters in the flares after the spin-down rate decreased. Change in n_H may be related to a change in the accretion geometry of the source. However, if there had been an

accretion geometry change accompanied with the change in the spin-down rate of the source, we would expect other spectral parameters to vary as well, especially the power law index as in the RXTE observations of SAX J2103.5+4545 ([11]), and 2S 1417-62 ([79]). New X-ray observations of the source will be useful to monitor any possible changes in the spin-down rate and its consequences.

CHAPTER 4

4U 1538-52

4.1 Introduction

4U 1538-52, a high mass X-ray binary pulsar, is an eclipsing system includes B0 I supergiant star QV Nor([144]) and a magnetized neutron star. It was discovered using the Uhuru satellite ([65]). Then Ariel 5 ([44]) and OSO-8 ([15]) also did observe this source and found X-ray pulsation with a period of 529 seconds. OSO-8 observations revealed orbital modulation as 3.7 days and found eclipsing as ~0.51 days.

The BATSE observations of this source permitted long-term monitoring pulse frequency and intensity histories([162]). In the pulse frequency history, Rubin 1997([162]) found short-term pulse frequency changes of either sign, and a power density spectrum of fluctuations of the pulse frequency derivative that is consistent with white torque noise on timescales from 16 to 1600 days.

One of the first eccentricity calculation was done as a result of ~0.082±0.047([39]). From RXTE observations between (MJD 50,449.93 - 50,453.69), Clark 2000([34]) obtained new orbital parameters of the source by using pulse-timing analysis. They did found the binary orbital period as ~3.728 days with an eccentricity of 0.174± 0.015, with a periastron at 64°±9° and orbital decay $\dot{P}_{orb}/P_{orb} = (-2.9 \pm 2.1) \times 10^{-6}$ yr^{-1}.

The system is almost bright in X-ray with an estimated flux of ~(5-20)×$10^{-10} erg^{-1} cm^{-2}$ in the 3-100 keV range([159]). From this measurement, a distance of the source is assumed as ~5.5 kpc ([15],[144]).

In this work, we present new orbital epoch and pulse frequency measurements based on our

analysis of archival RXTE observations of 4U 1538-52.

4.2 Observations and Timing Analysis

The observations of the source occurred in between July 31 and August 7, 2003 (MJD 52851-52858) and with an exposure of $\sim$ 75 ksec. The results presented here are based on PCA[87] data.

Again, we begin with generating our background subtracted light curves and X−ray spectra by using the binned Good Xenon data. For 4U 1538-52, X-ray emission coming from the galactic ridge is only a few percent of the total X-ray emission which should not affect our timing analysis (see [117]), so we did not include an estimation of the galactic ridge emission in our analysis. In Figure 4.1, the background subtracted light curve is presented. Although the number of active PCUs varied from 1 to 4 during the observations, Figure 4.1 shows count rates adjusted as if 5 PCUs had been active using the ”correctlc” tool in HEASOFT 6.

For the timing analysis, again we corrected the light curve to the barycenter of the solar system. We also corrected this barycentered light curve for binary orbital motion using both circular and elliptical orbital models given in Table 4.1 (see also Clark 2000 ([34])).

In order to find the pulse frequency and a new orbital epoch, we again used the cross-correlation technique as we described in Chapter 2. We obtained 12 pulse arrival times through the $\sim$ 2 binary orbits. For the method independent pulse profiles samples were made from each of the 12 independent RXTE observations. We used 10-term unweighted harmonic series to cross-correlate the template pulse profile with the pulse profiles for each RXTE observation. The maximum value of the cross-correlation is analytically well-defined and does not depend on the phase binning of the pulses.

The source 4U 1538-52 has a variable pulse profile which affects the pulse timing. In order to estimate the errors in the arrival times, the light curve of each RXTE observation was divided into approximately 4-5 equal subsets and new arrival times were estimated. The standard deviation of the arrival times obtained from each subset of the observation was taken to be the uncertainty in the arrival time for that observation.

Arrival time delays may arise from the change of the pulse frequency during the observation

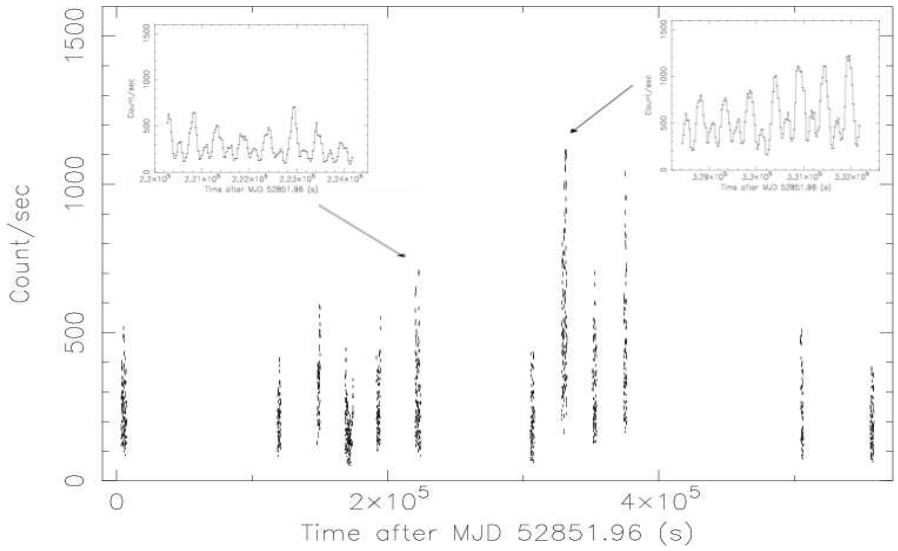

Figure 4.1: 2-30 keV RXTE-PCA light curve of 4U 1538-52 between July 31 and August 7, 2003. Two 26s binned ~ 3ksec samples of this light curve corresponding to single RXTE orbits are presented on the upper left and the upper right.

(or intrinsic pulse frequency derivative) and from the differences between the assumed and actual orbital and pulse parameters ([46]), and used elliptical model Equation 2 in Chapter 2. Corrected values of orbital and pulse parameters $\delta\nu$, $\delta T_{\pi/2}$ and $\dot{\nu}$ were estimated from the fits of above expression to pulse phase residuals. For both orbital and pulse parameters, the result of fits can be seen from Table 4.1.

We also reestimated the orbital epochs by varying the projected orbital radius $(a_x/c)sini$ in the

Table 4.1: Orbital Parameters of 4U 1538-52

Parameter	Elliptical Orbit	Circular Orbit
$T_{\pi/2}$ Orbital Epoch (MJD)	52855.0421±0.025	52855.0441±0.025
a_x sin i (lt-s)[a]	56.6±0.7	54.3±0.6
e[a]	0.174±0.015	
ω[a](deg)	64± 9	
P_{orbit}[a]	3.7228366±0.000032	3.7228366±0.000032
Epoch (MJD)	52855.0585±0.025	52855.0585±0.025
P_{pulse} (s)	526.8551±0.016	526.8535±0.013
$\dot{\nu}$ (Hz s^{-1})	(2.838±4.124)× 10^{-13}	(2.241± 2.764)× 10^{-13}
reduced χ^2	1.44	1.0

[a] Taken from Clark 2000([34])

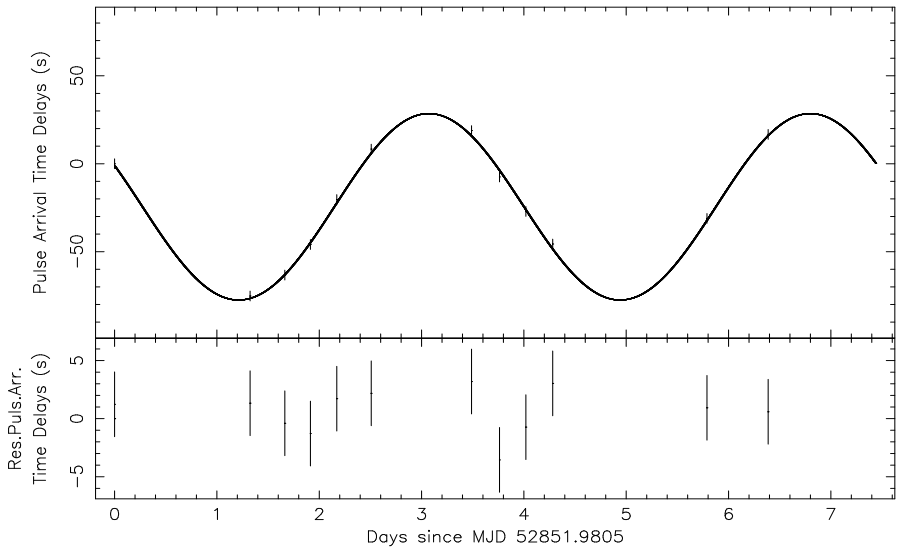

Figure 4.2: Top panel. Pulse arrival time delays and best-fit elliptical orbital model given in Table 4.1. (Note that pulse profiles are obtained with respect to the reference time 52855.0585 MJD). Residuals after removing best orbital model.

range of its uncertainty ($\pm$ 1 σ) and found that the resulting orbital epochs are consistent with the best fit value at the 1σ level. The error in the orbital epoch due to an error in $(a_x/c)\sin i$ may also be expressed ([46]) as

$$\sigma_{T_{\pi/2}} = \frac{P_{orb}\sigma_{(a_x/csini)}}{2\pi a_x/csini} \sim 0.0073 days \tag{4.1}$$

where $\sigma_{a_x/csini}$ is the uncertainty in the projected orbital radius. This value is small relative to our error estimate for the orbital epoch (see Table 4.1). In (Figure 4.2), we present the arrival time delay, the best fit elliptical orbit model, and arrival time residuals. In (Figure 4.3), we display the long-term pulse frequency history of the source.

As seen from Table 4.1, the orbital epochs for circular and elliptical orbital models agree with each other at the 1 σ level. In order to check our technique, we extracted observations of 4U 1538-52 done in 1997 (MJD 50449.93-50453.69) and estimated orbital epochs for those observations. The results agreed with the orbital epochs given by Clark 2000([34]). In Figure 4.4, we present observed minus calculated values of orbital epochs ($T_{\pi/2} - n < P_{orbit} > - < T_{\pi/2} - n < P_{orbit} >>$) relative to the constant orbital period ($< P_{orbit} >= 3.7228366$ days). A quadratic fit to the epochs from all experiments yielded an estimate of the rate of period change $\dot{P}_{orb}/P_{orb} = (0.4 \pm 1.8) \times 10^{-6}$ yr^{-1}. In Table 4.2, we present the orbital epoch measurements from different observatories and orbital cycle number (n).

4.3 Discussion

Before CGRO observations, 4U 1538-52 had been found to have a long-term spin down trend. A linear fit to pre-CGRO pulse frequency history gives $\dot{\nu}/\nu \sim -8 \times 10^{-12} s^{-1}$ and a linear fit to CGRO and our RXTE result yields $\dot{\nu}/\nu \sim 1.45 \times 10^{-11} s^{-1}$. Rubin 1997 ([162]) constructed the power spectrum of pulse frequency derivative fluctuations. Their analysis showed that the pulse frequency derivative fluctuations can be explained on timescales from 16 to 1600 days with an average white noise strength of $(7.6 \pm 1.6) \times 10^{-21}$ (Hz $s^{-1})^2$ Hz^{-1}. A random walk in pulse frequency (or white noise in pulse frequency derivative) can be explained as a sequence of steps in pulse frequency with an RMS value of $< (\delta\nu^2) >$ which occur at a constant rate R. Then the RMS variation of the pulse frequency scales with elapsed time τ as $< (\Delta\nu)^2 >= R < (\delta\nu)^2 > \tau$ (Hz), where $S = R < \delta\nu^2 >$ is defined as noise strength. Then, RMS scaling for the pulse frequency derivatives can be obtained as $< (\Delta\dot{\nu})^2 >^{1/2}= (S/\tau)^{1/2}$Hz.$s^{-1}$. As seen from Table 4.1, in our fits, upper limits on intrinsic pulse frequency derivatives are 7-10 times higher than the long-term spin up rates. If white noise in the pulse frequency derivative can be interpolated to a few days, then the upper limit on the change of frequency derivative obtained from a $\sim$ 1 week observation should typically have a magnitude that can be estimated from $< (\Delta\dot{\nu})^2_{week} >=< (\Delta\dot{\nu})^2_{1600days} \times 15^2 >$. This value is 15/7 - 15/10 times higher than the measured upper limit values. Therefore the measured upper limits on the intrinsic pulse frequency derivatives for 1 week are consistent with the values from the extrapolation of the power spectrum within a factor of a few.

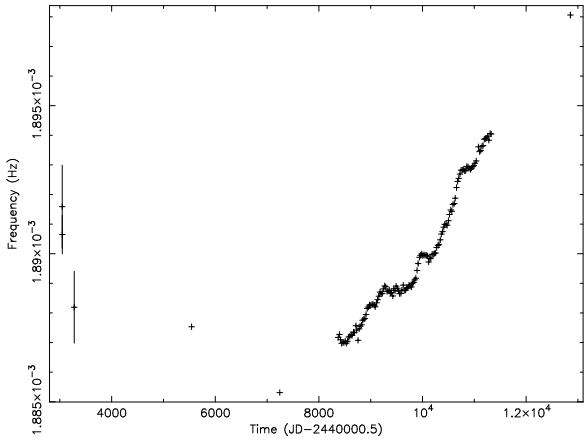

Figure 4.3: Pulse frequency history of 4U 1538-52. The rightmost point corresponds to most recent RXTE observation of ID 80016.

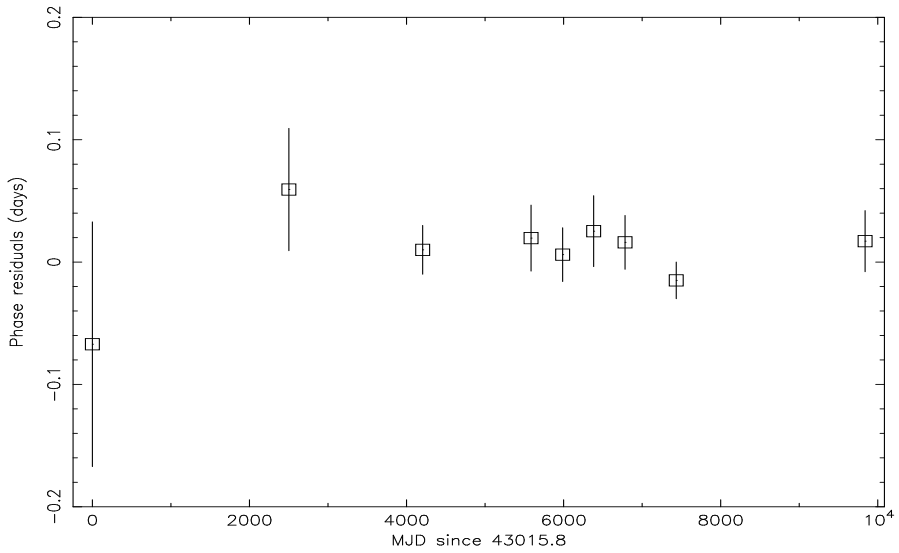

Figure 4.4: The phase residuals of orbital epoch for 4U 1538-52. The orbital phases are estimated relative the constant orbital period ($T_{\pi/2} - n < P_{orbit} > - < T_{\pi/2} - n < P_{orbit} >>$), where n is the orbital cycle number. The rightmost point corresponds to the most recent RXTE observation of ID 80016.

Previous marginal measurement of change in the orbital period, was (-2.9 ± 2.1)×10^{-6} yr^{-1} ([34]), and our new value for the orbital period change, $\dot{P}/P = (0.4 \pm 1.8) \times 10^{-6} yr^{-1}$, are consistent with zero. These two measurements are consistent with each other in 1σ level.

In most of the X-ray binaries with accretion powered pulsars, the evolution of the orbital period seems to be too slow to be detectable. Yet there are still some such systems in which this evolution was measured and $\dot{P}/P$ were reported. These systems include Cen X-3 with

Table 4.2: Orbital epochs by pulse timing analysis

Experiment	Orbit Number	Orbital Epoch (MJD)	Reference
OSO 8	-1128	43015.800± 0.1	[15]
Tenma	-457	45517.660± 0.050	[117]
Ginga	0	47221.474± 0.020	[39]
BATSE	370	48600.979± 0.027	[162]
BATSE	478	49003.629± 0.022	[162]
BATSE	584	49398.855± 0.029	[162]
BATSE	691	49797.781± 0.022	[162]
RXTE	866	50450.206± 0.014	[34]
RXTE	1511	52855.0421± 0.025	This work

(-1.8 ± 0.1)×10^{-6} yr^{-1} ([96];[138]), Her X-1 with (-1.32 ± 0.16)×10^{-8} yr^{-1} ([49]), SMC X-1 with (-3.36 ± 0.02) ×10^{-6} yr^{-1} ([110]), Cyg X-3 with (1.17 ± 0.44) ×10^{-6} yr^{-1} ([98]), 4U 1700-37 with (3.3 ± 0.6) ×10^{-6} yr^{-1} ([161]), and LMC X-4 with (-9.8 ± 0.7)×10^{-7} yr^{-1} ([111]). Change in the orbital period of Cyg X-3 was associated with the mass loss rate from the Wolf-Rayet companion star. For 4U 1700-37, the major cause of orbital period change was also thought to be mass loss from the companion star. For Her X-1, mass loss and mass transfer from the companion were proposed to be the reasons of the change in the orbital period of the system.

On the other hand, for the high mass X-ray binary systems Cen X-3, LMC X-4 and SMC X-1, the major cause of change in the orbital period is likely to be tidal interactions ([96], [111], [110]). For these three systems, orbital period decreases (i.e. derivative of the orbital period is negative). Our new measurement of orbital period change ($\dot{P}/P$) gives the value of about -10^{-6} yr^{-1} which is similar to the observed values of SMC X-1 and Cen X-3.

CHAPTER 5

OBSERVATIONS OF ACCRETION-POWERED PULSARS WITH FERMI/GBM

The latest gamma-ray satellite, after BATSE instrument, Fermi was launched on 2008 June 11 into a 26.5deg inclination orbit at an altitude of 565 km and begin to scientific operations on 2008 August 12. It was launched as in the name of GLAST (Gamma-ray Large Space Telescope) then was renamed the Fermi. It contains two instruments: the Large Area Telescope (LAT) and Gamma-ray Burst Monitor (GBM). LAT is sensitive to gamma-ray from ~ 20 MeV to ~ 300 GeV ([4]) and where as GBM is sensitive to X-rays and gamma ray from ~8 keV to ~40 MeV ([126]). GBM is the only instrument in orbit which is providing nearly continuous full-sky coverage in the hard x-ray/soft gamma-ray energy range. It consists of 14 detectors; 12 Sodium Iodide scintillation (NaI) detectors and 2 Bismuth Germanate (BGO) scintillation detectors. The NaI detectors cover the lower part of the energy range, from 8 keV to about 1 MeV. The BGO detectors cover the energy range of ~150 keV to ~40 MeV. Each detectors is 12.7 cm in diameter and 12.7 cm thickness. The NaI detectors are located on the corners of the spacecraft, with 6 detectors oriented with the normals to the faces perpendicular to the z-axis of the telescope (the LAT is pointed in the +z-direction), 4 detectors pointed at 45deg from the z-axis, and 2 detectors pointed 20deg off the z-axis. Nonetheless, two BGO detectors are located such as on opposite sides of the spacecraft and view a large part of the sky. With none of the GBM detectors, direct imaging can not be done. For general wiev, see Figure 5.1.

Figure 5.1: The LAT (silver box at the top) was integrated on the spacecraft at General Dynamics Advanced Information Systems in December 2006.

5.1 Pulsar Monitoring and Data Analysis Process

We use full sky coverage of GBM on Fermi for long monitoring of the brighter accreting pulsar systems. This continues monitoring allows us correct measurements of spin frequencies, frequency rates, so that studying spin-up and spin-down behaviour and orbital parameters for previously known or recently detected transient sources.

Each day the GBM data three types of data set; bursts, daily, trigger. In the daily type data set, there are 12 NaI ctime (0.256 s resolution), 2 BGO and 1 poshist (position history) data. In our pulse monitoring, we use ctime data (0.256 s resolution) from all the NaI detectors. The first step is to screening the count rates of these data. We remove high voltage transients, phosphorescence events, rapid spacecraft slews, South Atlantic Anomaly induced transients, electron precipitation events and gamma-ray bursts. Source pulses are then separated from the background by fitting the rates in all detectors with a background model, and subtracting the best fit model. This model includes bright sources (here we use Crab, Sco X-1, Cyg X-1) and their changing detector responses, including Earth occultation steps, and quadratic spline functions which account for the remaining long-term background trends. ”The spline models have statistical constraints on the changes in second derivative between spline segments to control the model stiffness. These fits are made jointly across detectors (with common bright

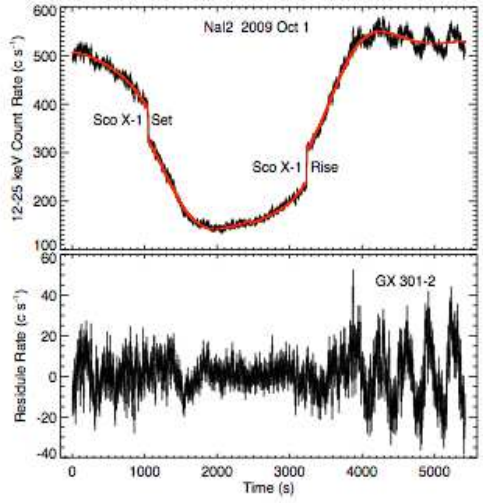

Figure 5.2: A fit of the background rates belongs to the data 2009 Oct 1 in the 12-25 keV band. The upper panel shows the rates and the fit, the bottom panel shows the residuals.

source fluxes) but separately for each channel of the CTIME data. Then we combine the residuals over detectors with time dependent weights which are proportional to the predicted (phase averaged) count rates from the pulsar. Short intervals (~300s) of these combined residuals are then fit with a constant plus a Fourier expansion to determine a pulse profile. The profiles are divided into six day intervals and the pulse frequency and mean profile determined in each interval with a search of pulse frequency for the maximum of the Y_n (n=2) statistic ([53]). Y_n was formulated for finding a pulse frequency from a series of pulse profiles, each represented by a finite Fourier expansion, and accounts for possible frequency dependent non-Poisson noise."

In the Figure 5.2 there is an example fit and residual for one channel and NaI detector 2. The model fits well to the occultation steps of Sco X-1, and the whole background trend underlying the pulsation of GX 301-2 is the evidence of the residuals. The pulses belong to the source can be seen clearly the figure.

5.2 Pulse Searches

In this work, We carry out two different pulse search monitoring: Daily Blind Search and Source Specific Searches.

For the first part, mainly we compute fluxes from the day data in 24 equally spaced source directions on the galactic plane. For each direction, we get the result of FFT based search between 0.5 and 1000 seconds to have strong estimate of the pulse period of previously know sources and to set off the pulse from unknown sources. Then, the final determination of galactic longitude of the source will be given by the longitude with the highest power peak. The latitude can also be restrainted by mapping the power of the source over a grid of source directions.

Source specific searches are performed using short intervals of ctime data. We use small ranges of frequency and frequency rates based on phase shifting and summing pulse profiles of these data which have barycentric and orbital corrections. This is more detail work according to blind pulse search, due to the using small ranges and using of source specic parameters such as longitude and latitude, orbital parameters, flux spectrum in the calculations.

5.3 Detected Sources

To date we have monitored 20 accreting pulsar systems which 8 of them are persistent systems, and 12 of them transient systems (Table 5.2). We are also monitoring five transients which we have not yet detected, using narrow frequency searches made with profile stacking techniques. In the analysis we use channels 1 (12-25 keV) and 2 (25-55 keV). The integration intervals used varies from source to source, ranging from one to four days. For eclipsing systems each egress to ingress interval is divide into an integral number of equal parts, with no measurement made during the eclipse. For sources where the binary orbit is known the frequencies are corrected for the binary motion after barycentered. The R.M.S. pulsed flux is given in the energy band that the pulse search was made. Mostly, it includes only the first and second harmonics.

We label these sources in the Corbet Diagram as in the Figure 5.3. Seven of detected sources, XTE J1946+274, Cep X-4, RX J0440.9+4431, MXB 0656-072, Swift J0513.4-6547, 1A 1118-615 and GX 304-1, can not be shown in Corbet Diagram since their orbital periods are unknown (Those information also given in the Table 5.2). Those seven sources are classified as Be/X-ray binary systems, either known or suspected systems. In the below, we can see some of these sources explicitly with frequency and the pulsed flux history in between 12-25 keV. We can detect outbursts from Be/Xray pulsar systems like XTE J1946+274, Cep

X-4, EXO 2030+375, V 0332+53, A 0535+26, MXB 0656-072, Swift J0513.4-6547, GRO J1008-57, A 1118-615, 2S 1417-624 and also XTE J1946+274, RXJ0440.9+4431, GX 304-1 are well known systems for being on quiescence state but during the GBM monitoring period renewed activities begin to occur. Those systems show two types of outbursts.

A 0535+26 shows many short outbursts, and it is a good example for mixed type I and II behaviour. With GBM, the first detected outburst belongs to time from MJD 54720 - 54730, the second from MJD 54832 - 54842, and the third from MJD 54936 - 54954 and on 2009 July 26 (MJD 55038) . We find that the higher flux outbursts begin at an earlier orbital phase, with the first outburst detected with Fermi/GBM beginning 4 days before periastron passage,

Table 5.1: Detected accreting pulsars with Fermi/GBM

Name	Spin Period (s)	Orbital Period (day)	Type
Persistent Sources			
Her X-1	1.24	1.70	Eclipsing LMXB
4U 1626-67	7.63	0.023	Super-Compact LMXB
OAO 1657-415	37.1	10.4	Eclipsing Wind-fed Supergiant
GX 1+4	158	1161	Symbiotic Binary (red giants)
Vela X-1	283	8.96	Eclipsing Wind-fed Supergiant
4U 1538-52	525	3.73	Eclipsing Wind-fed Supergiant
GX 301-2	686	41.5	Wind-fed Supergiant
Cen X-3	4.80	2.09	Eclipsing Disk-fed Supergiant
Transient Sources			
XTE J1946+274 (GRO J1944+26)	15.8	unknown	Be/X-ray binary
Cep X-4	66.3	unknown	Be/X-ray binary
EXO 2030+375	41.3	46.0	Be/X-ray binary
V 0332+53	4.37	34.2	Be/X-ray binary
RX J0440.9+4431	202	unknown	Be/X-ray binary
A 0535+26	103	111	Be/X-ray binary
MXB 0656-072	160	unknown	Be/X-ray binary
Swift J0513.4-6547	27.3	unknown	prob. Be/X-ray binary in LMC
GRO J1008-57	93.7	248	Be/X-ray binary
1A 1118-615	407	unknown	Be/X-ray binary
GX 304-1	272	unknown	Be/X-ray binary
2S 1417-624	17.5	42.1	Be/X-ray binary

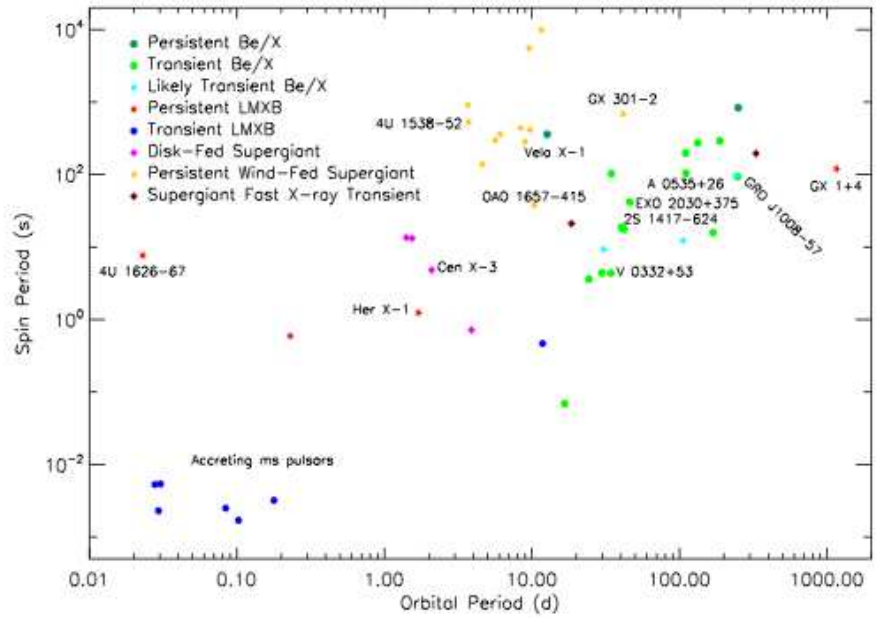

Figure 5.3: The Corbet Diagram showing distribution of accreting pulsars as in spin period versus orbital period configuration, with GBM detected sources

the second 3 days, and the third 10 days. The forth outburst was first detected 19 days before periastron, suggesting it will be brighter than any of the previous three observations([54]).

Later, It was detected in pulsations on 2010 June 23 (MJD 55370), 20 days before the next periastron passage. The source was initially detected with Earth occultations on 2010 June 25 the source was detected with a flux of about 150±40 mcrab (12-25 keV) ([25]). It continues to detect brightly. On 2009 November 30 (MJD 55165), Fermi GBM Earth occultation observations showed that the flux had risen rapidly to 480±100, 460±70, and 620±100 mCrab in the 8-12, 12-25, and 25-50 keV bands. On 2009 December 1 (MJD 55166), the flux continued to rise to 580±105, 640±50, 444±80 mCrab in the 8-12,12-25, and 25-50 keV bands respectively. After remaining fairly constant at 10 mCrab from November 19-24, the pulsed rms flux in the 12-50 keV band began to rise, reaching 70 mCrab on December 1. From Nov 29 to Dec 1 the pulse frequency increased at a rate of $1.22(7) \times 10 \times 10^{-12}$ Hz/s reaching 9.66094(4) mHz on Dec 1.5 ([36]).The general trend can be easily seen from Figure 5.4

”Swift J0513.4-6547 in the LMC is one of the recently discovered accreting system ([101])

had been detected between 2009 March 1 and March 28. Pulse searches were made for several multi-day intervals covering 2009 January 30 to April 15. In between March 18 and March 22, the pulsed flux (12-25 keV) reached 15 mCrab, with a lower limit of luminosity as 7×10^{37} erg/cm^2 s. The searches included both trial frequencies near the 36.66 mHz (27.28 s period) RXTE measurement ([101]), and trial frequency rates in the range expected for accreting pulsars near Eddington luminosity ([55]). The negative frequency rates in the last two intervals are most probably due to Doppler shifts from the binary orbit which we have not any information about it."

In Table 5.2, there is an detailed information belongs to frequency and frequency rate with used epoch.

Cepheus X-4 (GS 2138+56) is also another transient Be/X-ray binary pulsar which showed its pulsation between 12-25 keV energy band. The source was first detected on 2009 March 7 and was again detected on March 8. On both days, the pulse frequency was consistent with 15.07552(15) mHz, and the r.m.s. pulsed flux was consistent with 2.8(2)E-10 $erg/cm^2/s$ (12-25 keV) ([17]). Then, we continue to detect its steadily risen flux on March 15 of $5.1(3)10^{-10}$ erg/cm^2/s (12-25 keV), which is approximately twice that on March 7. The pulse frequency has also increased at an average rate of $3.8(5)\times10^{-12}$ Hz/s, reaching 15.07760(18) mHz on March 15.5([18]).

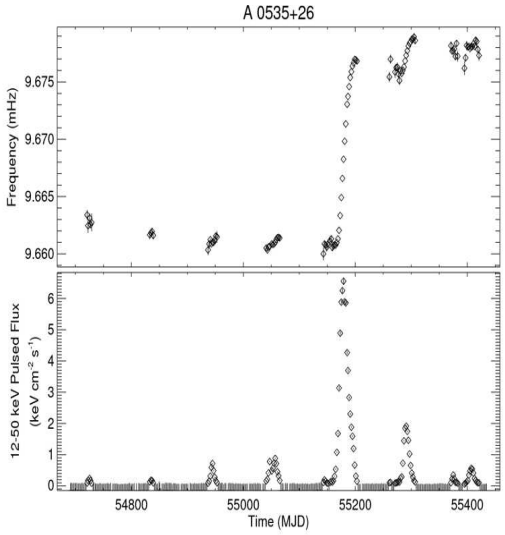

Figure 5.4: Frequency and the pulsed flux history between 12-25 keV for A 0535+26

Another transient Be/X-ray binary pulsar 2S 1417-624 was also detected in outburst. Coherent pulsations from the source at a 17.5 s period have been detected in the GBM data since 2009 October 18. The rms pulsed flux has been increasing, reaching 12 mCrab (12-52 keV) during October 28-29. From October 24.0 to 30.0, the spin frequency (corrected using the binary orbital elements of ([79]) increased at a rate of $(8.5 \pm 1.0) \times 10 \times 10^{-12}$Hz/s, reaching 57.09623(14) mHz on October 29.0 (MJD 55133.0). The Swift/BAT monitoring shows a flux of 40 mCrab on October 29 and 90 mCrab on October 30. ([16]).

EXO 2030+375 is one of the source we are monitoring continuosly with GBM. It is a good example of type I behaviour. In Figure 5.5 we can see the GBM pulse frequency and pulsed flux history of this source.

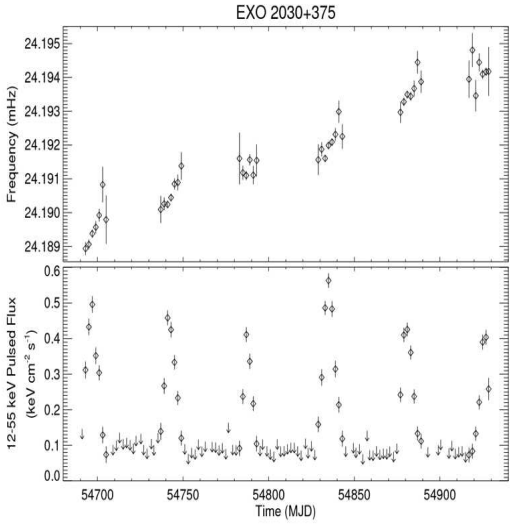

Figure 5.5: Frequency and the pulsed flux history between 12-25 keV for EXO 2030+375

Table 5.2: Detected accreting pulsars with Fermi/GBM

Time Range (MJD)	Epoch (MJD)	Frequency (mHz)	Frequency Rate (1E-12 Hz/s)
54819.0-54897.0	54893.984	36.59407(13)	48(2)
54897.0-54902.0	54899.339	36.62742(18)	102(5)
54904.6-54908.5	54906.509	36.67029(15)	30(3)
54908.5-54912.5	54910.552	36.67429(13)	-8(3)
54912.5-54918.0	54915.296	36.66989(13)	-6(3)

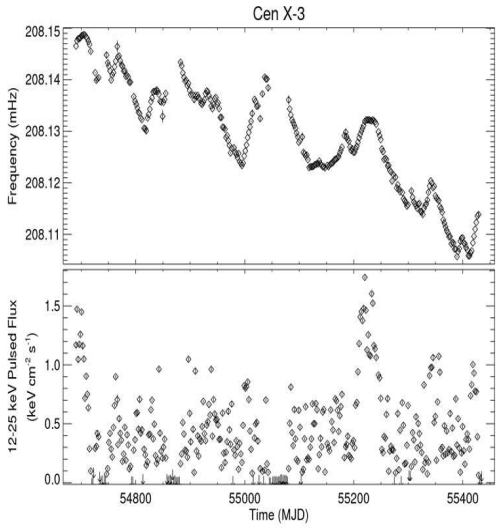

Figure 5.6: Frequency and the pulsed flux history between 12-25 keV for Cen X-3

Cen X-3 is a luminous eclipsing binary system and an example for the Disk-fed supergiant class. In this system, the supergiant companion is overflowing its Roche-lobe, and as a result a persistent disk is generated. From the precise orbit determinations which have been made over the past 40 years we know that the orbital period is decreasing. The pulsar's spin frequency history shows torque switching behavior with persistent spin-up changing with intervals of persistent spin-down. There are short transitions between two states. There is no correlation between torque behaviour and pulsed flux. We can see this behaviour in (Figure 5.6)

Vela X-1, GX 301-2, 4U 1538-52 and OAO 1657-415 are the sources in which the accretion flow is occurred via stellar wind, since the Roche-lode is underfilled. Vela X-1 is one of the eclipsing binary which is well known and well studied source since 1967 ([33]). As it can be seen from Figure 5.7, the frequency history is consistent with a random walk (or white torque noise). The frequency history is consistent with random walk.

Three accreting pulsars with low mass companions, 4U 1626-67, Her X-1 and GX 1+4, can be classified as persistent LMXBs. Her X-1 is again one of the mostly studied pulsar, it an eclipsing Roche-lobe overflow system with an 35 day cycle in the X-ray intensity. This 35 day flux cycle is due to obscuration of the pulsar by accretion disk. This flux cycle includes "main-on" state then off-state and then "short on" state and again off-state. With GBM, we can easily detect these states and continue to detect (Figure 5.8).

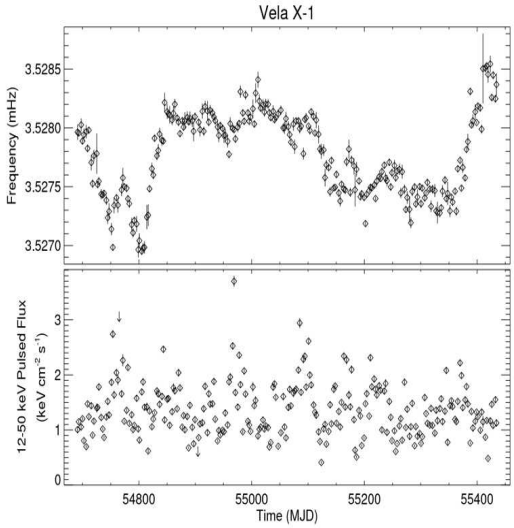

Figure 5.7: Frequency and the pulsed flux history between 12-25 keV for Vela X-1

5.4 4U 1626-67

It was discovered by Uhuru ([64]). Rappaport et al. 1977([153]) mentioned that it steadily spun up on a timescale, $\nu/\dot{\nu}$ ~5000 yr (see Figure 5.9). The system consists of a 7.66s X-ray pulsar accreting from an extremely low mass companion (0.04 M$\odot$ for $i = 18^o$) ([108]). The

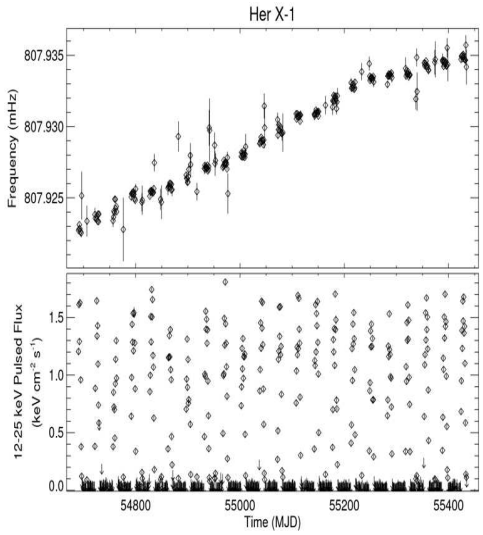

Figure 5.8: Frequency and the pulsed flux history between 12-25 keV for Her X-1

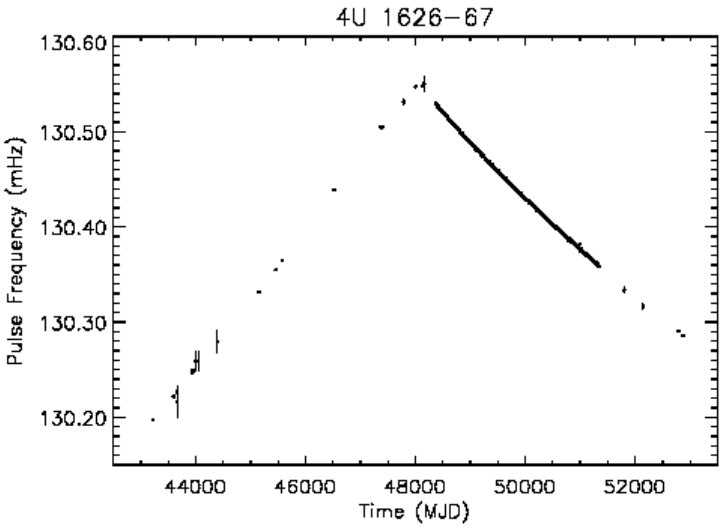

Figure 5.9: Pulse frequency history of 4U 1626−67, showing all available historical data from 1997 to 2003. The 1990 June (∼MJD 48000) torque reversal is clearly seen.

orbital period determined as 42 min ([29]). The binary has faint optical counterpart (KZ TrA, V∼17.5) with a strong UV excess and high optical pulse fraction ([124], [125]).

A persistent quasi-periodic oscillation (QPO),48 mHz, has been detected in the X-ray emission ([165], [102]). The QPO frequency evolution during the previous 22 years changed from a positive to a negative trend is similar to the frequency seen during the June 1990 torque reversal ([93]).

After the discovery of pulsations ([153]) the source underwent steady spin-up at a mean rate of $\sim \dot{\nu} = 8.5 \times 10^{-13}$ Hz s^{-1} ([28]) (see Figure 5.9). Monitoring of the source by the Burst and Transient Source Experiment (BATSE) on board the Compton Gamma Ray Observatory (CGRO) starting in April 1991 showed that the source changed sign in the accretion torque ([194],[21]) and spin-down trend. During the 7 years after the first torque reversal, the pulsar spun-down at a rate of $\sim \dot{\nu} = -7.2 \times 10^{-13}$ Hz s^{-1} ([28]).

5.5 Observations and Timing Analysis

We firstly present a long term timing analysis using continuosly monitoring of 4U 1626-67 with Fermi-GBM starting in 2008 August. Pulsar is founded that it is spinning-up rather

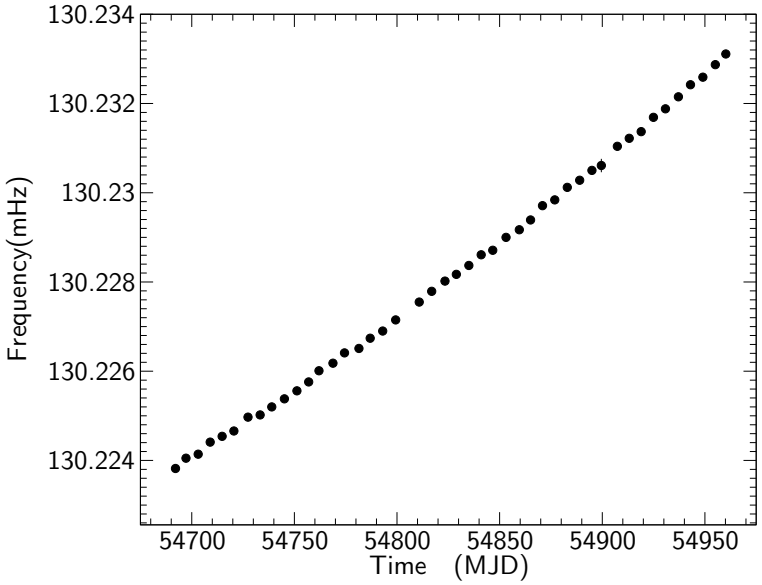

Figure 5.10: Fermi/GBM pulse frequency measurements of 4U 1626-67 since 2008 August. A change in the sign of the torque was found after 18 years of the source spinning down.

than spinning-down. Figure 5.10 shows the pulse frequency history using data from this monitoring. 4U 1626-67 seems to be increasing in $\dot{\nu}$. Follow-up Fermi-GBM observations confirm that the pulsar it is currently spinning-up at a mean rate of $\sim \dot{\nu}=4\times10^{-13}$ Hz s^{-1}.

5.6 Swift/BAT observation and Timing Analysis

The source conte continued to be monitored by also hard X-ray Swift-BAT from 2004 up to 2009. It allows us to cover the evolution of the second torque reversal shown by the source. The Swift Gamma-ray mission ([66]) was launched on 2004 November 20. The hard X-ray (15-150 keV) Burst Alert Telescope (BAT) on board Swift monitors the entire sky searching mainly for GRBs. Behind this main business, BAT also make a hard X-ray survey of the entire sky covering 2 sr at any particular time. Therefore it produces continuous detecting of rate data. The rate data include (quadrant rates) (1.6 sec sampling; four energy bands; four separate spatial quadrants), not background subtracted (total exposure time $\sim$ 13 Ms).

”A similar procedure was followed for the Swift-BAT (quadrant rates) timing analysis. Initial good time interval (GTI) files are obtained using the ”maketime” ftool (heasoft-6.6.1)[1]. Then

[1] http://heasarc.gsfc.nasa.gov/docs/software.html

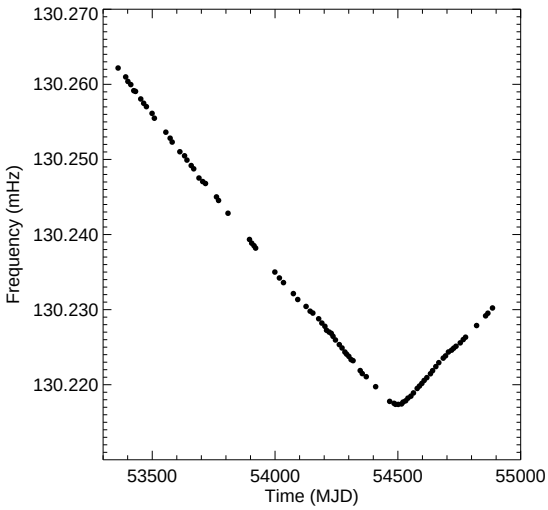

Figure 5.11: Swift-BAT pulse frequency history covering this second reversal torque (from 2004 Oct to the present time). Error bars are smaller than the plotted symbols.

a filtered version of the (quadrant rates) is obtained, rejecting those times when the source is below the horizon, to then finally be barycentered using the ftool ”barycorr”. Data are then inspected and cleaned as in the previous section. With the ftool ”batmasktgimg”, the pixel exposure fraction for each quadrant is computed for the center of each (refined) GTI interval. Pulse profiles for each good GTI interval are computed. First the rates for each quadrant are fit to a quadratic+Fourier expansion. Then the Fourier coefficients are combined using the quadrant exposures to produce mean profiles (with units of counts s^{-1} cm^{-2}). In a final stage, the Y_n (n=2) statistic is again used in intervals of 35 days and a frequency search for pulsations is carried out. The spin rates were computed by fitting a linear function to the frequencies, which were divided into 21 time intervals.”

As a result of analysis we found that the pulsar spun-down at a mean rate of $\sim \dot{\nu} = -4.8\times10^{-13}$ Hz s^{-1} until the source reversed torque. Figure 5.11 shows that the transition took place at around MJD 54500 (2008 Feb 04) and lasted approximately 150 days. In the bottom panel of Figure 5.12 we can see that there is a strong correlation between the Swift-BAT count rate and the spin-up rate especially during the reversal. It is not known if this occurred in the 1990 torque reversal because of the missing of observations for that duration. In order to see any other possible change, we created pulse profiles in the 15-50 keV band. We have not observed any significant change in pulse shape, not even during the reversal. They all are single-peaked

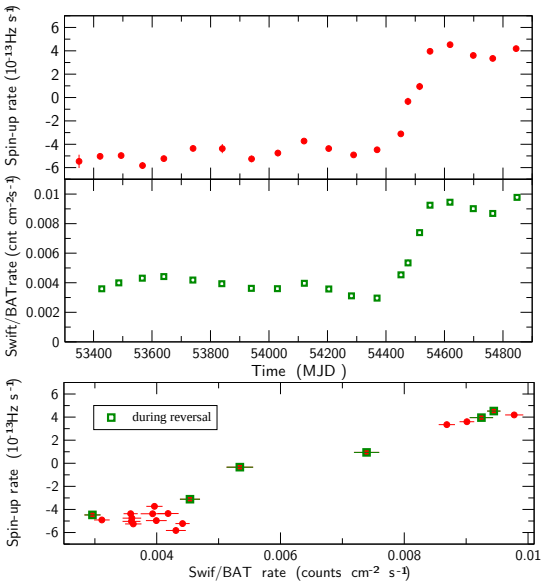

Figure 5.12: Top panel. Swift-BAT spin-up rate history of 4U 1626-67. Middle panel. Average 15-50 keV BAT count rate vs. time. Error bars are smaller than the plotted symbols. Bottom panel. BAT count rate vs. spin-up rate for all the period (circles). A correlation pattern is observed specially during the torque reversal (only square symbols).

and sometimes not entirely symmetric as was recently reported by Krauss et al. 2007([99]).

5.7 RXTE Observation and Analyse

Two RXTE/PCA observations from 2008 March 5 and 13 were used (ID 93431-01-01-00 and 93431-01-02-00; 7.174 ksec). For spectral analysis we selected PCA Standard-2 data which contains 129-channel range spectra taken every 16 seconds and HEXTE Standard Modes (Archive) data which contains Spectral Bin (64-bin spectra produced every 16s). For the long-term hardness ratio analysis we used the ASM daily flux averages in the 1.5-12 keV energy range from the HEASARC archive[2].

5.7.1 Hardness Ratio

The two RXTE-HEXTE observations do not provide us any direct comparison between before and after the torque reversal. So in hardness ratios, we use BAT and ASM light curves. For

[2] http://he//heasarc.gsfc.nasa.gov/docs/archive.html

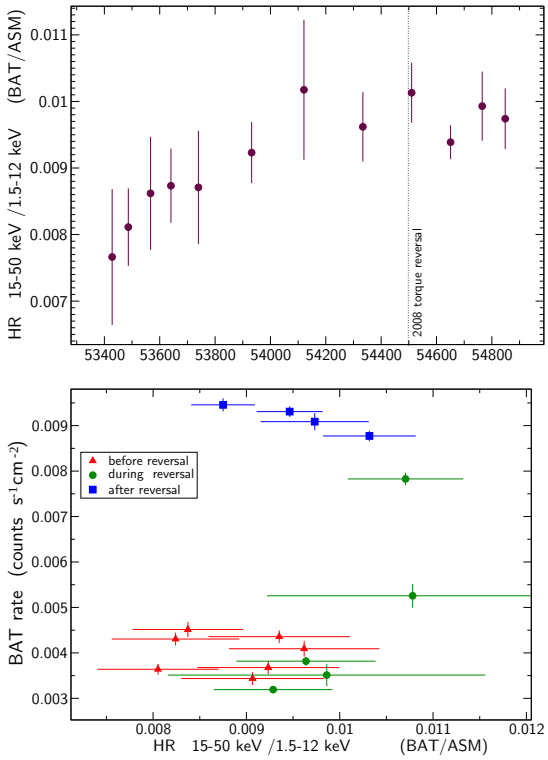

Figure 5.13: Top panel. Long term hardness ratio analysis of 4U 1626-67. Swift-BAT count rates (15-50 keV) were selected as the hard band and RXTE/ASM count rate (1.5-12 keV) as the soft band. Bottom panel. Hardness-intensity diagram. During the reversal a transition from hard to soft is seen.

the hardness ratio analysis from BAT data, we used count rates from the Swift-BAT transient monitor results provided by the Swift-BAT team[3].

Figure 5.13 (top panel) shows the hardness ratio (HR) analysis of this source. The HR was defined as the ratio of 15-50keV BAT light curves to 1.5-12.0keV ASM lightcurves. All lightcurves was rebinned. We can see that there is a smooth hardening evolution of the source before the reversal.

In the bottom panel of Figure 5.13 we have replaced the intensity with the BAT count rate in order to perform Hardness-intensity diagram (HID), to study the long term spectral variability of 4U 1626-67, including the transition. From that figure we can see that there is a transition from hard to soft during this new reversal of 4U 1626-67.

[3] http://heasarc.gsfc.nasa.gov/docs/swift/results/transients

5.7.2 Spectral analysis

For spectral analysis we used RXTE/PCA (2.5-20 keV) and HEXTE (18-100 keV) data by using XSPEC 11.3.2. Belongs to that source, firstly a ~37 keV absorption cyclotron feature is founded in the 0.1-200 keV BeppoSAX spectrum ([143]). Then X-ray broad-band continuum (0.7-100 keV) was fitted with a low-energy absorption, a blackbody, a power law and a high energy cutoff at ~20 keV (*(wabs (gauss+bbody+powlaw) highecut)*), with a braod iron line near 6.5 keV ([149]).

When we try this model we fixed the hydrogen column density of cool material in the line of sight at a value of $1.3 \times 10^{21} \mathrm{cm}^{-2}$. This constraint was taken from Krauss et al. 2007([99]) study.

The spectral parameters obtained from our fitting are shown in Table 5.3. Reprocessing of photons either at the base of the accretion column or the inner edge of the accretion disk might explain the origin on the blackbody component. From the blackbody flux and temperature we obtain an emission area of 9×10^{12} cm^{-2} (assuming a source distance of 10 kpc), which is inconsistent with either of those possibilities.

Then, we fit same model with a bremsstrahlung instead of a blackbody component to obtain a compatible fit (*(wabs (gauss+bremss+powlaw)highecut)*). Table 5.3 summarizes the spectral parameters that we obtained. Fluxes for the first model in the 2-10 keV, 2-20 keV and 2-50 keV bands are $3.24(2)\times10^{-10}$, $7.003(11)\times10^{-10}$ and $9.98(2)\times10^{-10}$ erg $\mathrm{cm}^{-2}\mathrm{s}^{-1}$, for the first RXTE observation (similar values for the second one).

5.8 Discussion

By using ctime data belongs 12 NaI detectors of Fermi/GBM, we can monitoring brighter accretion pulsars continuosly by using full sky coverage of GBM. By using this full sky coverage of GBM we can able to monitor both persistent and transient accreting systems. During GBM life time, since 2008 August 12, we can be able to detect new detected transient sources and new outbursts of known sources. We are producing long term histories of the pulse frequency, frequency rates, flux and pulse profiles in 8-50 keV, according to be softness or hardness systems. We are using two main challenges while producing them: a daily blind search for

Table 5.3: RXTE/PCA and HEXTE continuum spectral fits

Observation (MJD)	α^{*}	$E^{\dagger}_{cut}$	$E^{\dagger}_{Fold}$	Gaussian†	Gauss. $\sigma^{\dagger}$	Gauss. norm**	$T^{\dagger}_{BBody}$ $T^{\dagger}_{Bremss}$	norm $^{BBod^{1}}_{Brem^{2}}$	Flux***	χ^2_r(DOF)
93431-01-01-00	0.75(2)	$18.2^{+0.1}_{-0.3}$	8.5(4)	$6.05^{+0.5}_{-0.17}$	$1.6^{+0.3}_{-0.2}$	$2.4^{+4}_{-0.8}$	$0.615^{+0.006}_{-0.018}$	0.0013	1.01(8)	1.15(114)
(54530)	0.74(2)	$18.2^{+0.3}_{-0.2}$	$8.5^{+0.3}_{-0.4}$	$6.42^{+0.17}_{-0.4}$	$1.4^{+0.1}_{-0.2}$	$1.5^{+1.2}_{-0.6}$	$1.74^{+0.12}_{-0.14}$	0.108	1.01(1)	1.15(114)
93431-01-02-00	$0.71^{+0.06}_{-0.04}$	$17.90^{+0.19}_{-0.3}$	$8.4^{+0.5}_{-0.6}$	$6.2^{+0.6}_{-0.4}$	$1.5^{+0.4}_{-0.2}$	$2.23^{+1.9}_{-0.08}$	$0.654^{+0.04}_{-0.009}$	0.0013	1.006(12)	1.29(114)
(54538)	$0.71^{+0.04}_{-0.05}$	$17.96^{+0.14}_{-0.2}$	8.4(6)	6.9(2)	$0.5^{+0.4}_{-0.3}$	$0.396^{+0.14}_{-0.015}$	$2.47^{+0.3}_{-0.08}$	0.068	1.004(9)	1.28(114)

($N_{\rm H} = 1.3 \times 10^{21}$ cm^{-2} fixed)

* Photon Index

† keV

** $\times 10^{-3}$

^{1} (Lumin/10^{39} erg s^{-1})(d/$10kpc$)$^{-2}$

^{2} $3.05 \times 10^{-15}(4\pi d^2)^{-1}\times$ Emission measure

*** $\times 10^{-9}$erg cm^{-2} s^{-1} (2-100 keV)

^{a} Uncertainties at 3σ level.

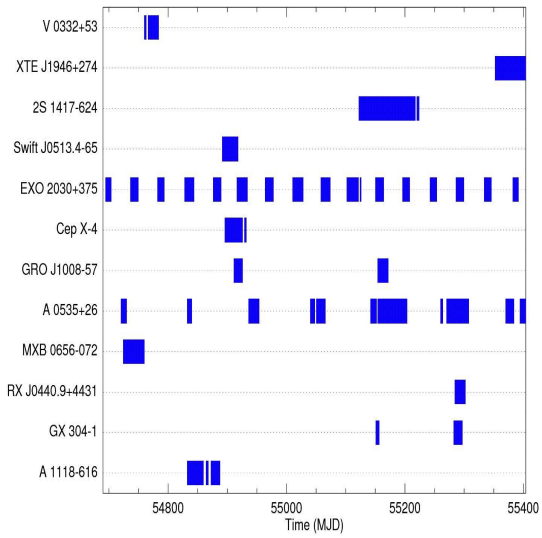

Figure 5.14: Times of transient outburst observed with GBM

pulsed sources and source specific searches by using narrow band pulse searches specific to every source. In Figure 5.14 we can see some of the transient systems since beginning of the detection.

4U 1626-67 is one the source monitored continuosly with Fermi-GBM. As well as GBM, by also using continuosly monitoring of the source by Swift-BAT and archival RXTE-PCA and HEXTE data we can could be able to study the torque reversal in 2008(see Figure 5.15). This reversal has shown us that the spin behaviour of that source to be more complicated than previously thoughts. Firstly, while the continuous decrease of total X-ray flux during almost two decades was expected to bring the source into quiescence ([99]), a new spin reversal with a rapid increase of the flux occurred. This inconsistency make us to search physical processes responsible from the spin evolution of the pulsar.

”All previous studies of 4U 1626-67 were focused on modeling the spin-up torque applied to the neutron star from the accreted material. It was widely believed that the spin behavior of the pulsar depended mainly on variations of the mass accretion rate onto the stellar surface. Using variable equilibrium period ([67]), the torque reversal in 1990 (transition spin-up to spin-down) has been tried to explain by Vaughan & Kitamoto 1997([182]). The neutron star phase transition in their model includes decrease of mass accretion rate and, possibly, change of the structure of the accretion flow beyond the magnetosphere. This scenario is based on some

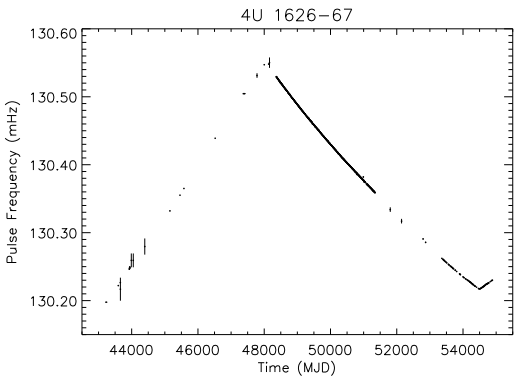

Figure 5.15: Pulse frequency history of 4U 1626-67 from 1997 up to 2009. The 1990 June and the 2008 Feb reversals are clearly seen.

evidence for a connection between torque and X-ray luminosity observed in 4U 1626-67 and being hard in the spectrum after the torque reversal. But, with that approach they encounter some problems in explaining the observed behavior of QPOs, which have been interpreted in terms of the MBFO ([107]). Their analysis suggests that either this interpretation of QPOs is incorrect or the torque reversal in 1990 occurred as the magnetospheric radius of the neutron star, $r_{\rm m}$, had increased beyond its corotation radius, which for the parameters of 4U 1626-67 is ([104])

$$r_{\rm c} = \left(\frac{GM_{\rm ns}}{4\pi^2\nu^2}\right)^{1/3} \simeq 6.7\times10^8\ m^{1/3}P_{7.7}^{2/3}\ \text{cm}. \tag{5.1}$$

Here m and $P_{7.7}$ are the mass and spin period of the neutron star in units of 1.4 M_{sun} and 7.7 s. A dramatic change in the power spectra between the last observation of 4U 1626-67 during the spin-down phase (2003) ([93]), and observations made soon after the new torque reversal has been recently reported by Jain et al. 2009([88]), with the 35-48 mHz QPO no longer being present, and wide shoulders on the pulse fundamental appearing. They claimed that the observed behavior of the source cannot be a simple case of increased mass transfer rate, but is also a change in the accretion flow parameters.

Analyzing the evolution of the source energy spectrum and possible correlation between the torque and X-ray luminosity of the pulsar, Yi & Vishniac 1999([197]) proposed a scenario in which the torque reversal in 1990 can be related with a state transition of the accretion disk to a geometrically thick, hot and, possibly, sub-Keplerian phase. The same idea can be said also for the 2008 torque reversal with an transition of geometrically thin Keplerian phase to its original disk. However, the reason for such a transition is rather unclear since the level

of X-ray flux measured before and even after the 2008 reversal is smaller than that measured during the reversal in 1990. Furthermore, both reversals have occurred at almost the same timescale (about 150 days), which significantly exceeds the dynamical timescale in the hot disk in which its transition to the ground state is expected.

A correlation between the torque applied to the neutron star in 4U 1626-67 and X-ray flux of the system in the above mentioned models has been accepted as one of the basic assumptions. To check reality of this assumption, Figure 5.16 is a good illustration showing the 4U 1626-67 X-ray flux history. We can see all previous flux measurements and two RXTE/PCA recent values from the present work (in the 2-20 keV band). These values are relative to the flux measured in 1978 by HEAO 1 in the same energy band ([143], [99], [28]). The cross point before the 2008 reversal has been inferred by scaling the PCA fluxes according to the observed change (2.5 factor) in the Swift-BAT rate, since no spectral changes across the transition have been observed according to the present work. It should be noted, however, that all these relative flux values were computed in different energy bands, therefore the general decreasing trend we see since 1977 might not be the real picture. Points could misrepresent the HEAO1 0.7-60 keV flux by a $\sim$ 20% due to spectral changes. Moreover, rather than a continuous decline (ignoring the 1990 point) 4U 1626-67 might present a flat behavior until the first reversal, then a sudden drop after that and a decreasing tendency until the 2008 reversal, in which this source experienced a rapid increase of flux. It therefore appears that the spin-down phase is the only suitable part of the light curve for testing the correlation between the torque and mass accretion rate onto the neutron star surface.

As seen from Figure 5.16, the X-ray flux during the spin-down phase has decreased by a factor of 2. This indicates that the mass accretion rate onto the surface of the neutron star, $\dot{M}$, and, correspondingly, the spin-up torque applied to the star ([152]),

$$K_{\rm su} = \dot{M}(GM_{\rm ns}r_{\rm m})^{1/2}, \tag{5.2}$$

during this phase have also decreased by at least the same value. If the spin-down torque applied to the neutron star during this time were constant one would expect the pulsar to brake harder at its fainter state close to the end of the spin-down phase. However, observations show the situation to be just the opposite. The spin-down rate of the neutron star during this phase has decreased from $|\dot{\nu}| \simeq 7\times10^{-13}\,\mathrm{Hz\,s^{-1}}$ ([28]) to $5\times10^{-13}\,\mathrm{Hz\,s^{-1}}$ (see Figure 5.9), implying that the pulsar was braking harder at its brighter stage just after the torque reversal in 1990.

According to the equation governing spin evolution of an accreting neutron star,

$$2\pi I\dot{\nu} = K_{\rm su} - K_{\rm sd}, \tag{5.3}$$

this means that the spin-down torque, $K_{\rm sd}$, during the spin-down phase has been decreasing simultaneously with the spin-up torque but at a higher rate and, therefore, the pulsar spin evolution during this time has been governed mainly by variations of $K_{\rm sd}$ rather than $K_{\rm su}$ (here I is the moment of inertia of the neutron star). This conclusion seriously challenges the possibility of modeling the spin history of 4U 1626-67 solely in terms of variations of $\dot{M}$, and suggests that the dramatic increase of X-ray flux observed in 2008 torque reversal may be a consequence rather than a reason for this event.

Finally, the spectral evolution of 4U 1626-67 during the torque reversal differs from that expected in models which suggest significant changes of the accretion flow structure in spin-up/spin-down transitions ([197], [189]). As seen from (Figure 5.13), the spectrum becomes the hardest during the reversal and the value of the hardness ratio before and after these events does not differ significantly. This indicates that the recent torque reversal can be related with changes of physical conditions in the inner part of the disk or/and in the region of its interaction with the magnetosphere rather than a significant change of the accretion flow geometry.

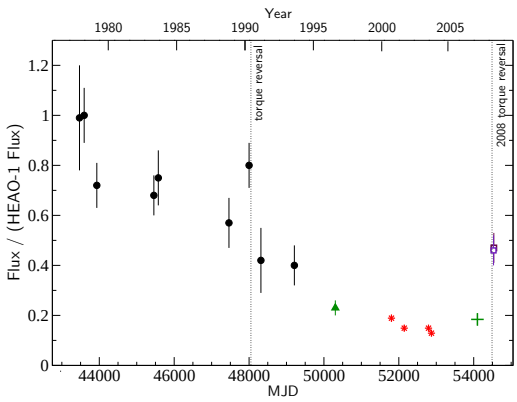

Figure 5.16: The X-ray flux history of 4U 1626-67 relative to the flux measured by HEAO 1, in the same energy band, from previous works ([28]) circles; ([143]) triangle; ([99]) stars) and two recent RXTE/PCA observations (unfilled squares) in the 2-20 keV band. The cross point is inferred from PCA flux and the fractional change in the Swift-BAT rate, since no spectral changes during the transition have been observed in this work.

However, the errors of the observations are too large for a justification of particular transition model. Therefore, a more precise spectral measurements of the pulsar during its next spin-up/spin-down transition is strongly desired. Assuming the recurrent time of the transition to be about 18 years one can suggest to pay more attention to the pulsar in 2025-2028. Since the typical duration of the transition is about 150 days, a regular monitoring of the pulsar, frequently enough to provide a spin-up rate measurement every two months, would prevent us from missing its next torque reversal."

For general wiev see the spacecraft web page[4] and the updated figures of the detected and other sources are available also at GBM pulsar web page[5]

[4] http://www.nasa.gov/mission_pages/GLAST
[5] http://gammaray.nsstc.nasa.gov/gbm/science/pulsars

CHAPTER 6

SPECTROSCOPIC AND PHOTOMETRIC OBSERVATIONS OF IGRJ 06074+2205 AND IGRJ 01583+6713

6.1 Introduction

IGRJ06074+2205 was discovered by INTEGRAL JEM-X during public observations of the Crab region that took place on 15 and 16 February 2003. The best-fit position was RA=06h07.4m DEC=22d05m (±2')([31]). The obtained flux values were ∼ 7 mCrab (±2 mCrab) in the energy range 3-10 keV and 15 mCrab in the range 10-20 keV range during the 67-ks exposure on 15 February 2003. A day later the flux had decreased to less than 5 mCrab during a 16 ks exposure.

Optical spectroscopic observations performed with the MDM 2.4 m telescope of the brighter stars in the field around the INTEGRAL position on 27 December 2005 found a Be star within 1' of the INTEGRAL position. It is suggested that the radio source discussed ([148]) was an another source. It showed Hα in emission with an equivalent width of 66 Å. Its magnitudes obtained from the USNO A2.0 and 2MASS catalogues are B=13.3, R=12.1, J=10.49, H=10.19, K=9.96 ([70]).

The radio source NVSS J060718+220452 lies 80" from the reported position of the X-ray source, and was stated as a possible radio counterpart ([148]). However, subsequent observations made with Chandra did not find any X-ray source at the location of the radio counterpart ([174]). The source also is classified as B0.5 Ve according to high mass binaries catalogue by Liu et al.2006([113]).

From low-resolution spectroscopic observations obtained using the G. D. Cassini 1.5m tele-

scope In Loiano observatory Masetti et al. 2006([121]) suggested a B8III star as the classification of the optical counterpart to it. However, their spectra did not have the spectral resolution for a proper analysis.

On 2 December 2006 a 5-ks observation with Chandra-ACIS improved the accuracy of the X-ray position and allowed the confirmation of the Be star suggested by Halpern and Tyagi 2005 and Masetti et al. 2006b([70], [122]), it is catalogued as CXOU J060726.6+220547. Using by extrapolating power-law fits to Chandra observation between 20-40 keV, the flux value is found as 2.6 ($\pm$0.7) $\times$ 10^{-12} $ergs/cm^2/s$, so the flux ratio of Chandra value to INTEGRAL value is 0.021 $\pm$ 0.009. Such a flux ratio between outburst and quiescence would not be a normal range for Be X-ray binary, it shows us probably there is a binary orbit with eccentricity. The Chandra Spectral results gives $N_H = (7.2 \pm 2.0) \times 10^{22}$ cm^{-2} and a photon index of 0.9 $\pm$ 0.5 (90 % confidence errors). Unabsorbed flux between 0.3-10 keV is 3.5$\pm$0.5 $\times$ 10^{-12} cm^{-2} s^{-1} ([175]).

Lastly, spectroscopic observations of the optical counterpart to the X-ray binary
IGRJ 06074+2205 were obtained from the 1.3m telescope of the Skinakas observatory in Crete (Greece) and from the 1.5m telescope of the Fred Lawrence Whipple Observatory at Mt. Hopkins (Arizona) on several occasions throughout 2006-2008 by Reig and Zezas 2009 ([156]). From their results, they identify the spectral type of the companion star and its long term spectral variability.

IGRJ 01583+6713 was first detected on 6-7 December 2005 during the observation of the Cassiopeia A region by IBIS/ISGRI, and later again by ISGRI on 8-10 December 2005. The source position reported as RA =29.57, Dec=+67.22 degree (error radius:2') and it was detected always outside the JEM-X error box([169]). The source flux is 14 mCrab in the 20-40 keV energy range and no detection in the 40-80 keV.

Swift/XRT observed this source on 13 December 2005 with 5ks. The position was reported to be RA=01h58m18.2s Dec=+67d13m25.9s [J2000]([97]) (error radius:3.5") which is 17" from the previously reported position. According to the USNO catalogue it has magnitude R=13.9, B=15.3. Although it had a low flux of 1.5 x 10^{-11} erg/s/cm^{-2} (0.2-10 keV), the spectral analysis showed that it was highly absorbed with N_H approximately 10^{23} cm^{-2} ([97]). Halpern & Tyagi Atel#681 reported, according to the low resolution optical spectrum taken with MDM 2.4m telescope on 24 December 2005, strong Hα (EW 7 nm) and weak Hβ (EW

0.6 nm) emission lines with diffuse interstellar bands. The spectroscopic results were similar to those characteristics reported above by Halpern & Tyagi 2005 ([70]), obtained from the observation by 1.5m G.D. Cassini telescope on 23 December 2005 by using the INTEGRAL error circle for positioning.

Addition to those characteristics, Na doublet was seen at 5980 A with the reported values of EW(Hα)=(74±2)Å and EW(Hβ)=(6.4±0.4)Å. The observational color excess 2.04 and Galactic color excess 1.41 mag ([164]) are different from each other, which is suggested that it is a remote star. But using the optical magnitudes for this object, the distance was estimated to be 11.6 kpc and 6.4 kpc from two different optical calculations ([121]). Also the luminosity values were calculated from the distance estimation as 7.3×10^{34} ergs^{-1} (0.2-10 keV) and 5.2 $\times 10^{35}$ ergs^{-1} (20-40 keV)(showed that it was in its active phase).

From both luminosity values and the spectral type discussions, Masetti et al. 2006([121]) concluded that IGRJ01583+6713 is a transient Be/X-ray HMXB. Again according to high mass catalogue of Liu et al.2006([113]), it is identify as also Be type star, this is also classified like that in Belczynski et al.2009([20]). Lastly, Kaur et al.2008([94]) had made some assumption from their calculations about the orbital period of the binary as the range of 216-561 d.

6.2 Observations

Optical spectroscopic and photometric observations of both IGRJ 06074+2205 and IGRJ 01583+6713 counterparts were obtained from the 1.3m telescope of the Skinakas observatory in Crete (Greece) with optical resolution 1 Å pixel^{-1}. It was observed through the Johnson B, V, R and I filters, shown in (Table 6.1). For the photometric observations the telescope was equipped with a 1024×1024 SITe CCD chip, containing 25 μm pixels.

For optical spectroscopic observations of counterpart an equipment with a 2000×800 ISA SITe CCD and a 1302L/mm blaze 550 grating with nominal dispersion of ∼1 Å pixel^{-1} is used.

The reduction and analysis of photometric and spectroscopic observations were made by using the package Longslit context of IRAF.

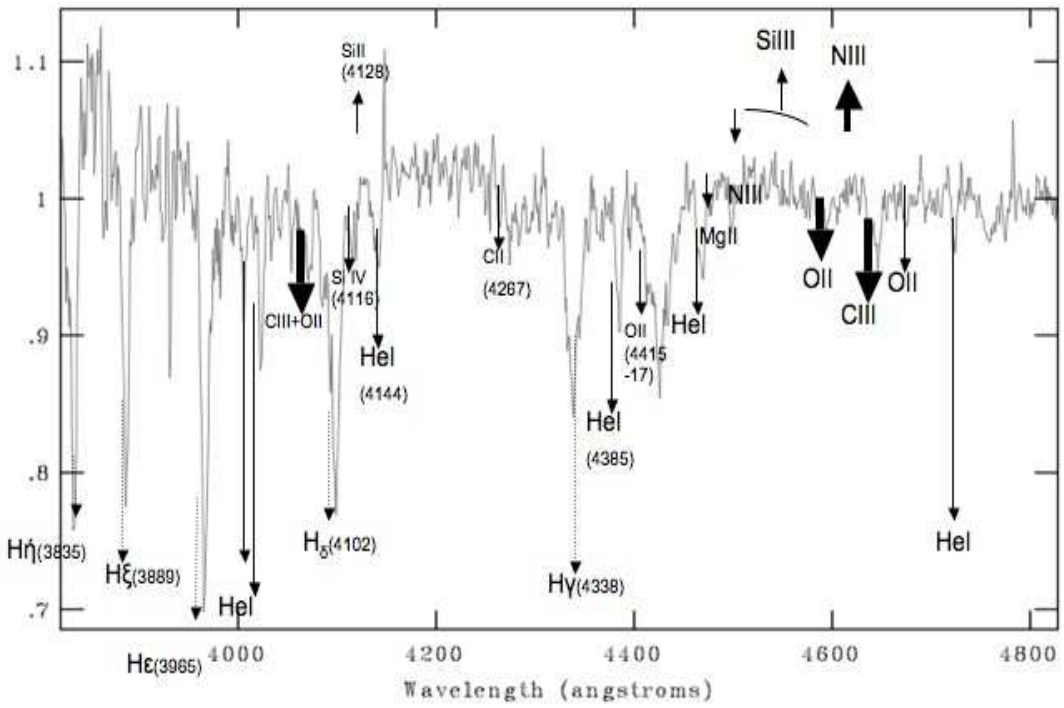

Figure 6.1: The blue band spectrum (3800-4800 (Å)) of IGRJ 06072+2205 taken on 26 December 2007

6.3 Results

6.3.1 Photometric Results

The results of photometric observations are presented in Table6.1. The photometric results of IGRJ06074+2205 and IGRJ01583+6713 for 2007, 25-26 October are completed by using the

Table 6.1: Results of photometric measurements of the counterparts

Date	MJD	B	V	R	I
IGRJ06074+2205					
25 October 2007	54399.62	12.88±0.02	12.28±0.03	11.90±0.02	11.47±0.02
26 October 2007	54400.29	12.81±0.03	12.26±0.03	11.89±0.04	11.43±0.05
IGRJ01583+6713					
16 July 2007	54298.07	15.57±0.03	14.37±0.03	13.48±0.03	12.62±0.03
25 October 2007	54399.62	16.37±0.02	15.25±0.03	14.71±0.02	
26 October 2007	54400.29	16.68±0.03	15.76±0.03	15.21±0.04	

values given by Table 1 in Reig et al. 2010([157]).

6.3.2 Spectral Classification

When we get appropriate spectrum belongs to different wavelength ranges in optical studies, we can identify the lines seen in spectrum. From those lines we can predict the type and characterize of the lines of the secondary star. To start with identifying the type, we get spectrum in between (3800-4800 (Å)) range. Figure 6.1 shows the blue spectrum (3800-4800 (Å)) of IGRJ 06074+2205. The Blue band spectrum shows various members of the Balmer series (Hα,Hη, Hξ, Hϵ, Hδ, Hγ) in absorption clearly. Balmer lines are specific emission lines created by hydrogen. The sets of transitions from n≥3 to n=2 are called the Balmer series.

No HeII lines are seen and except H and HeI lines, the spectrum shows some other metallic lines as NII, SiIV, SiII, CII, CIII+OII blends, MgII, NIII. The presence of H, HeI and SiIV lines clearly shows that the source contains an early-type stars. HeIIλ4686 in normal conditions is seen at B0.5. The other metallic lines classified the spectral type range as between B0-B2. The maximum strength of the HeI lines is reached in early B classes, around B2. In this spectrum, the strength of HeI lines are less than the ones of the standard stars in 'OB stars Atlas' ([184]). The ratio SiIIIλ4552 over SiIVλ4089 increases smoothly toward later spectral types, in our case it is smaller than one. Moreover, the spectral features CIII+OII$\lambda\lambda$4070,4650 blends and some SiIIIλ4552-68, although it is weak, indicate a B1-1.5 spectral type. As a luminosity class, the strength of CIII+OIIλ4650 blends is strong to classify it as a giant type. There are some line ratios to be used. HeIλ4121 over HeIλ4144, with λ4144 weakened out of the main sequence. Also, HeIλ4121 over SiIVλ4116 is bigger than one in the main sequence. As a result, the optical counterpart to IGRJ06074+2205 is a B1-1.5 III/V type.

Hα has a wavelength of 656.281 nanometers. It is visible in the red part of the electromagnetic spectrum and is the easiest way for astronomers to trace the ionized hydrogen content of gas clouds. If the star is in Be phase, then we expect to see emission in Hα. After we detect Hα line in the spectrum, we make Gaussian fit to this emission line with whole continuum by using IRAF program. We make some measurements of the strength of the spectral line according to continuum such as equivalent width (EW), flux value. The equivalent width of a spectral line is a measure of the area of the line on a plot of intensity versus wavelength. It is found by forming a rectangle with a height equal to that of continuum emission, and finding

the width such that the area of the rectangle is equal to the area in the spectral line.

The equivalent width (EW) values were obtained from Gauss fit to the emission features (see Table 6.2). The spectral line can be appeared in either emission or absoption form. In our table, we can understand from its minus sign of λ as it is appearing in emission form.

6.3.3 Reddening and Distance Measurements

The gas and dust along the line of sight to a star, starlight dims by absorbing and scattering the light. It is called interstellar extinction. Extinction is stronger at shorter wavelentghs, as shorter wavelentghs interact more strongly with dust particles. Red light passes through gas and dust more easily than the blue light. The more gas and dust between the source and the observer, the stronger the reddening. The reddening of starlight due to the interstellar extinction is known as interstellar reddenning.

In the red spectrum (5800-7200Å) besides the Hα and HeIλ6678 lines, there are several strong diffuse interstellar bands (DIBs). DIBs can be used to estimate the amount of interstellar absorption toward the source ([74], [75], [61]). Accoring to Herbig et al. 1975([74]), we use the correlation of EW(DIBs) with E(B-V),

$$EW(DIBs)(m\text{Å}) = aE(B-V) + b \tag{6.1}$$

$$EW(DIBs)(m\text{Å}) = a_o E(B-V) \tag{6.2}$$

Table 6.2: Equivalent widths of the Hα lines

Date	MJD	(λ_{obs})(Å)	Equivalent Width(Å)	Flux
IGRJ06074+2205				
22 October 2006	54394.58	6563.7	11.6873±0.8502	-11.3839±0.2626
24 October 2006	54394.59	6563.7	11.8766±0.6641	-11.6306±0.8840
06 September 2007	54349	6562.3	10.7274±0.5624	-11.1762±0.7522
04 October 2007	54377	6561.5	-9.2855±0.6236	9.3857±0.2771
IGRJ01583+6713				
29 May 2007	54249	6559.6	-49.4633±3.1871	70.2603±2.5212
04 September 2007	54347	6559.6	-56.1383±2.9352	72.0671±1.4951
07 September 2007	54350	6560.1	-54.7586±5.8930	73.0568±3.0311
02 October 2007	54375	6560.9	-53.5988±4.5186	73.7877±2.0351
04 October 2007	54377	6559.7	-52.5542±4.7984	78.0833±1.9687

where a, b, a_o are coefficients to define of each Diffuse lines belong to three different regions in space. They are taken from Table 4 given by Herbig et al. 1975([74]). Using the coefficient measurements of strongest lines, firstly 6203.06 and 6613.63, secondly 5797, 5849.79, 6376-79 combined, totally for 14 observations, in red spectrum for IGRJ 06074+2205, we get E(B-V)~0.79 mag.

To estimate the distance, we need to determine the amount of interstellar extinction to the source, $A_v = R_v \times E(B-V)$, where E(B-V) is an color excess and R_v can be determined from the reddening curve within the Galaxy, as R_v=3.1 (Reddening curve is obtained from ([68])). The visual extinction, A_v~2.43 mag. If we know the spectral type and luminosity class of the star, we can estimate the stars' luminosity, which is closely related to absolute magnitude. By using absolute (M) and apparent (m) magnitudes, we can estimate distance, as

$$m - M = -5 + 5log_{10}d \tag{6.3}$$

$$d = 10^{0.2(m-M+5-A_v)} \tag{6.4}$$

where d in pc. Taking an average absolute magnitude (for V band) for a known spectral type M_v ([178],[187]), we can use for IGRJ06074+2205 for M(B1 III)= -4.10 and also M(B1 V)= -2.95. From this calculation, the distance estimation can be done as around 4.03 kpc.

Another way to estimate the color excess is using the photometric observations results. We performed this method to IGRJ01583+6713 to find its color excess so hence the distance. We firstly used the photometric B and V magnitude results in Table6.1 and find the difference between two bands.

$$(B-V)_(observed) = 1.20 \pm 0.06 for MJD 54298.07 \tag{6.5}$$

$$(B-V)_(observed) = 1.12 \pm 0.05 for MJD 54399.62 \tag{6.6}$$

$$(B-V)_(observed) = 0.92 \pm 0.06 for MJD 54400.29 \tag{6.7}$$

We know the spectral type and luminosity class of the source as B2 IV([94]), by using the intrinsic color value for this known type ([186]) as $(B-V)_o$= -0.24 mag,

The below equation gives us the excess color

$$E(B-V) = ((B-V)_(observed)) - ((B-V)_o) \tag{6.8}$$

where $(B-V)_o$ is an intrinsic color value.

As a result, we get excess color values as

$$E(B-V) = 1.44 \pm 0.06 for MJD 54298.07 \quad (6.9)$$

$$E(B-V) = 1.36 \pm 0.05 for MJD 54399.62 \quad (6.10)$$

$$E(B-V) = 1.16 \pm 0.06 for MJD 54400.29 \quad (6.11)$$

The mean average excess color value for IGRJ01583+6713 is found as
E(B-V)=(1.32±0.06) mag.

By using V band magnitudes in Table6.1 and spectral type M_v=-2.32([187]) for IGRJ01583+6713, we can make distance estimation around 3.3 and 4.9 with an upper limit 6.2 kpc.

6.4 Discussion

Be stars can be define as stars with observation between late O to early A stars. Studies about Be stars show that Hα line is an important information for these stars. Especially the structure and the shape of the line provides importance about the structure of the disc. Negative value of EW(Hα) shows the line appears in emission (as an example see Table 6.1 and Figure 6.2). Hα profile can be appear as double peak, single peak, emission with a shell profile, absorption, emission with a split profile, quasi emission peak ([157]). The absorption lines are formed in the photosphere of the star which means there is no disc formation, while the emission profile is due to radiation from ionized hydrogen in the hot circumstellar envelope around the Be star. The optic photometrical and spectroscopical measurements give us information about the interstellar medium between the source and the observer.

IGRJ 06074+2205 is a binary system discovered with INTEGRAL JEM-X in 2003. The observed Hα lines show it is a Be type star, the spectroscopic measurements also confirm this result, with more specific determination. Using both photometric and spectroscopic measurements, we could be able to interstellar reddening which make prediction about the distance. The estimated distance measurement of IGRJ06074+2205 is around 4.03 kpc, which is also same as the value found by Reig et al. 2010([157]).

IGRJ 01583+6713 is a binary system discovered by INTEGRAL IBIS/ISGRI in 2005. For this source strong Hα and weak Hβ (as in [121]) make us to confirm the optical counterpart

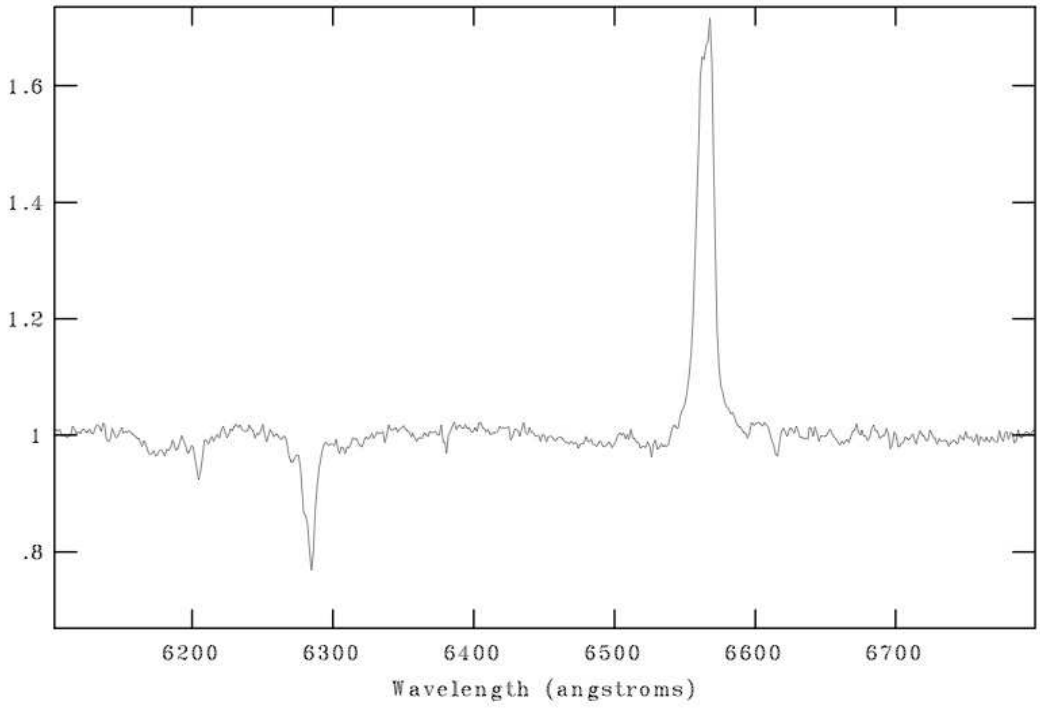

Figure 6.2: Hα emission line in the red spectrum of IGRJ 06074+2205 taken on 07 November 2007

as Be type. The lack of blue spectrum for this source, we can not be able to to determine the spectral type of the companion star. We have only photometric observations and from their results we could be able to calculate the amount of reddening so the excess color. The results are compatible with the value founded by Kaur et al. 2008([94]).

Finally, the multiband optical photometric variability and stability of the Hα line prole of IGR J01583+6713 shows almost the same results which is investigated by Kaur et al. 2008([94]). They determine the spectral type as B2 IVe and the distance to the source was estimated as ~ 4.0 kpc. Our distance calculation for this source gives a range ~3-6 kpc, which is compatible with their distance estimation.

CHAPTER 7

CONCLUSION

In this work, we presented the analysis of RXTE, Fermi-GBM, Swift observations of SMC X-1, 4U 1907+09, 4U 1538−52, 4U 1626−67 with analysis of spectroscopic and photometric observations of counterparts of IGRJ 06074+2205 and IGRJ 01583+6713 done with Skinakas Observatory (Crete).

An accreting powered system SMC X-1 continues to show spinning up. Analysis of 8 years RXTE/PCA observations show that the spin-up rate is $\dot{P}_{pulse}/P_{pulse}$=1.61805096(6863)×$10^{-6}$ s^{-1}. There is an increase in spin-up rate according to previous spin-up trend. By timing studies we could be able to see a ∼ 30 year long pulse period history of the source. Also with this study, we see that eccentric orbit model gives better solution in obtaining orbital parameters. Hence we obtain a new orbital epoch and using this new and previous results we could be able to find orbital period decay, $\dot{P}_{orbit}/P_{orbit}$ of $-3.402(7) \times 10^{-6}$ yr^{-1}, and see that it is consistent with previous values. Spectral analysis shows the variations only in hydrogen column density, other parameters did not show any variability according to previously founded values. Moreover hydrogen column density increases as the X-ray flux value deceases.

The spin-down rate of 4U 1907+09 obtained in between March 2001 and March 2002 was found to be ∼ 0.60 times lower than both the previous RXTE measurements of spin-down rate between November 1996 - December 1997 by ([10]) and the long term spin-down trend of the source in between 1983 and 1997 (See Figure 1 in [10]). In the recent studies and the previous RXTE observations show that time span of the observations were similar (∼ over year) and in both observations posses low timing noise. However, spin down rate is lowered by a factor of 0.6 in last RXTE observations. It is also interesting to observe that the spin-down rate

is consistent with zero around MJD 51000 before this significant change in spin-down rate. Since the discovery of the source, our pulse frequency measurements are significant due to including the first time resolved spin-down rate variations. The steady spin-down rate ([10]) and the presence of transient oscillations ([85],[136]) in 4U 1907+09 support the idea that the source accretes from retrograde transient accretion disc. The possibility of a prograde disc for which the magnetospheric radius should be close to the corotation radius so that the magnetic torque overcomes material torque is not likely to be the case for this system ([85]). If the disc is retrograde and the material torque is dominant, using ([67]) accretion disc model, a decrease in spin-down rate of the neutron star should be a sign of a decrease in the mass accretion rate coming from the accretion disc. If the disc accretion is the only accretion mechanism, this decrease in mass accretion rate should also lead to a decrease in X-ray flux of the system.

From the X-ray spectral analysis of the source, we found no clear evidence of a correlation between 3-25 keV flux and the change in spin-down rate. The flux levels were about the same for latter observations with low spin-down rate compared to the rest of the observations. This was not our expectation if we only consider disc accretion and may be because of the fact that the total mass accretion rate is not only due to only disc accretion, but also accretion from stellar wind may contribute to the total mass accretion rate (see also [158]). In case of accretion from both transient disc and wind, the change in mass accretion rate from the accretion disc might not cause a substantial change in X-ray flux. However, it is important to note that the orbital coverage of the latter (proposal ID 60061) observations is poor and limited to the phase locked flares in orbital phases $\sim$ 0.05 and $\sim$ 0.6. Future observations of the source may be helpful to have a better understanding of a possible relation between spin-down rate and X-ray flux.

For flaring parts of the source, we found evidence an increase in Hydrogen column density (n_H) for the latter observation with lower spin-down rate. Except Hydrogen column density, there is no any significant variations or evidence in other spectral parameters after the spin-down rate decreased.

The timing analysis for 4U 1538−52 between July 31 and August 7, 2003 with RXTE/PCA give information about orbital epoch, orbital period and derivatives, pulse frequency and derivatives. We calculate the new orbital epoch by using $< P_{orbit} >= 3.7228366$ days and a quadratic fit to that epoch gives us orbital period change rate as $\dot{P}_{orb}/P_{orb} = (0.4 \pm 1.8) \times 10^{-6}$

yr^{-1}, as in some other HMXBs, this change can be explained by tidal interactions. Previous observations also found long term spin-down trend for this source, and a linear fit gave the frequency history as $\dot{\nu}/\nu \sim -8 \times 10^{-12} s^{-1}$, and when we fit to our RXTE observation, the result becomes $\dot{\nu}/\nu \sim 1.45 \times 10^{-11} s^{-1}$.

By analyzing of the all RXTE observations archive data, the trend of spin period show that the neutron star spins up for 30 years, with different spin-up rate. According to RXTE observations duration, source's spin-up rate shows increasing within 20% according to previous spin-up behavior.

Mass transfer or loss, the gravitational radiation, the gravitational effects by a third body and the tidal interactions are the possible explanations for the orbital decay in a period of a binary system. For SMC X-1 system, the effects of mass transfer or loss can be negligible, the system does not include a third body so that a period decaying due to the gravitational acceleration can not be reason. The long negative orbital period decaying of the system, as in Cen X-3 and LMC X-4, is mostly likely due to the tidal interaction between the neutron star and the companion star.

Hydrogen column density changes just during the low flux values, the hydrogen column density is very high when the flux is low as expected but after some flux value the column density although the flux increases, the density goes constant. The increased soft X-ray pulsation is absorbed due to hydrogen column. Whereas, the other parameters belongs to model do not show any changes according to flux.

We established a pulsed source monitoring by using rates of 12 NaI detectors on Fermi/GBM instrument between 8-55 keV. In our continuous monitoring we can be able to detect outbursts from the Be/X-ray transient, disk-fed supergiants, and persistent LMXB systems. We are producing long term histories of the pulse frequency, flux, pulse profile and make precise measurements of orbital parameters. One of these systems, 4U 1626−67 was investigated in detail. Since GBM discovers a new spin-down to spin-up torque reversal belongs to that source. It occurred after about 18 years of the pulsar's steadily spinning down and was centered on 2008 Feb 4. The transitions was lasted ~150 days and accompanied by an increase in the Swift/BAT count rate of a 2.5 factor (~150%). The pulsar spectrum was harder during the torque transition than before or after. A strong correlation between torque and luminosity is obviously appeared only during the transition. The spin-up and spin-down rates before and

after the transition were almost identical ($\sim \mid \dot{\nu} \mid = 5 \times 10^{-13}$ Hz s^{-1}). However, the pulsar was braking harder at the beginning of the spin-down epoch in 1990 than at its end in 2008. Furthermore, the spin-down rate during this epoch was decreasing simultaneously with the decreasing of the source X-ray luminosity. Finally, the spin-down to spin-up torque reversal in 2008 has occurred at lower luminosity as the spin-up to spin-down torque in 1990. These properties cannot be explained with existing models and it can be interesting step for further studies in understanding the mechanism of the torque reversals in the accretion-powered pulsars.

The optical photometric and spectroscopic observations of the optical counterpart to IGR J06074+2205 and IGRJ01583+6713 show that they are binary systems with Be type. For both sources Hα lines appear in emission which means that there is circumstellar disk around Be star. The spectral type of the companion star of IGR J06074+2205 is found as B1-1.5 III/V class. The photometric magnitudes give the value of interstellar reddening for each sources. From the reddening value we predict the distance of IGR J06074+2205 as around 4 kpc which is compatible with the results of Reig et al.2010([157]). For IGRJ01583+6713 from photometric observations we estimate the distance in between ~3-6 kpc which is compatible with the results of Kaur et al.2008([94]).

REFERENCES

[1] Alpar M. A., Shaham J., 1985, Nat, 316, 239

[2] Angelini L., Stella, L., Parmar, A.N. 1989, ApJ, 346, 906

[3] Angelini L., Stella, L., White, N.E. 1991, ApJ, 371, 332

[4] Atwood W. B. et al., 2009, ApJ, 697, 1071

[5] Camero-Arranz A., Finger M. H., Ikhsanov N. R., Wilson-Hodge C. A., Beklen E. 2010, Apj, 708, 1500

[6] Coburn W., Heindl W. A., Rothschild R. E., Gruber D. E., Kreykenbohm I., Wilms J., Kretschmar P., Staubert R., 2002, ApJ, 580, 394

[7] Casumano G, Salvo T.D., Burderi L., Orlandini M., Piraino S., Robba N., Santangelo A., 1998, A&, 338, L79

[8] Baade W., & Zwicky, F., 1934, Phys. Rev., 45, 138

[9] Baykal A., Ogelman H., 1993, A&A, 267, 119

[10] Baykal A., İnam, Ç., Alpar M.A., in 't Zand J., Strohmayer T., 2001, MNRAS, 327, 1269

[11] Baykal A., Stark M., Swank J. 2002, ApJ, 569, 903

[12] Baykal A., İnam S. Ç., Beklen E. 2006, MNRAS, 369, 1760

[13] Baykal A., İnam S. Ç., Beklen E. 2006, A&A453, 1037

[14] Baykal, A., Kızıloğlu Ü., Kızıloğlu N., Beklen, E., Özbey M. 2008, A&A, 479, 301

[15] Becker R.H., Swank J.H., Bold E.A., Holt S.S., Pravdo S.H., Saba J.R., Serlemitsos P.J., 1977, ApJ. Lett., 216, L11

[16] Beklen E., Finger H.M., 2009, Atel#2275

[17] Beklen E., Finger H. M. 2009, Atel#1956

[18] Beklen E., Finger H. M. 2009, Atel#1972

[19] Belczynski K., Sadowski A., Rasio F.A., Bulik T. 2006, ApJ, 650, 303

[20] Belczynski K., Ziolkowski J. 2009, ApJ, 707, 807

[21] Bildsten L., Chakrabarty D., Chiu J., Finger M. H., Grunsfeld J. M., Koh T., Prince T. A., & Wilson R., 1994, in AIP Conf. Ser. 304, The Second

[22] Bildsten L., Chakrabarty D., Chiu J., Finger M. H., Koh D. T., Nelson R. W., Prince T. A., Rubin B. C., Scott D. M., Stollberg M., Vaughan B. A., Wilson C. A., Wilson R. B. 1997, ApJS, 113, 367

[23] Blondin J.M., Kallman T.R., Fryxell B.A., Taam R.E., 1990, ApJ, 356, 591

[24] Bonnet-Bidaud J. M., van der Klis M., 1981, A&A, 97, 134

[25] Caballero et al., 2010, Atel#2541

[26] Casumano G., Salvo T.D., Burderi L., Orlandini M., Piraino S., Robba N., Santangelo A., 1998, A& A, 338, L79

[27] Chadwick J. 1932, Nature, 129, 312

[28] Chakrabarty D., et al. 1997, ApJ, 474, 414

[29] Chakrabarty D., Levine A. M., Clark G. W., Takeshima T., 1998, IAUC, 7048

[30] Chakrabarty D., Wang, Z., Juett A. M., Lee J. C., & Roche P. 2002, ApJ, 573, 789

[31] Chenevez J., Budtz-Jorgensen C., Lund N., Westergaard N. J., Kretschmar P., Rodriguez J., Orr A., Hermsen Wim, Atel#223

[32] Chitnis V.R., Rao A.R., Agrawal P.C., Manchanda R.K., 1993, A& A, 268, 609

[33] Chodil G., Mark H., Rodrigues R., et al. 1967, ApJ 150, 57

[34] Clark G.W. 2000, ApJL, 542, 133

[35] Coburn W.,,Heindl W. A., Wilms J., Gruber D. E., Staubert R., Rothschild R. E., Postnov K. A., Shakura N., Risse P., Kreykenbohm I., Pelling M. R. 2000, ApJ, 543, 351

[36] Wilson-Hodge A.C., Finger H.M., Camero-Arranz A.and Connaughton V., The GBM Occultation Project and GBM Pulsar Project teams ,2009, Atel#2324

[37] Cook M.C., Page C.G., 1987, MNRAS, 225, 381

[38] Corbet R.H.D. 1986, MNRAS, 220, 1047

[39] Corbet R.H.D., Woo, J.W., Nagase, F. 1993, A& A, 276, 52

[40] Corbet R.H.D., Negueruela I., 2007, MNRAS, 382, 743

[41] Cox N.L., Kaper L., Mokiem M.R., 2005, A& A, 436, 661

[42] Casumano G., Salvo T.D., Burderi L., Orlandini M., Piraino S., Robba N., Santangelo A., 1998, A& A, 338, L79

[43] Davidson K., Ostriker J.P. 1973, ApJ, 179, 585

[44] Davison P. J. N., 1977, MNRAS, 179, 15

[45] Day C. S. R., Nagase F., Asai K., Takeshima T., 1993, ApJ, 408, 656

[46] Deeter J. E., Boynton P. E., Pravdo S. H., 1981, ApJ, 247, 1003

[47] Deeter J. E., Boynton P. E., 1985, in Proc. Inuyama Workshop on Timing Studies of X-ray Sources, Nagoya Univ., Nagoya, p.29

[48] Deeter J.E., Boynton P.E., Lamb F.K., Zylstra G. 1989, ApJ, 336, 376

[49] Deeter J.E., Boynton P.E., Miyamoto S., 1991, ApJ, 383, 324

[50] Dupree A. K., et al. 1980, ApJ, 238, 969

[51] Finger M.H., Wilson R.B., Chakrabarty D., 1996, A&AS, 120, 209

[52] Finger M.H., 1998, Adv. Space Res., 22, 1007

[53] Finger M. H., Bildsten L., Chakrabarty D., Prince T. A., Scott D. M., Wilson C. A., Wilson R. B., & Zhang S. N. 1999, ApJ, 517, 449

[54] Finger, M. H., Beklen, E., Camero-Arranz, A., Atel # 2142, 2009

[55] Finger M. H., Beklen E., 2009, Atel#2023

[56] Finger et al. 2009 Fermi Symposium, Washington

[57] Finger M. H., Wilson-Hodge C., Camero-Arranz A., Jenke P., 2010 HEAD 11.4208

[58] Finger et al. 2010 Cesme, Turkey ASTRONS meeting

[59] Fritz S., Kreykenbohm I., Wilms J., Staubert R., Bayazit F., Pottschmidt K., Rodriguez J., Santangelo A. 2006, AAP, 458, 885

[60] Galache J. L., Corbet R. H. D., Coe M. J., Laycock S., Schurch M. P. E., Markwardt C., Marshall F. E., Lochner J., 2008, ApJS, 177, 189

[61] Galazutdinov G.A., Musaev F.A., Krelowski J., & Walker G. A. H., 2000, PASP, 112, 648

[62] Giacconi R., Gursky H., Paolini F. R., & Rossi B. B., 1962, Phy. Rev, 9, 439

[63] Giacconi R., Kellogg E., Gorenstein P., Gursky H., Tananbaum H., 1971, ApJ, 165, L27

[64] Giacconi R., Murray S., Gursky H., Kellogg E., Schreier E., & Tananbaum H. 1972, ApJ, 178, 281

[65] Giacconi R., Murray S., Gursky H., Kellog E., Schreier E., Matilsky T., Koch D., Tananbaum H., 1974, ApJS, 27,37

[66] Gehrels, N., et al. 2004, ApJ, 611, 1005

[67] Ghosh P., Lamb F.K., 1979, ApJ, 234, 296

[68] Gordon K. D., Clayton G. C., Misselt K. A., Landolt A. U., Wolff M.J. 2003, ApJ, 594, 279

[69] Gruber D. E., Rothschild R. E., 1984, ApJ, 283, 546

[70] Halpern J.P., Tyagi S., 2005, Atel#682

[71] Studies of X-Ray Sources, ed. S. Hayakawa & F. Nagase (Nagoya: Nagoya Univ.), 29

[72] Hayakawa S.,& Matsuoka M., 1964, PThP, 30, 204

[73] Henry P., Schrier E., 1977, ApJ, 212, L13

[74] Herbig, G.H., 1975, ApJ, 196, 129

[75] Herbig, G.H., &Leka, K.D., 1991, ApJ, 382, 193

[76] Hinkle K. H., Fekel F. C., Joyce R. R., Wood P. R., Smith V. V., & Lebzelter T. 2006, ApJ, 641, 479

[77] Hoyle F., Narlikar J. V., & Wheeler J. A. 1964, Nature, 203, 914

[78] Hui Chung Yue, PhD Thesis, 2007

[79] İnam S.C., Baykal A., Swank H.J., Stark M., 2004, ApJ, 616, 463

[80] İnam S.C., Baykal A., Scott D.M., Finger, M., Swank J., 2004, MNRAS, 349, 173

[81] İnam S.Ç., Baykal A., 2005, MNRAS, 361, 1393

[82] İnam S.Ç., Baykal A., Beklen E. 2010, MNRAS, 403, 378

[83] İnam S.Ç., Şahiner Ş., Baykal A. 2009, MNRAS, 395, 1015

[84] in't Zand J.J.M., Strohmayer T.E., Baykal A., 1997, ApJ, 479, L47

[85] int Zand J.J.M., Baykal A., Strohmayer T.E. 1998a, ApJ, 496, 386

[86] in't Zand J.J.M., Strohmayer T.E., Baykal A., 1998b, Nucl.Phys. B, 69, 224

[87] Jahoda K., Swank J. H., Giles A. B., Stark M. J., Strohmayer T., Zhang W., Morgan, E. H., 1996, SPIE, 2808, 59

[88] Jain C., Paul B., & Dutta A. 2009, MNRAS, submitted

[89] Jain C., Paul B., Dutt A., 2010, MNRAS, 403, 920

[90] James M., Biswajit P., Indulekha K., 2010, MNRAS, 407, 285

[91] Kahabka P., Li X.D., 1991, A&A, 345, 117

[92] Kaur R., Paul B., Raichur H., Sagar R., 2007, ApJ, 660, 1409

[93] Kaur R., Paul B., Kumar B., Sagar R., 2008, ApJ, 676, 1184

[94] Kaur R., Paul B., Kumar B., and Sagar R. 2008, MNRAS, 386, 2253

[95] Keller S.C., Wood P.R., 2006, ApJ, 642, 834

[96] Kelley R.L., Rappaport G., Clark G.W., Petro L.D. 1983, ApJ, 268, 790

[97] Kennea J.A., Racusin J.L., Burrows D.N., Hunsberger S., Nousek J.A. and Gehrels N., 2005, Atel#673

[98] Kitamoto S., Hirano A., Kawashima K. et al. 1995, PASJ, 47, 233

[99] Krauss M. I., Schulz N. S., Chakrabarty D., Juett A. M., & Cottam J. 2007, ApJ, 660, 605

[100] Krivonos R., Produit N., Kreykenbohm I., Staubert R., von Kienlin A., Winkler C., Gehrels N. 2003, ATel211

[101] Krim et al., 2009, Atel #2011

[102] Kommers, J. M., Chakrabarty, D., & Lewin, W. H. G. 1998, ApJ, 497, L33

[103] Kunz M., Gruber D.E., Kendziorra E. et al. 1993, A&A, 268, 116

[104] Lamb F.K., Pethick C.J., Pines D. 1973, ApJ, 184, 271

[105] Lamb F.K., Shaham J., Pines D. 1978, ApJ, 224, 969

[106] Lamb F.K., Pines D., Shaham J. 1978, ApJ, 225, 582

[107] Lamb F. K., Shibazaki N., Alpar M. A., & Shaham J. 1985, Nature, 317, 681

[108] Levine A., Ma C. P., McClintock J., Rappaport S., van der Klis M., & Verbunt F. 1988, ApJ, 327, 732

[109] Leahy D. A., Darbro W., Elsner R. F., Weisskopf M. C., Kahn S., Sutherland P. G., Grindlay J. E., 1983, ApJ, 266, 160

[110] Levine A., Rappaport S., Deeter J.E., Boynton P.E., Nagase F., 1993, ApJ, 410, 328

[111] Levine A.M., Rappaport S.A., Zojcheski G., 2000, ApJ, 541, 194

[112] Liller W., 1973, ApJ, 184, L37

[113] Liu Q.Z., van Paradijs J., van den Heuvel E.P.J., 2006, A&A, 455, 1165

[114] Liu Q.Z., van Paradijs J., van den Heuvel E.P.J., 2007, A&A, 469, 807

[115] Lucke R., Yentis D., Friedman H., Fritz G., Shulman S., 1976, ApJL, 206, 25

[116] Makishima K., Kawai N., Koyama K., Shibazaki N., Nagase F., Nakagawa M., 1984, PASJ, 36, 679

[117] Makishima K., Koyama K., Hayakawa S., Nagase F., 1987, ApJ., 314, 619

[118] Makishima K., Ohashi T., Kawai N. et al. 1990, PASJ, 42, 295

[119] Makishima K., Mihara T., 1992, in Tanaka Y., Koyama K., eds. Proc. XXVIII Yamada Conf., Frontiers of X-ray Astronomy, Universal Academy Press, Tokyo, p. 23

[120] Marshall N., Rickets M.J., 1980, MNRAS, 193, 7

[121] Masetti N., Bassani L., Bazzano A., Bird A. J., Dean A.J., Malizia A., Norci L., Palazzi E., Schwope A. D., Stephen J. B., Ubertini P., Walter R. 2006, A&A, 455,11

[122] Masetti N., Morelli L., Palazzi E., Galaz G., Bassani L., Bazzano A., Bird A. J., Dean A. J., Israel G. L., Landi R., Malizia A., Minniti D., Schiavone F., Stephen J. B., Ubertini P., Walter R.

[123] McBridge V.A. ,Coe M.J., Bird A.J., Dean A.J., Hill A.B., McGowan K.E., Schurch M.P.E., Udalski A., Soszynski I., Finger M., Wilson C.A., 2007, MNRAS, 382, 743

[124] McClintock J. E., Bradt H. V., Doxsey R. E., Jernigan J. G., Canizares C. R., & Hiltner W. A. 1977, Nature, 270, 320

[125] McClintock J. E., Li F. K., Canizares C. R., & Grindlay J. E. 1980, ApJ, 235, L81

[126] Meegan C. A., et al. 2009, ApJ, 702, 791

[127] van der Meer A., Kaper L., van Kerkwijk M. H., Heemskerk M. H. M., van den Heuvel E. P. J., 2007, A&A, 473, 523

[128] Meszaros P., Nagel W., Ventura J., 1980, ApJ, 238, 1066

[129] Middleditch and Priedhorsky 1986, Astrophysical Journal 306, 230

[130] Mihara T., 1995, PhD thesis, Univ. Tokyo

[131] Moon, D., Eikenberry, S.S. 2001a, ApJ, 549, L225

[132] Moon D., Eikenberry S.S. 2001b, ApJ, 552, L135

[133] Morrison R., McCammon D., 1983, ApJ, 270,119

[134] Motch C., Stella L., Janot-Pacheco E., Mouchet M. 1991, ApJ, 369, 490

[135] Mukherjee U., Bapna S., Raichur H., Paul B., Jaaffrey S. N. A., 2006, JA&A, 27, 25

[136] Mukherjee K., Agrawal P.C., Paul B., Rao A.R., Yadav J.S., Seetha S., Kasturirangan K. 2001, ApJ, 548, 368

[137] Nagase F. 1989, Bubl. Astron. Soc.Japan, 41, 1

[138] Nagase F., Corbet R.H.D., Day C.S.R., et al. 1992, ApJ, 396, 147

[139] Naik S. and Paul B., 2004, A&A, 418, 655

[140] Neilsen J., Hickox R. C., Vrtilek S. D., 2004, ApJ, 616, 315

[141] Okazaki A.T., Negueruela I. 2001, A&A, 377, 161

[142] Oppenheimer, J. R., & Volkoff, G. M. 1939, Phy. Rev., 55, 374

[143] Orlandini M., et al. 1998, ApJ, 500, L163

[144] Parkes G.E., Murdin P.G., Mason K.O. 1978, MNRAS, 184, 73

[145] Paul B., Rao A.R. 1998, A& A, 1998

[146] Paul B., Nagase F., Endo T., Dotani T., Yokogawa J., Nishiuchi M., 2002, ApJ, 579, 411

[147] Petterson J. A., Rothschild R. E., & Gruber D. E. 1991, ApJ, 378, 696

[148] Pooley G. 2004, Atel#226

[149] Pravdo S. H., et al. 1979, ApJ, 231, 912

[150] Price R. E., Groves D. J., Rodrigues R. M., Seward F. D., Swift C. D., Toor A., 1971, ApJL, 168, 7

[151] Primini F.A., 1977, PhD thesis submitted to Massachusetts Institute of Technology

[152] Pringle J., Rees M.J., 1972, A&A, 21,1

[153] Rappaport S., Markert T., Li F. K., Clark G. W., Jernigan J. G., & McClintock J. E. 1977, ApJ, 217, L29

[154] Reynolds A.P., Hilditch R. W., Bell S. A., Hill G., 1993, MNRAS, 261, 337

[155] Reynolds A.P., Quaintrell H., Still M.D., Roche P., Chakrabarty D., Levine S.E. 1997, MNRAS, 288, 43

[156] Pablo R. & Andreas Z., 2009, Atel#2085

[157] Reig P., Zezas A., Gkouvelis L., 2010arXiv1006.4935R

[158] Roberts M.S.E., Michelson P.F., Leahy D.A., Hall T.A., Finley J.P., Cominsky L.R., Srinivasan R. 2001, ApJ, 555, 967

[159] Rodes, J. J. 2007, Ph.D. Thesis, University of Alicante

[160] Rodes-Roca J.J., Torrejn J.M., Kreykenbohm I., Martnez Nez S., Camero-Arranz A., Bernabu G., 2009, A&A, 508, 395

[161] Rubin B.C., Finger M.H., Harmon B.A. et al. 1996, ApJ, 459, 259

[162] Rubin B.C., Finger M.H., Scott D.M. et al. 1997, ApJ, 488, 413

[163] Schreier E., Giacconi R., Gursky H., Kellogg E., Tananbaum H., 1972, ApJL, 178, 71

[164] Schlegel D.J., Finkbeiner D.P., Davis M. 1998, ApJ, 500, 525

[165] Shinoda K., Kii T., Mitsuda K. 1990, PASJL, 42, 27

[166] Shibazaki N., Lamb F. K., 1987, ApJ, 318, 767

[167] Schwartz D. A., Griffiths R. E., Bowyer S., Thorstensen J. R., Charles P. A., 1980, AJ, 85, 549

[168] Soong Y., Swank J. 1989, in Proc. 23d ESLAB Symp., Two Topics in X-ray Astronomy, Vol.1, ed. N. White (Garching: ESA), 617

[169] Steiner C., Eckert D., Mowlavi N., Decourchelle A., Vink J., 2005, Atel#672

[170] Stella L., White N. E., Rosner R., 1986, ApJ, 308, 669

[171] Takeshima T., Dotani T., Mitsuda K., Nagase F., 1991, PASJ, 43, L43

[172] Takeshima T., Dotani T., Mitsuda K., Nagase F., 1994, ApJ, 436, 871

[173] Takeshima T. 1997, BAAS, 19111104

[174] Tomsick J.A., Chaty S., Rodriguez J., Walter R., Kaaret P., 2006, Atel#959

[175] Tomsick J. A., Chaty S., Rodriguez J., Walter R., Kaaret P. 2008, ApJ, 685, 1143

[176] Trowbridge, S., Nowak M. A., Wilms, J., 2007, ApJ, 670, 624

[177] Tuohy I. R., Rapley, C. G., 1975, ApJL, 198, 69

[178] Vacca W. D., Garmany C. D., Shull J.M., 1996, ApJ, 460, 914

[179] Valinia A., Marshall F.E., 1998, ApJ, 505, 134

[180] van der Klis et al. 1985, Nature, 316, 225

[181] van der Klis M., 1989, in Timing Neutron Stars, ed. H. Ogelman, E.P.J. van den Heuvel (Dordrecht:Kluwer), p.27

[182] Vaughan B. A., & Kitamoto S. 1997, arXiv:astro-ph/9707105

[183] Vrtilek S.D., Raymond J.C., Boroson B., McCray R. 2005, ApJ, 626, 307

[184] Walborn N. R., Fitzpatrick E. L. 1990, PASP, 102, 379

[185] Webster B. L., Martin W. L., Feast M. W., Andrews P. J., 1972, Nat, 240, 183

[186] Wegner W. 1994, MNRAS, 270, 229

[187] Wegner W., 2006, MNRAS, 371, 185

[188] White N. E., Swank J. H., Holt S. S., 1983, ApJ, 270, 711

[189] Wijers R. A. M. J., & Pringle J. E. 1999, MNRAS, 308, 207

[190] http://en.wikipedia.org/wiki

[191] Wilms J., Nowak M.A., Dove J.B., Fender R.P., di Matteo T. 1999, ApJ, 522, 460

[192] Wilson C.A., Finger M.H., Coe M.J., Laycock S., & Fabregat J. 2002. ApJ. 570, 287

[193] Wilson C.A., Fabregat J., Coburn W. 2005. ApJLett. 620, L99

[194] Wilson R. B., Fishman G. J., Finger M. H., Pendleton G. N., Prince T. A., & Chakrabarty D., 1993, in AIP Conf. Ser. 280, Compton Gamma-ray

[195] Wojdowski P., Clark George W., Levine Alan M., 1998, ApJ, 502, 253

[196] Yentis D., Shulman S., Mckee J.D., Rose W.K., 1977, Astrophys. Lett., 19, 53

[197] Yi I., & Vishniac E. T. 1999, ApJ, 516, L87

[198] Zel′dovich Ya. B. & Guseynov O. H. 1965, ApJ, 144, 840

[199] Zhang W., Morgan E.H., Jahoda K. 1996, ApJ, 469, L29

CURRICULUM VITAE

PERSONAL INFORMATION

Surname, Name: Beklen, Elif

Nationality: Turkish (TC)

Date and Place of Birth: 1 December 1977, Ankara

Phone: +90 312 210 43 24

email: elif@astroa.physics.metu.edu.tr, elif.beklen@gmail.com

EDUCATION

Ph.D: Middle East Technical University (METU), The Graduate School of Natural and Applied Sciences, Physics Department, Ankara, February 2004-September 2010

M.Sc: METU, The Graduate School of Natural and Applied Sciences, Physics Department, Ankara, February 2004.

B.Sc.: Ankara University, The Graduate School of Natural and Applied Science, Physics Department, Ankara, June 2000.

High School: TED Ankara College, Ankara, June 1996.

PUBLICATIONS

1. İnam S.C., Baykal A., Beklen E., 2010, Analysis of RXTE-PCA Observations of SMC X-1, MNRAS, 403, 378-386

2. Camero-Arranz A., Finger M. H., Ikhsanov N. R., Wilson-Hodge C. A., Beklen E., 2010, New Torque Reversal and Spin-up of 4U 1626-67 Observed by Fermi/Gamma-ray Burst Monitor and Swift/Burst Alert Telescope, ApJ, 708, 1500-1506

3. Baykal A., Kızıloğlu Ü, Kızıloğlu N., Beklen E., Özbey M., 2008, Recent RXTE/ASM

and ROTSEIIId observations of EXO 2030+375 (V2246 Cygni), A&A, 479, 301 - 306

4. Baykal A., İnam S. C., Beklen E., 2006, Recent timing studies on RXTE observations of 4U 1538-52, A&A, 453, 1037- 1040

5. Baykal A., İnam S. C., Beklen E. 2006, Evidence of a change in the long-term spin-down rate of the X-ray pulsar 4U 1907+09, MNRAS, 369, 1760 -1764